DEVELOPMENT OF COMPUTATIONAL FLUID DYNAMICS (CFD) BASED EROSION MODELS FOR OIL AND GAS INDUSTRY APPLICATION

by

DEVAL PANDYA

Presented to the Faculty of the Graduate School of

The University of Texas at Arlington in Partial Fulfillment

of the Requirements

for the Degree of

DOCTOR OF PHILOSOPHY

THE UNIVERSITY OF TEXAS AT ARLINGTON

December, 2013

Acknowledgements

I would like to express my deepest appreciation and gratitude to my advisor, Dr. Brian Dennis, for his continuous guidance and mentorship, right from the time I decided to apply for the Ph.D. program through the completion of this degree. Dr. Dennis' intellectual heft is matched only by his ever enthusiastic nature and inspiring humility.

I would like to thank my committee member Dr. Kent Lawrence, Dr. Dereje Agonafer, Dr. Bo Wang and Dr. Seiichi Nomura for their support and thought provoking suggestions.

I am extremely grateful to Baker Hughes Inc. for providing me continuous support in terms of experimental data without which this work would have been impossible. I would like to thank Dr. Mike Wells, Director of Research, for his continued interest and support. I would like to thanks Dr. Shashi Talya and Dr. Rajani Satti for being an excellent mentor throughout this work. My special thanks to Mr. Ronnie Russell, for his expert guidance and insight in the subject which was a guiding light for my work.

Finally, I'd be remiss if I did not acknowledge support and patience of my parents, Vatsala Pandya and Anil Pandya.

Last but not the least; I thank love of my life, Nivisha , for without her this work would have been impossible. It’s because of her inspiration during dull times, support during dark hours and continuous faith in my capabilities that I have been able to achieve the successful completion of this work.

November 22nd ,2013

Abstract

DEVELOPMENT OF COMPUTATIONAL FLUID DYNAMICS (CFD) BASED EROSION MODELS FOR OIL AND GAS INDUSTRY APPLICATION

Deval Pandya,PhD

The University of Texas at Arlington, 2013

Supervising Professor: Brian Dennis

Erosion prediction plays a critical role in different oil and gas industry segments including drill bit manufacturing, measurement & logging while drilling (M&LWD), and reservoir engineering/completions tools. Recently, Computational Fluid Dynamics (CFD) is used to predict erosion due to multiphase flows in complex geometries. Currently used CFD-based erosion models are able to predict erosion regions fairly accurately in various applications but they are highly inaccurate when it comes to predictions of quantities like erosion rate. Predicted quantities within an order of magnitude of the measured values are common and may be considered acceptable for many applications in the industry simply because more accurate prediction tools do not exist. This research aims at

developing a more robust and accurate CFD-based erosion model and formulating best practice CFD guidelines for the application of the model. An extensive set of experimental data was made available by Baker Hughes for experiments conducted on a 900 elbow. The present Baker Hughes erosion model was studied and modified to better fit the experimental data. The model was prepared for low sand concentration (1-10%) applications and was validated by comparing the predicted erosion region to that observed in the experimental results. Effect of various computational turbulence models and wall treatments were studied. A grid convergence study was performed to see the effect of near wall resolution on erosion prediction accuracy. Just by improving the CFD modeling approach, the mean percentage error decreases from around 60% to 40%. A statistical analysis was performed on the CFD output parameters to identify the parameters that effect erosion rates the most. Correlation analysis and non-parametric statistical analysis was carried out. Various regression models were employed for approximating the erosion rates as a function of the identified parameters. A new model specific to different y+ range was proposed and a considerable decrease in mean percentage error was observed. Two new regression models based on turbulent kinetic energy and surface shear stress were also developed. They provide excellent results with a further decrease in mean

percentage error to around 30%. Finally, an artificial neural network model was developed. A multilayer feedforward model with backpropogation algorithm and Levenberg-Marquardt training was used. The model gave a mean error percentage of less than 30%. Bayesian regularization was used with the training algorithm to avoid over fitting of the model. This model with regularization gave less than 10% mean percentage error for 920 data points.

Contents

List of Illustrations

List of Tables

Chapter 1

Introduction

1.1 Background

Erosion is defined as, “Gradual destruction or diminution of something”, by oxford dictionary. Damage is caused by the solid particles when they impinge on a surface. This mechanical damage, Erosion, is a big problem in various engineering applications. Erosion phenomenon is critical in failure of various tools that encounter multiphase flow where solid particles are present in fluid phase. Oil and Gas industry experiences erosion challenges in various applications. Sand erosion resulting from sand production in various high-rate wells is a common phenomenon. High erosion rates are observed even with low sand concentrations due to high production velocities. Hence, erosion modeling is a handy tool in sand control in completion and production. Predicting erosion regions and rates can be critical in drill bits design as well. It is a fairly recent practice to use erosion modeling for design and development of Measurement while Drilling (MWD) and Logging while Drilling (LWD) tools. Solid particle erosion thus, can be a limiting factor in design phase and a big concern for scheduling maintenance. It can be costly and may cause premature failure of components if not predicted within certain accuracy.

Chapter 2 Erosion is a complex phenomenon. It is observed that various factors affect erosion in oil and gas application. Geometry of the tool, material of the tool, particle size, particle concentration, particle shape, fluid velocity, viscosity of fluid, etc. affect the erosion region and rate.

Chapter 3 Oil and gas manufacturers, operators as well as service industry, all are interested in methods to predict erosion. A erosion prediction method that is reliable, can not only save money but also lives but predicting failure accurately and help in maintaining the safety of the equipment. Equipment used in sand production, drill-bits or MWD /LWD tools, all operate at extreme conditions. Thus, it is extremely difficult to replicate working condition for laboratory testing. Even if it is possible in some cases like drill-bits to test it before deployment, it is extremely expensive and time consuming to predict erosion using experiments.

Chapter 4 Computational Fluid Dynamics (CFD) based erosion modeling has been employed and explored extensively. CFD- based erosion models offer a cheaper and faster solution to the erosion modeling problem. But erosion modeling using CFD is a complex task involving various physical phenomenon that need to be accounted for. Flow modeling, particle interaction with fluid, wall effects, fluid properties, as well as the erosion model characteristics are just some of the properties that need to be considered. In addition, adequate modeling of the

geometric and discretization of the domain (meshing) are critical aspect in the success of the overall CFD-based erosion modeling procedure. The biggest advantage of CFD-based erosion modeling over other simplistic models is that complex geometries and flow fields can be easily accounted for using CFD. It is a powerful tool that can predict erosion regions accurately presenting a low cost, qualitatively accurate and timely method to predict erosion in various tools and geometries.

1.2 Research Purpose and Approach

There are two main goals of this research, improving CFD modeling techniques using the existing Baker Hughes model and developing a new more robust model including more physical parameters.

The CFD- based erosion modeling procedure essentially consists of three steps. (1) Flow modeling using CFD, (2) Modeling of Discrete phase (DPM) to obtain particle trajectories and wall interactions and finally (3) Erosion calculations based on an empirical equation. Each of these steps affects the accuracy of final erosion prediction and is critical to overall analysis. This analysis presents guidelines for each of the above steps. The results of CFD simulations are largely affected by the quality of the CFD mesh. Flow results can vary substantially with mesh, hence a thorough grid dependency study was performed to determine the

appropriate grid density required to achieve the most accurate erosion results. Turbulence modeling and the near wall treatment is another major factor that plays a role in accurately capturing the physics of erosion. FLUENT is a commercial finite volume code available from ANSYS Inc. and is the software employed for CFD modeling in this research. Various turbulence models are available in fluent which were explored for this study. An important consideration of turbulent flow modeling is near wall treatment. Different Wall Functions as well as wall integration approaches are explored in this work as well as various parameters in DPM calculations. These include the number of particles, particle restitution coefficients and method of injection into the flow field. Once, satisfactory results are obtained a suitable erosion equation is employed to obtain accurate erosion region and rate results. The predicted erosion regions are then validated qualitatively with available experimental data. Historically, CFD based erosion models adequately identify regions of erosion but are not sufficiently accurate in predicting the extent of erosion. A major effort in this research is focused on improving quantitative erosion rate predictions.

The major milestones in this research are summarized below:

- Fluid flow modeling
    - Grid dependency study
    - Turbulence models exploration
    - Near wall treatment effects
- Discrete Phase Modeling (DPM)
    - Restitution coefficient effect
    - Number of particle
- New erosion models
    - Correlation analysis to identify dependent parameters
    - Evaluation of current models
    - Improved grid specific model
    - New Surface Shear stress model
    - New turbulent kinetic energy model
    - New Artificial Neural Network model

Chapter 2

Literature Review

2.1 Introduction

Erosion damage is seen in almost any industrial application where a solid-fluid multiphase flow occurs. The particles are carried across the streamline due to momentum and they impinge on the walls causing material damage. Erosion can be sometimes limiting factor in design of equipment and might even cause failure. Thus, erosion process has been studied extensively since decades even though CFD based erosion modeling is fairly recent compared to experimental investigations. This chapter discusses pervious work on erosion predictions that can be helpful in understanding and realizing the potential of present work.

2.2 Solid Particle Erosion

Erosion mechanisms vary for brittle and ductile materials. Material is removed from surfaces differently in brittle and ductile materials due to material and surface properties like ductile strength, shear strength, etc. A significant amount of research has been conducted investigating the

mechanisms of the erosion in ductile and brittle materials some of these are presented below.

2.2.1 Erosion in Brittle Materials

Erosion in brittle materials is believed to occur as a result of crack formation. Cracks are formed on the material when particles collide on the surface. These cracks continue to grow as the impact load increases. Plastic defragmentation along the fracture occurs when impact load exceeds a defined level that is dependent on the hardness of the material. This phenomenon is discussed by Levy (1995) in detail. Figure 1, taken from Levy's book, shows how stress fields can develop inwards from the plastically deformed crater produced by the initial particle impact.

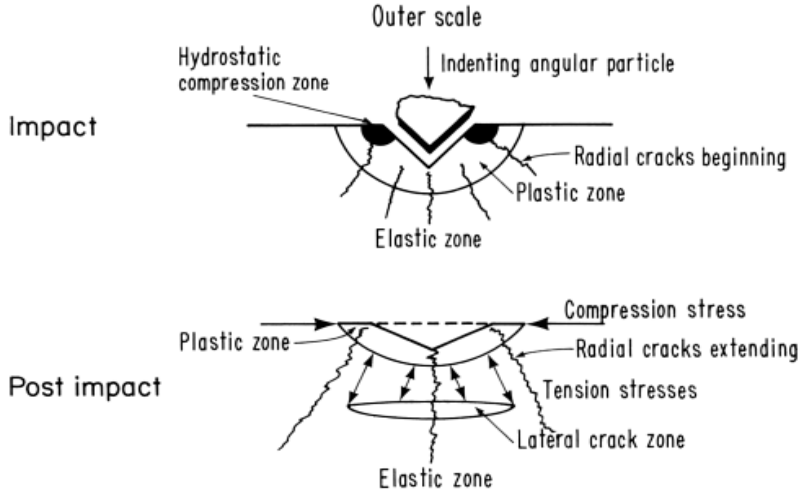

Figure 1 Schematics of stress fields and crack orientation under particle impact area (Levy, 1995)

Planer cracks are formed along the interface when the area is unloaded after particle rebounds from the surface. A network of cracks is formed by material near the surface in contact. These pieces can are then removed by particle impact thereafter. A.G. Evans, M.E. Gulden and M. Rosenblatt published a paper on impact damages in brittle materials (1978). Crack zones are clearly observed in ZnS material impacted by glass using optical reflected light micrographs as shown in Figure 2 below.

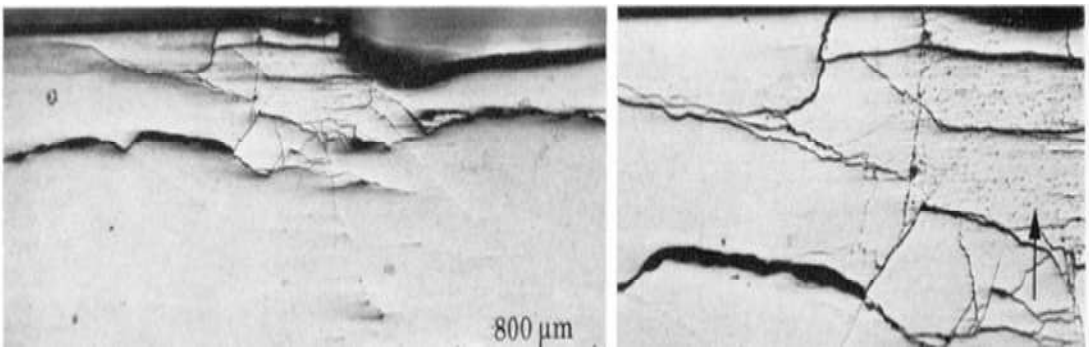

Figure 2 The extent of radial and lateral cracks in ZnS material impacted by glass projectiles (Evans, et.al. 1978)

2.2.2 Erosion in Ductile Materials

Finnie (1960, 1972), JGA Bitters (1963), Hutchings and Winter (1974) and Hockey et.al (1977) conducted some of the early work focused on understanding erosion mechanisms. An analytical erosion model that predicts erosion in ductile materials was presented by Finnie(1960). He later published more detailed paper on erosion phenomenon in ductile

materials in 1972. The model presented my Finnie was based on the assumption that the erosion mechanism is a process of micro-cutting in which the surface material is removed in form of cuttings. Particles striking the surface at low impact angles form a crater. Material is then continually removed by further particle impacts. The inherent drawback of Finnie's cutting theory model is that it neglects the effect of particles hitting the surface at right angles. This was accounted for by Finnie, (Finnie, 1960) who made modifications to his theory indicating that particles impacting a surface at larger angels will result in the surface material being piled up. This raised material is then removed by further particle impacts. J.G.A. Bitters (1963) also presents an erosion model based on two different mechanisms, repeated deformation and cutting wear, rather than just micro-cutting.

The model based on micro-cutting phenomenon was found to be inaccurate. Experiments were conducted using scanning electron microscope to understand the erosion phenomenon in ductile materials (Hutchings, 1974) which led to observation of physical phenomenon occurring on the surface of materials. A theoretical analysis of erosion of metals by spheres at normal incidence was presented by Hutchings (1981). The new model employed the criterion of critical plastic strain to determine when material will be removed.

A two stage mechanism of erosion is proposed by G.P, Tilly (1973). The first stage is when impacting particles strike the surface and produce an indentation and may remove a chip of metal. The second stage occurs when subsequent The fragments in the hole left by chip of metal break up and fragments are projected radially from the primary site (Tilly, 1973). A platelet mechanism of erosion in ductile materials was presented by R. Bellman and A.V. Levy(1981). They suggested that erosion occurs by generation and loss of platelet like pieces of surface material. The impacting particles make shallow craters which then form platelets from the deformed surface. These platelets are forged, strain hardened, into the distressed condition which makes them vulnerable to being knocked off the surface by further particle impacts. Sequence of erosion by platelet mechanism is presented in Figure 3. Adiabatic shear heating occurs to the immediate surface region of the impact. A work-hardened zone forms beneath the surface in the immediate region of impact during this platelet formation. Platelets continue to form by subsequent particle impacts until they are eventually knocked free and removed. This mechanism explains low initial erosion rate compared to steady-state erosion rate (Levy, 1995).

Various other mechanisms for solid particle erosion can be found in the literature. Target melting (Smeltzer et al., 1970 and Hutchings, 1979), subsurface cracking (Sargent, 1982), delamination wear (Jahanmir,1980)

and ploughing (Chase et al., 1992) are some of the more prominent theories available in literature. It is out of the scope of this work to discuss in details each one of them.

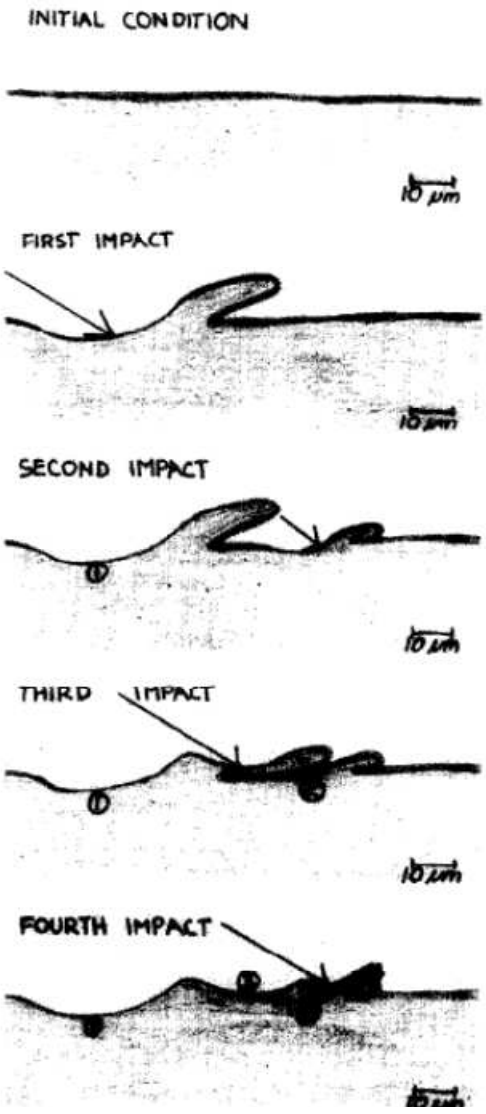

Figure 3 Proposed sequence of erosion of copper-plated steel specimen (Levy,1986)

2.3 Factors Affecting Erosion

More than 100 different erosion models have been proposed by different researchers over the past few decades. Based on these studies it was determined that the three most important factors that govern erosion are: 1) Velocity of the particles 2) Angle of impact of these particles and 3) Type of material being eroded. Particle density plays a very important role in erosion rate. As the density increases so does the erosion rate and significant changes can occur to the distribution of the erosion coefficient with respect to impact angle. Erosion of the down-hole tools used in the oil and gas industry is primarily caused by solid particle concentration in drilling fluids, fluid and particle velocities and densities, size and shape of particles, angle of impingement, hardness and fracture toughness of the impacted surface. Due to the multitude of variables involved in the erosion phenomena, predicting erosion rate is difficult. This section presents work done focused on some of the main factors affecting erosion process.

2.3.1 Particle Impact Velocity

Almost all the researchers since early studies of erosion agree that particle velocity is the most important factor affecting erosion. Each one of

them has concluded that erosion rate (ER) is proportional to particle impact velocity raised to some exponent.

$$ER = V_p^n$$

Various investigators have proposed different values for the exponent n. Finnie's model considers that kinetic energy of the impacting particles determines its ability to cause erosion (Finnie, 1958,1960 and proposed the value of n as 2. Smeltzer et al. (1970) and Burnett et al. (1995) curve fitted the experimental data and proposed values of n varying from -0.3 to 4.5. The aerodynamic effects in the erosion process were studied by Laitone (1979) and he suggested that change in local fluid velocities could affect the erosion and a better fit was achieved with higher n values up to 4. It is important to note that most of the experimental studies considered only fluid velocity rather than actual particle impact velocity, assuming the particles exactly followed the flow.

A more recent model proposed by Oka et al. (2005a, 2005b), considers the exponent as a function of hardness of the eroded material which then is not a fixed number. There are various mechanisms causing erosion and exact details of which are not yet clear but most of the experimental evidence suggests that the velocity exponent, n, varies from

2.0 to 3.0 for most applications. It will be assumed in this study that, 2.5 should be a good estimate for velocity exponent n.

2.3.2 Particle Impact Angle

The angle at which a particle impinges on the surface is critical in determining erosion. The effect of angle of impact has been studied by numerous researchers including Finnie et al. (1992) , Oka et al. (1997) and Sheldon (1970) . Typical curve for normalized erosion rate as a function of impact angle for various materials is shown in Figure 4.

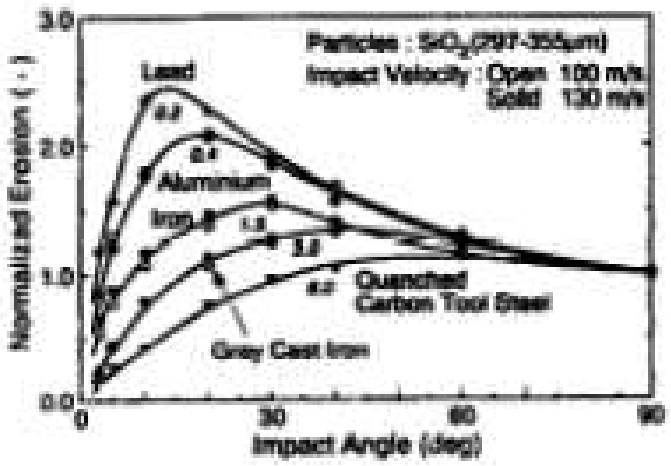

Figure 4 Normalized erosion rates at impact velocities 100 m/s and 130 m/s for five metallic materials (Oka et al., 1997)

Cutting action and platelet formation are observed to be more prevalent mechanisms at lower impact angles for ductile materials

whereas the repeated plastic deformation is considered dominant erosion mechanism in brittle materials. Both of these can be identified from the erosion vs. impact angle graph in Figure 5

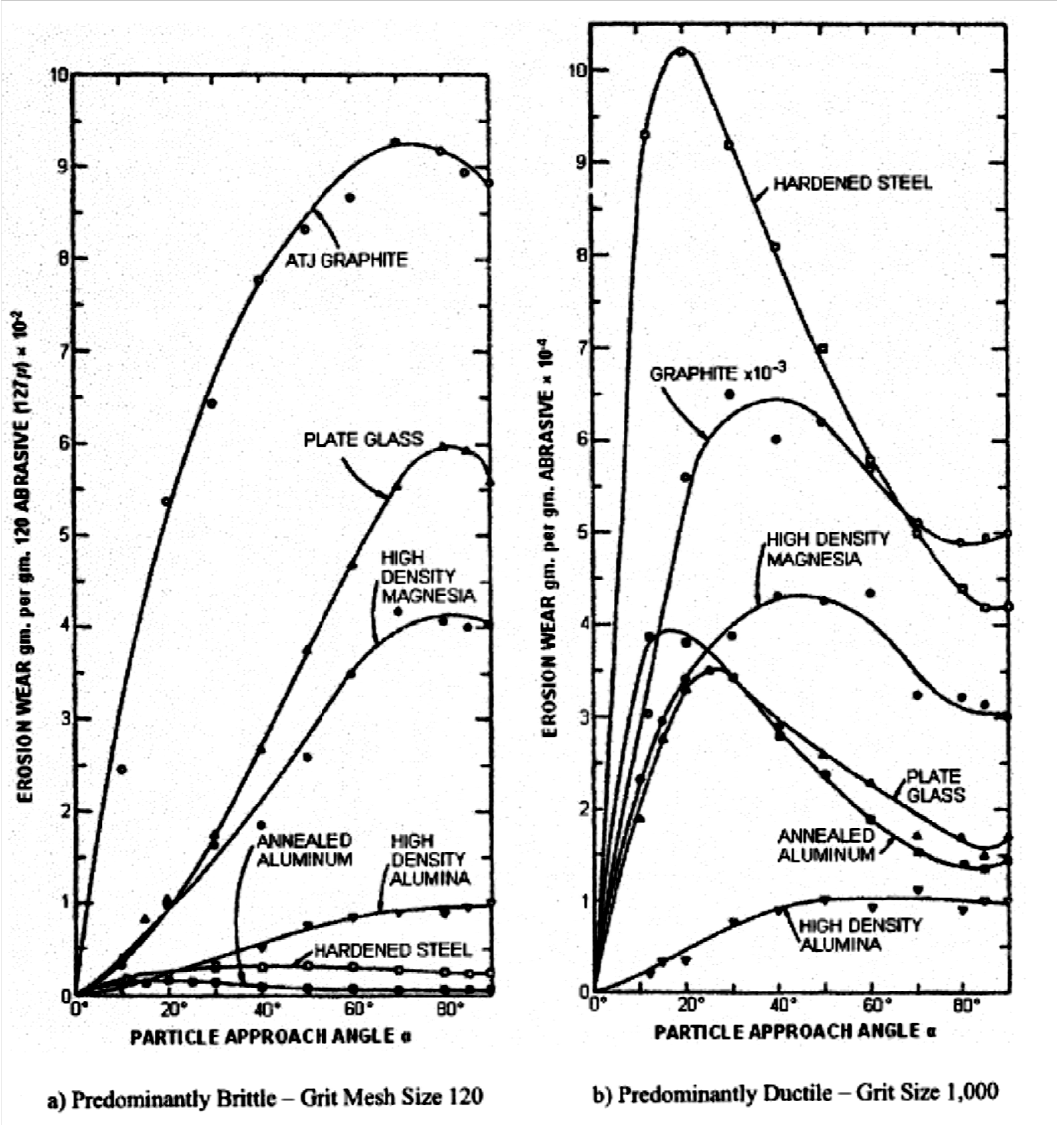

Figure 5 Erosion versus Particle Impact angle for various materials at particle velocity of 500fps (Sheldon,1970)

Although, a considerable amount of research has been done to predict impact angle dependency of erosion rate, no single function for particle impact angle that satisfies all conditions has been identified.

2.3.3 Properties of Particles

Erosion occurs in a variety of applications as borne out by numerous investigations. The particles in each of these applications have different hardness, size, shape etc. This variation in particle properties also has a significant effect on erosion rate.

Numerous researches have conducted investigations into the effect of particle shape and size on erosion rate which ultimately present different parameters to account for these effects. Oka et al. (2005a, 2005b) published a model which incorporated different constants for different shape of particles. The University of Tulsa's erosion –corrosion research center's model (McLaury et at., 1997, 1998, 1999, Ahlert, 1994), incorporates shape factors for particles varying from 1.0 for sharp angular particles to 0.53 for semi-rounded particles and 0.2 for round particles. Salik et al., (1981) were amongst the first to suggest that angular particles, crushed glass in this case, cause much more erosion than rounded particles. Levy et al., (1983) concluded that angular particles can cause

four times more erosion as compared to rounded particles under the same conditions. Cousens and Hutchings (1983) found out that the shape of particles not only affects erosion rate but also the impact angle at which maximum erosion occurs. Bahadur and Badruddin (1990) presented an extensive study of effect of shape and size of particle on erosion. The behavior of erosion was analyzed considering the effect of rake angle in ploughing and micro-cutting. They found out that it is possible to explain the variation in erosion behavior with change in shape factors in terms of relative ploughing and micro-cutting contribution to total erosion.

Also, the erosion rate increases with increased particle size for SiC and Al2O3 particles when impinging on maraging steel up to an asyomptotic value dependent on the size (Figure 6)

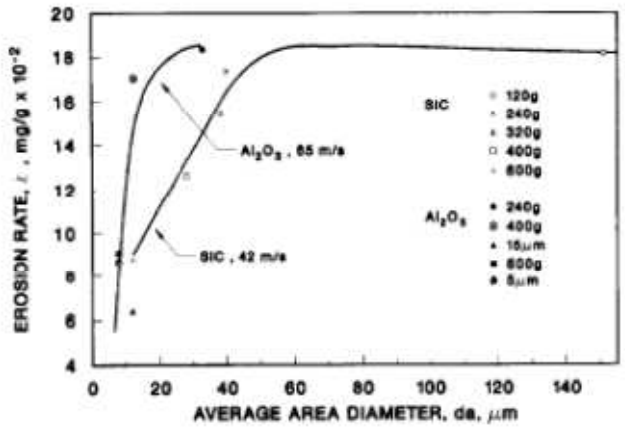

Figure 6 Variation of erosion rate of 18Ni(250) marging steel with average area diameters of SiC and alumina particles (Bahadur and Badruddin , 1990)

Tilly (1973) proposed a model where the erosion rate is a function of particle size. In his study, the measured erosion rates closely matched the experimental results.

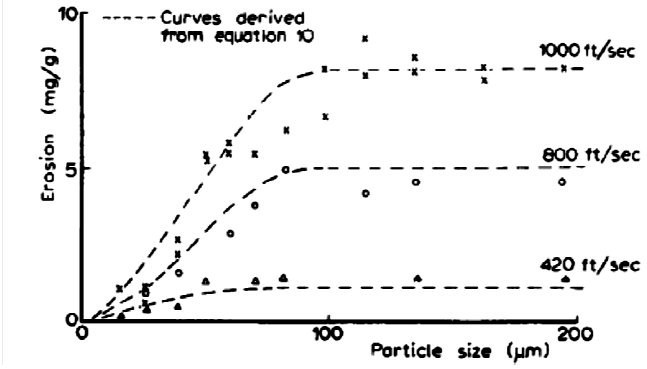

Figure 7 Estimated and experimental data for different particle sizes and velocities (Tilly, 1973)

Oka et al. (2005a, 2005b) also included a particle size term in their erosion model. They used an exponential model stating that erosion increased with particle size raised to power 0.19. The significant conclusion to be made is that almost all investigators agree that the rate of erosion due to increases in particle size becomes relatively constant at sizes above around 100 µm.

The effect of particle concentration is also studied by various researchers. Andrews and Horsfield (1983) proposed a shielding mechanism in erosion to explain the effect of particle concentration on erosion rate. It states that, in low particle concentration flow, less number of inter particle collisions occur due to large distance between them. Thus, more particles can impact the wall surface. With increase in particle concentration more inter particle collision occur and more particle rebound this contributes in lesser erosion. Turenne et al. (1989,1990), Liebhard and Levy, (1991), Shipway and Hutchings (1994) all investigated the effect of particle concentration. Turenne et al. (1990) varied the sand volume concentration ranging from 0.38% to 8.61 % in the tests and found out that erosion ration decreased following a power law of sand volume concentration.

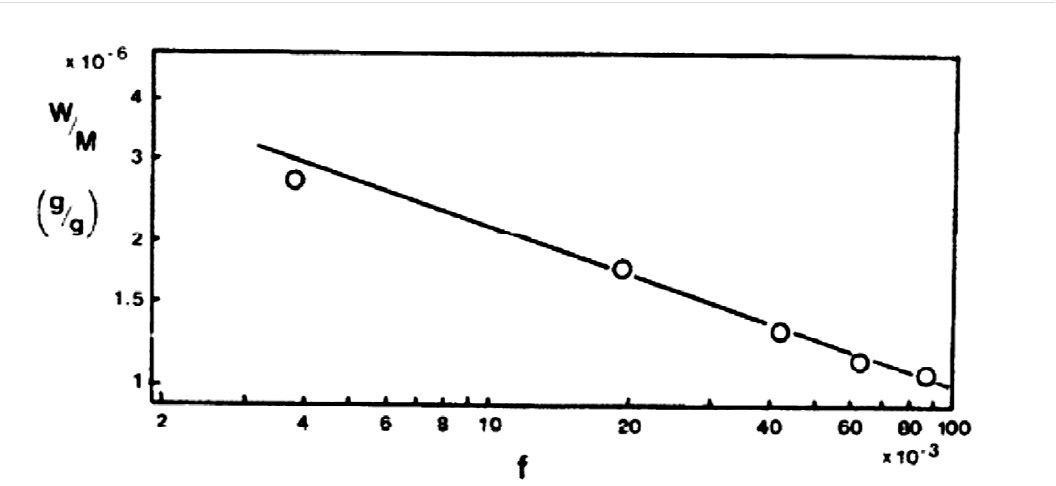

Figure 8 Empirical relation between the erosion rate W/M and the sand volume fraction f for aluminum eroded for 20 min. (Turenne et al., 1990)

2.3.4 Material Properties

Properties of target material affect the erosion rate. Various properties of target material are studied to see its effect on erosion rate. Material hardness is the most widely used property representative of mechanical properties affecting erosion. Finnie et al.(1967) studied the effect of hardness and concluded that higher hardness leads to greater erosion rate. This widely accepted conclusion was slightly changed by Levy's platelet mechanism model (1981). The research suggested that ductility is more important and can give an indication of erosion resistance of material. Erosion is higher for extra hard material. This is due to the fact that ductile materials resist erosion by distributing the kinetic energy of

impacting particles by the plastic deformation of a large region under the surface impact point. Many other properties like thermal properties, strain hardening, etc. have been studied and reported to affect erosion in some way or the other. A complex phenomenon like erosion cannot be successfully characterized by just one material parameter.

2.3.5 Fluid Properties

Fluid flow and its interaction with the particles is a complex phenomenon in itself. Various interactions like heat transfer and momentum transfer occur between fluid and particles. Thus, it is evident that fluid properties like density and viscosity have an effect on particles motion resulting in erosion caused by these particles. With increase in density and viscosity of fluid, drag force acting on the particle increases. In addition this can also be directly related to conclusion of research conducted by Smeltzer et al. (1970), that erosion rate decrease at higher test temperatures. At higher temperatures, density and viscosity of fluid is observed to decrease in most cases. Hence; particles tend to follow streamlines in liquid as compared to gases. The effect of turbulence has been studied by Pourahmadi and Humphry (1983, 1990). Impingements occur in region of high turbulence due to higher momentum transfer to the particles.

Russell et al. (2004) observed during this test with 90o elbows that secondary flow causes major erosion damage on the inner-side of walls rather than outer-side as might be expected. Secondary flow can change the particle trajectories greatly and hence the erosion pattern. Particle concentration at some location can vary drastically as compared to inlet mixture due to flow path and geometries of component. Boundary layer affects the particle motion in near wall regions. This in turn affects the erosion. Clark and Burmeister (1992) proposed a squeeze film model to account for cushioning effect due to fluid boundary layer. A phenomenon of boundary layer filtration in which particles are deflected due to high normal gradients in flow was observed by Clark (1992).

2.4 Erosion Modeling

In the oil and gas industry, the guideline followed for erosive service is, the American Petroleum Institute recommended practice API 14E that suggests a limiting flow velocity (Maximum allowable erosional velocity). The practice states that severe erosion does not occur if the production velocities are maintained below the flow velocity limit, which is calculated considering only the fluid density.

$$V_e = \frac{c}{\sqrt{\rho_m}}$$

Where

V_e= fluid erosional velocity, ft/sec

C = empirical constant

ρ_m= gas/liquid mixture density at flowing pressure and temperature, lb/ft^3

However, as we have seen in the previous section, the mechanism of erosion is very complex and the severity of erosion depends on many factors that are not included in API guidelines. Furthermore these guidelines do not take into consideration the shape of the material being eroded.

As a results, several investigators and scientists have proposed erosion models to replace API 14E. Most of these erosion models can be primarily divided into two types; Theoretical models and Empirical models. While theoretical models can be applied to wide range of applications empirical models are developed for a specific application. It is impossible to discuss in detail each of these models but a few important ones are discussed below.

2.4.1 Theoretical Models

There are several theoretical models available in literature. Three of the commonly available models are listed below:

2.4.1.1 Finnie's Model

Finnie (1958) was amongst the earliest investigator to propose a theoretical model of erosion mechanism. It is based on the assumption that cutting wear is the major mechanism leading to erosion by solid particles. It has been improved constantly and equation loss for volume of material lost was presented by Finnie and McFadden (1978) :

$$V = \frac{cMU^2}{4P(1 + mr^2/I)}\left[cos^2 \propto -\left(\frac{x_0'}{U}\right)^2\right]$$

Where, V = Volume removed from surface

M = mass of eroding particle

m = mass of individual particle

I = moment of inertia of particle about its center of gravity

r = average particle radius

α = impact angle

U = particle impact velocity

P = horizontal component of flow stress

c = fraction of particles cutting in an idealized manner

$x_o^{'}$= horizontal velocity of the tip of the particle after cutting

The major drawback of this model is that it predicts no erosion at right angle and erosion is overestimated for shallow impact angles and under estimated for large impact angles.

2.4.1.2 Neilson and Gilchrist Model

Neilson and Gilchrist (1968) suggested a model that accounts for erosion due to both deformation wear as well as shearing wear. The eroded mass of the material is given by:

$$\alpha \leq \alpha_0 : \mathrm{W} = \frac{\mathrm{M}}{2}\left(\frac{\mathrm{V}^2 \times \cos^2\alpha \times \sin \mathrm{n}\alpha}{\varphi} + \frac{(\mathrm{V}\sin\alpha - \mathrm{K})^2}{\varepsilon}\right)$$

$$\alpha \geq \alpha_0 : W = \frac{M}{2}\left(\frac{V^2 \times cos^2\alpha}{\varphi} + \frac{(V\,sin\,\alpha - K)^2}{\varepsilon}\right)$$

Where

M = mass of eroded particles

W = eroded mass produced by M at impact angle of α and velocity of V.

K = velocity component normal to the surface below which no erosion takes place in certain hard materials.

α = angle of attack at which the residual parallel component of particle velocity is zero.

α_0 = angle of attack at which the residual parallel component of particle velocity is zero. Therefore at this angle (αo) both the above erosion equations predict the same erosion.

The erosion rate is obtained by dividing the eroded mass of the material (W) by the mass of the erosive particles (M).

2.4.1.3 ANSYS Fluent Standard Erosion Model

It is important to mention that ANSYS Fluent also has an inbuilt erosion model.(ANSYS Fluent , User Manual, 2006, Theory guide ,2009). The erosion rate is defined by ANSYS FLUENT's standard erosion model as a product of the mass flux, and specified functions for the particle diameter, impact angle, and velocity exponent. It is given as

$$R_{erosion} = \sum_{p=1}^{N\ Particles} \frac{m_p\, C(d_p)\, f(\alpha) v^{b(v)}}{A_{face}}$$

Where

$C(d_p)$ = function of particle diameter

α = impact angle of the particle path with the wall face

$f(\alpha)$ = function of impact angle

υ = relative particle velocity

$b(\upsilon)$ = function of relative particle velocity

A_{face} = area of the cell face at the wall

Default values are $C = 1.8 \times 10^{-9}$, f =1, and b=0.

As with any model there are certain advantages and disadvantages with theoretical models. Theoretical models can be readily tuned to fit a particular application. For example, in FLUENT the parameters such as impact angle function and diameter function can be tuned to match the test results. But the disadvantage is that tuning may provide a perfect match for a particular variation of the application but they may not yield good results for other variations of the application.

2.4.2 Empirical Models

Several empirical models have been developed by researchers for specific applications. These models are generally developed through a combination of experimentation and modeling. Empirical models can be incorporated into FLUENT with the help of a User Defined Function (UDF) or a Custom Field Function (CFF).

2.4.2.1McLaury et al. Erosion model

The McLaury (1996) and Ahlert (1994) developed erosion model at the Erosion Corrosion Research Center (E/CRC), University of Tulsa, Oklahoma. The primary application areas for this model are chokes, pipe elbows, and oil & gas production equipment.

$$ER = AF_s V^n f(\alpha)$$

$$f(\alpha) = a\alpha^2 + b\alpha \quad \alpha \leq a$$

$$f(\alpha) = x\cos^2(\alpha)\sin(\alpha) + y\sin^2(\alpha) + z \quad \alpha > a$$

Where

a, b, c, w, x, y, z = constants for the impact angle function

A = 1559 $HB^{-0.59}$ x $^{10-9}$, wher HB is Brinell Hardness

n = velocity exponent

2.4.2.2TULSA EROSION Model

The Tulsa erosion model was also developed at the Erosion Corrosion Research Center (E/CRC), University of Oklahoma, Tulsa. It can also be used for Erosion prediction in chokes, pipe elbows, and oil & gas production equipment.

$$ER = \frac{AF_s F_p V^n m}{D_p^2 B^b}$$

Where

A = constant

F_s = sand sharpness correction factor

F_p = penetration factor for wall material

B = brinell hardness of the material

n = velocity exponent

D_p = pipe diameter

b = hardness exponent

2.4.2.3 Salama and Venkatesh Erosion Model

The Salama and Venkatesh model is primarily used for erosion prediction in Pipe flows and elbows. (1983)

$$ER = \frac{S_k V^2 m}{d_{pipe}^2}$$

Where

S_k = geometry dependent constant

= 0.038 for short radius elbows

= 0.019 for ells and tees

d_{pipe} = diameter of the pipe

m = sand flow rate

V = particle impact velocity

Similar to the theoretical model, the empirical models also have some of the advantages and disadvantages. The empirical models are very accurate for the application they are developed for. Once the model is developed, it can be used for different variations of the application. The biggest disadvantage with these models though, is that the constants in an empirical model are generally fixed for the application they were developed and cannot be tuned further.

2.4.2.4Oka et al. model

Oka et al. presented an erosion model considering impact angle dependence (1997). The model is as follows:

$$E(\alpha) = g(\alpha)E_{90}$$

$$g(\alpha) = (sin\theta)^{n_1}(1 + Hv(1 - sin\theta))^{n_2},$$

$$E_{90} = K(Hv)^{k_1}\left(\frac{V_p}{V}\right)^{k_2}\left(\frac{D_p}{D}\right)^{k_3}$$

Where:

$$n_1 = s_1(Hv)^{q_1}$$

$$n_2 = s_2(Hv)^{q_2}$$

$$k_2 = 2.3(Hv)^{0.038}$$

K, k_1,k_2,k_3,s_1,s_2,q_1, q_2,n_1 and n_2 are constants and exponent values for particles material and targeted material. (Oka et al, 1997, Oka and Yoshida 2005, Oka et al. 2005)

The equation for g (α) is a combination of two terms, the first term represents repeated plastic deformation and the second term represents cutting wear. Plastic deformation term represents brittle characteristics and increases with particle impact angle. Cutting wear term has biggest value when particle impact angle is zero and is more effective for smaller angles. H*v* term represents Vicker's hardness.

Chapter 3

CFD Based Erosion Modeling

3.1 Introduction

Very complex tools with complicated geometries are involved in industrial applications where erosion damage can occur. In oil and gas industry, it is most of the time impossible to simulate the exact working conditions on a laboratory scale. Computational Fluid Dynamics (CFD) is a great tool that can be utilized to analyze flow in complicated scenarios and very complex geometry. With the advance in computing science, very large scale of problems can be solved and simulated using CFD within very little time. Various CFD tools have been developed for simulate complex multiphysics problem in oil and gas industry in past decade. Many complex commercial codes have also been developed to cater to oil and gas industry problems. CFD analysis not only saves a lot of time and money but also is more environmentally friendly in most of the cases.

CFD has been widely used for erosion prediction since early 1990's. University of Tulsa, Oklahoma has been the hub for most of CFD-based erosion prediction research since past two decades. McLaury (,1993,1996), was amongst the first to propose a CFD-based erosion prediction procedure. Edwards (2000), Chen et al. (1998.2004), Zhang

(2006), all have contributed in advancing capabilities of CFD-based erosion prediction procedure and models. Zhang et al. also recently presented procedures and improved guidelines for using commercial CFd code for erosion prediction (2009).

Erosion modeling using CFD consists of three main parts: a flow model, a particle tracking model and an erosion model.

3.2 Flow Modeling

Flow modeling is the first step in CFD-based erosion prediction. It is critical as flow structure, velocity and turbulence greatly affect the particle motion and behavior in the flow. As it is the first step, any error or inclusion of non-physical behavior can magnify in the further steps. The flow field predicted is the input for particle tracking used to determine particle trajectories. Fluent is a finite volume code that solved Navier-Stokes equations to model motion of fluid. ANSYS meshing was utilized to create computational mech. Information about boundary conditions, turbulence models, and numerical schemes to follow are then selected. Finally, flow solver gives the flow filed information.

3.2.1 Conservation Equation

Following are the conservation equation.

$$Mass: \quad \frac{\partial \rho}{\partial t} + div(\rho\, \mathbf{u}) = 0$$

$$x - momentum: \quad \frac{\partial(\rho u)}{\partial t} + div(\rho u \mathbf{u}) = -\frac{\partial p}{\partial x} + div(\mu\ grad\ u) + S_{Mx}$$

$$y - momentum: \quad \frac{\partial(\rho v)}{\partial t} + div(\rho v \mathbf{u}) = -\frac{\partial p}{\partial y} + div(\mu\ grad\ v) + S_{My}$$

$$z - momentum: \quad \frac{\partial(\rho w)}{\partial t} + div(\rho w \mathbf{u}) = -\frac{\partial p}{\partial z} + div(\mu\ grad\ w) + S_{Mz}$$

Where, $\vec{V}$ = Velocity vector

ρ = density

u,v,w = velocity components in x,y and z directions

p = pressure

μ = dynamic viscosity

S_M = other bodily forces

The key step in finite volume is to integrate the differential form of equation. The general integral form of conservation equations for mass, momentum and energy transport that are solved by the fluent to calculate the flow pattern and associated scalar fields is:

$$\frac{\partial}{\partial t}\left(\int_{CV} \rho\varphi \, dV\right) + \int_{A} \mathbf{n}\cdot(\rho\varphi\,\mathbf{u})\, dA = \int_{A} \mathbf{n}\cdot(\Gamma \, grad\, \varphi)\, dA + \int_{CV} S_{\varphi}\, dV$$

Where, Φ = 1 for continuity

= u for x-momentum

= v for y-momentum

= w for z- momentum

= h for energy

S = is corresponding source term

3.2.2Turbulence Modeling

Fluent has several turbulence models such as standard k- epsilon , Renormalization-group (RNG) k- epsilon, realizable k- epsilon, standard k-omega , shear-stress transport (SST) k-omega, Reynolds stress model (RSM) and large eddy simulation (LES) model. There is a trade-off between accuracy and computational cost for each of these models as shown in Figure 9 .

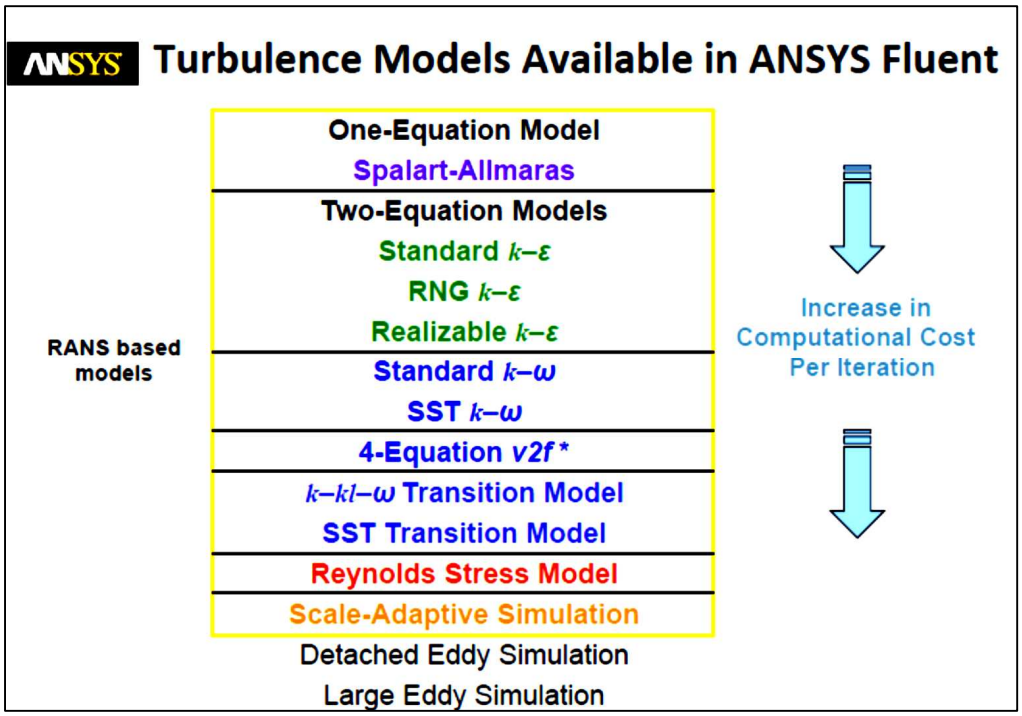

Figure 9 Fluent Turbulence models overview (ANSYS Fluent documentation)

Standard k- □ model and realizable k- □ models has proved to give good results for various applications and offer good balance between accuracy and computational effort. (ANSYS Fluent, User manual, 2006). Hence, these two models were investigated. The k- □ model focuses on mechanism that affects the turbulent kinetic energy k.

All the K-□ models have similar transport equations for k and □. The major differences are:

- The way in which turbulent viscosity is calculated

- Turbulent Prandtl numbers governing the turbulent diffusion k and □
- The generation and destruction terms in □ equation

3.2.2.1Standard k-epsilon Model

Standard k-epsilon model is a robust model which provides reasonable accuracy for wide range of flows. Hence, it becomes the first choice for any industrial problem. It does suffer with the weakness of over diffusivity and is weak at predicting jet spreading rates accurately. It is a semi empirical model. The model of transport equation for *k* is derived from exact equations mathematically whereas that for epsilon is obtained from physical reasoning. It assumes that the effects of molecular viscosity are negligible and hence is valid only for a fully turbulent flow.

Turbulent kinetic energy transport equation:

$$\underbrace{\rho U_i \frac{\partial k}{\partial x_i}}_{Convection} = \underbrace{\mu_t \left(\frac{\partial U_j}{\partial x_i} + \frac{\partial U_i}{\partial x_j} \right) \frac{\partial U_j}{\partial x_i}}_{Generation} + \underbrace{\frac{\partial}{\partial x_i} \left\{ (\mu_t / \sigma_k) \frac{\partial k}{\partial x_i} \right\}}_{Diffusion} - \underbrace{\rho \varepsilon}_{Destruction}$$

Dissipation rate transport equation:

$$\underbrace{\rho U_i \frac{\partial \varepsilon}{\partial x_i}}_{Convection} = \underbrace{C_{1\varepsilon}\left(\frac{\varepsilon}{k}\right)\mu_t\left(\frac{\partial U_j}{\partial x_i}+\frac{\partial U_i}{\partial x_j}\right)\frac{\partial U_j}{\partial x_i}}_{Generation} + \underbrace{\frac{\partial}{\partial x_i}\left\{(\mu_t/\sigma_\varepsilon)\frac{\partial \varepsilon}{\partial x_i}\right\}}_{Diffusion} - \underbrace{C_{2\varepsilon}\rho\left(\frac{\varepsilon^2}{k}\right)}_{Destruction}$$

Where $\sigma_{k,}\sigma_\varepsilon, C_{1\varepsilon}, C_{2\varepsilon}$ are empirical constants

3.2.2.2Realizable k- epsilon Model

The two most important distinctions of this model from standard model are:

- It contains alternative formulation for turbulent viscosity

$$\mu_t \equiv \rho C_\mu \frac{k^2}{\varepsilon}$$

  Where

$$C_\mu = \frac{1}{A_o + A_s \frac{U^* k}{\varepsilon}}$$ Is a variable

- (A_0, A_s, and U* are functions of velocity gradients)
- Ensures positivity of normal stresses; $\overline{u_i^2} \geq 0$
- Ensures Schwarz's inequality; $(\overline{u_i u_j})^2 \leq \overline{u_i^2}\ \overline{u_j^2}$
- The □ transport equation is derived from an exact equation for the transport of mean-square vorticity fluctuations.

The term “realizable” is attached to the fact that this model satisfies constraints on the Reynolds stresses, and is consistent with physics of turbulent flows. The limitation of this model is that it produces non-physical turbulent viscosities in situation when domain contains both rotating and stationary fluid zones. But that not being the case in this analysis, this model is as robust as any other for our analysis. For our analysis and sensitivity study, Realizable k- epsilon model has proved to capture the physics with best accuracy and hence this model is finalized for further studies. It is thus important here to describe the mathematical formulation of this turbulence model. It is also a 2 equation model.

Turbulent kinetic energy transport equation is same as standard model.

Dissipation rate transport equation:

$$\rho\frac{D\varepsilon}{Dt}=\underbrace{\frac{\partial}{\partial x_j}\left[\left(\mu+\frac{\mu_t}{\sigma_\varepsilon}\right)\frac{\partial\varepsilon}{\partial x_j}\right]}_{Diffusion}+\underbrace{\rho c_1 S\varepsilon}_{Generation}-\underbrace{\rho c_2\frac{\varepsilon^2}{k+\sqrt{\nu\varepsilon}}}_{Destruction}+\underbrace{c_{1\varepsilon}\frac{\varepsilon}{k}c_{3\varepsilon}G_b}_{Boyancy}$$

3.2.3Wall Treatment

Walls are the main source of vortices and turbulence. The presence of walls gives rise to turbulent momentum and thermal boundary layer. An

accurate near wall treatment can save a lot of computational time as a very fine mesh to resolve the steep velocity profile is not possible many times. Since the equations cannot be integrated down to the wall, some special near wall treatments are necessary. The following figure shows subdivision of near wall regions namely the viscous laminar layer, buffer layer and the fully turbulent layer.

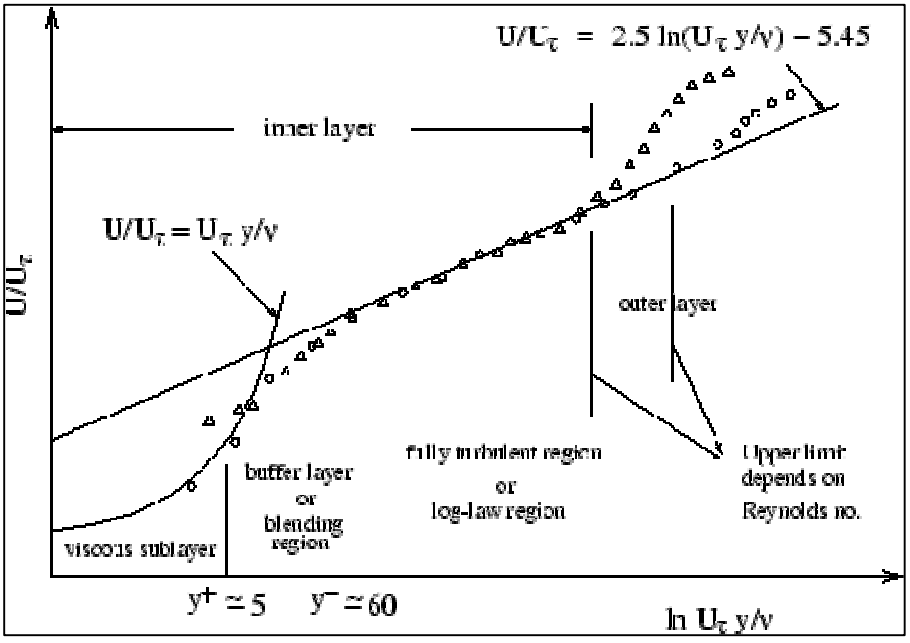

Figure 10 Subdivisions of the near wall region (Fluent User's Guide)

Many basic turbulence models like k-ε models, RSM and LES model are valid only in flow region far from walls. Other models like Spalart-Allamaras and k-ω are valid in viscous sub layers but that requires much higher density of grid in laminar region and hence is computationally

much more expensive. Fluent gives us two major options to model near wall region. First is wall functions approach which uses semi-empirical formulas called 'wall functions' to bridge the viscosity affected regions between wall and fully developed turbulent region. The second is near wall modeling approach or popularly called wall integration approach. In this approach the boundary layer is sufficiently resolved with a mesh all the way to the wall. Figure 11 shows pictorial comparison between them.

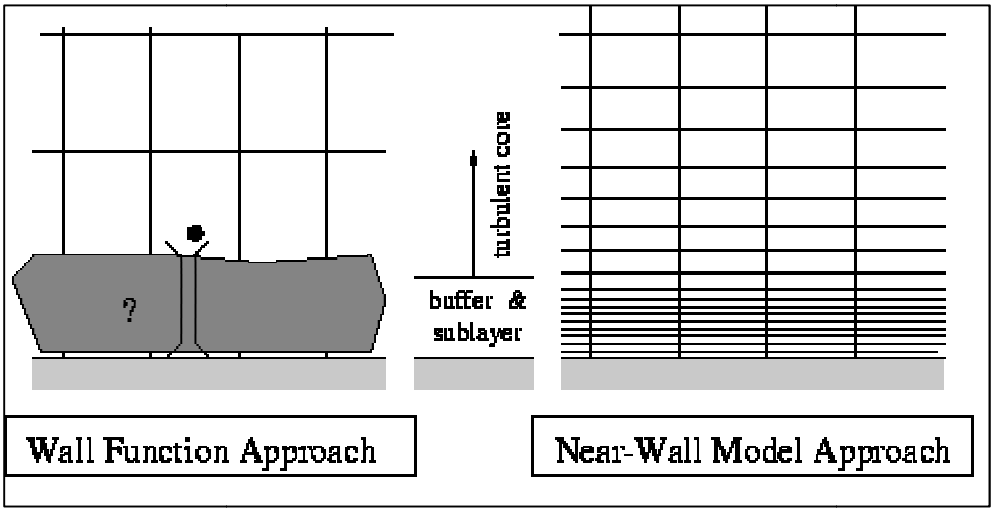

Figure 11 Wall functions (Left) and Wall integration approach (Right) for near wall modeling (Fluent User Guide)

3.2.3.1Standard Wall Function

Standard function options are specifically designed for high Re flows. The viscosity affected regions near the wall are not resolved. Also a coarse mesh can be used near wall with these options. The standard wall

function becomes less reliable when flow departs from the conditions assumed. E.g. local equilibrium assumption may not be valid in strong pressure gradients or large curvatures. Small gaps are also present in their formulation.

3.2.3.2Scalable Wall Functions

These are much similar to standard wall function but it puts a limiter on the y* calculations. i.e to say that the wall surface collides with the edge of the viscous layer if the first grid point is too close. Thus it also helps to reduce dependency on y + values when wall functions are employed. Again this does require adequate boundary layer resolution.

3.2.3.3Enhanced Wall Treatment

This model combines enhanced wall functions and the two-layer model, it has been proved efficient for low Re flows with complex near wall phenomena. It requires a really fine mesh for resolving the near wall region. In enhanced wall function approach, the momentum boundary layer condition is based on blended law- of –the-wall and similar laws are applied for energy as well. This incorporated the effect of pressure gradient and thermal effects. The two layer model is used to determine the near-wall epsilon field. The domain is divided into viscosity-affected region and turbulent core region based on turbulent Reynolds number. Also , this is dynamic zoning and adapts to the solution.

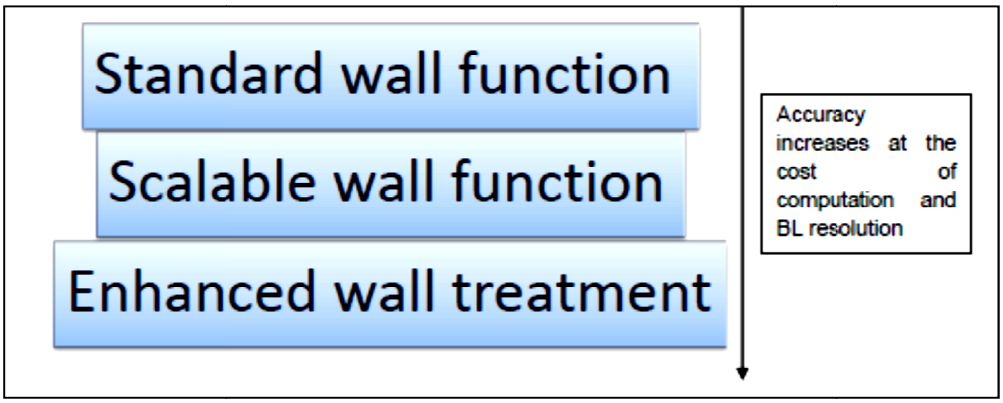

Figure 12 Near wall treatment trade offs

The discussion on the mathematics and numerical details of all the models as well as wall treatment is out of scope of this document and FLUENT Theory Manual can be referred to for better and deeper understanding of turbulence modeling in fluent.

3.3Discrete Phase Modeling (DPM)

Particle tracking is the second major step in CFD-based erosion modeling. In the Eulerian-Lagrangian approach, after the continuous flow field converges, the discrete phase is solved by tracking a large number of particles. A fundamental assumption of this approach is that the dispersed second phase occupies a low volume fraction (less than 10%). For flow conditions of interest in a drilling operation, the sand concentration is fairly

small so that the effect of sand particles on the carrier fluid is assumed negligible. Thus one-way coupling method, that assumes the presence of solid particles has little or no effect on the flow field, is employed to calculate sand particle trajectories. FLUENT's Discrete Phase Model (DPM) is used to model the sand particle flow and erosion on the tool geometry. FLUENT computes the trajectories of the discrete phase entities using a Lagrangian formulation, by solving the governing equations of particle motion by taking into account the drag force, pressure gradient force, buoyancy force etc. acting on the particles.

Fluent predicts the trajectory of a discrete phase particle (or droplet or bubble) by integrating the force balance on the particle, which is written in a Lagrangian reference frame. This force balance equates the particle inertia with the forces acting on the particle, and can be written as Particle transport equation as presented below.

$$\frac{p}{6}d_p^3\rho_p\frac{\partial\vec{v}_p}{\partial t}=\frac{p}{6}d_p^3\rho_p F_D\left(\vec{v}-\vec{v}_p\right)+\frac{p}{6}d_p^3\rho_p\frac{\vec{g}\left(\rho_p-\rho\right)}{\rho_p}+\vec{F}$$

where,

$$F_D = \frac{18\mu}{\rho_p d_p^2}\frac{C_D \,\mathrm{Re}}{24}$$

$$\mathrm{Re} = \frac{\rho d_p \left|\vec{v}_p - \vec{v}\right|}{\mu}$$

C_D is drag coefficient and that can be calculated by any of the following equations:

$$C_D = \frac{24}{\mathrm{Re}_r}\left[1 + 0.15\,\mathrm{Re}_r^{0.687} + 0.0175\left(1 + 4.25\times 10^4\,\mathrm{Re}_r^{-1.16}\right)^{-1}\right] \quad \text{(a)}$$

$$C_D = a_1 + \frac{a_2}{R_e} + \frac{a_3}{R_e^2} \quad \text{(b)}$$

$$C_D = \frac{24}{\mathrm{Re}_r}\left(1 + b_1\,\mathrm{Re}_r^{b_2}\right) + \frac{b_3\,\mathrm{Re}_r}{b_4 + \mathrm{Re}_r} \quad \text{(c)}$$

Cliff and Gauvin (1971) proposed equation (a) . Equation (b) was proposed by Mosri and Alexander (1972) where a_1 , a_2 , a_3 are constants for spherical particle over large range of Re_r. Haider and Levenspiel (1989) proposed equation (c) where,

b_1 = $\exp(2.3288 - 6.4581\varphi + 2.446\varphi^2)$

b_2 = $0.0964 + 0.5565\varphi$

b_3 = $\exp(4.905 - 13.8944\varphi + 18.4222\varphi^2 - 10.2599\,\varphi^3)$

b_4 = $\exp(1.4618 + 12.2584\varphi - 20.7322\varphi^2 + 15.8855\,\varphi^3)$

and φ is the shape factor defined as

$$\varphi = \frac{s}{S}$$

s is the surface area if a sphere having same volume as the particle and S is the actual surface area of the particle.

Various other forces like pressure gradient, gravity and buoyancy and added mass can be included in the model as well.

Discrete random walk model is applied to account for effect of turbulent eddies on particles. The model assumes that the particles travel through as succession of turbulent eddies that are present in the flow. Each eddi that the particle encounters is characterized by Gaussian distribution random velocity fluctuations and tam time scale called eddy lifetime. This model accounts for the deviation of particle from their trajectories caused by turbulent eddies. A complete details about the theory of random walk model can be studied from Fluent theory guide.(2009). It is important in erosion modeling to include this Discrete random walk model as turbulent can change particle trajectories and this can in turn affect erosion prediction regions and rates.

Particle wall interaction is an important phenomenon that should be accounted for in DPM. The particle's momentum is changed during particle-wall interaction. This change is accounted by restitution coefficients that are ratios of particle velocity components after

impingement to the corresponding component before impingement. Tabakoff and Wakeman (1982) proposed that restitution coefficients e_n and e_t define the amount of momentum that is retained by the particle after the impingement with the boundary, in the direction normal and tangential to the wall. Various other investigators have proposed various values of restitution coefficient. Foder et al. (1998) , Grant and Tabakoff (1974) are prominent amongst others .

3.4Erosion Model

Third and final step in CFD-based erosion modeling is to calculate the erosions. In Fluent, erosion predictions can be made considering empirical relations that can incorporated either by custom field function (CFF) or use defined function (UDF). We will be incorporating the erosion equation as CFF to determine the erosion rate in required units. CFF approach is relatively simple as Fluent allows the users to define a custom function incorporating properties that are already calculated by fluent like velocity or DPM concentration.

Chapter 4

Baker Hughes Erosion Test and Erosion Model

All the analysis done in this research is based on experimental results provided by Baker Hughes. Tests were conducted at Baker Oil Tools for four different flow conditions considering two different flow rate i.e. 50 ft/s and 85.8 ft/s and for two different size of particles i.e. 256 microns and 25 microns.(Russell ,2004) The test was performed on a 90^{o} elbow with 1 inch inner diameter. Inconel 718, Nickel Alloy 825, 25% Cr, Nickel Alloy 925 , and 13% Cr L-80 material elbows were placed in series. The sand concentration was approximately 1% of liquid weight and 0.38 % by volume. (Russell, 2004). Erosion rate was measured at 230 different locations on the elbow. The experimental set up is shown in a schematic below:

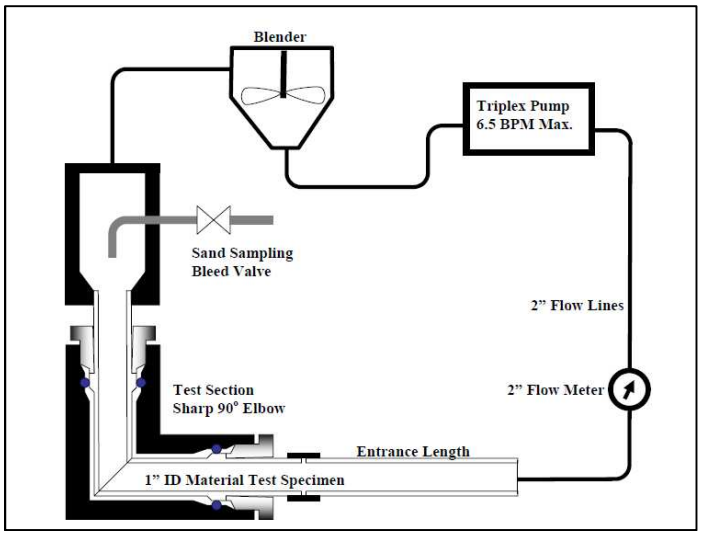

Figure 13 Experimental setup for erosion experiment (Russell,2004)

The details of erosion test fixture (elbow) are given below

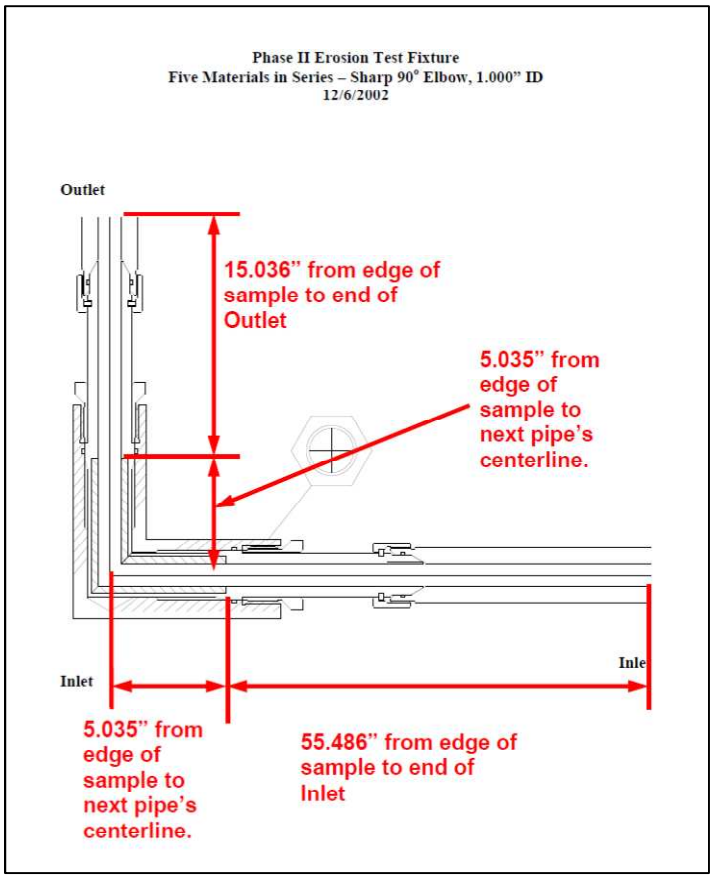

Figure 14 Erosion test fixture

4.1Baker Hughes -ERC Erosion Model

The Baker Hughes-ERC-2003 erosion model was developed at Baker Oil Tools. Ronnie Russell et al. (2004) presented this model that was based on extensive experiments on a 90 ^{o} elbow. Series of erosion tests were performed with different materials and under different flow conditions and sand concentrations. A predictive model was then created

based on the obtained results. The model is primarily used for straight line flows.

$$\mathrm{E} = \mathrm{K}\,\mathrm{C}\,\mathrm{V}^{\mathrm{n}}$$

Where

K = empirical constant

C = sand concentration

V = velocity

n = velocity exponent

The Baker Hughes-ERC-2008 model is an improvement over the Baker Hughes-ERC-2003 model and is an exponential fit model. This model is more accurate when compared to the Baker Hughes -ERC-2003 model for low flow velocities.

$$E = K\ C\ e^{(R\ V)}$$

K = empirical constant

C = sand concentration

V = velocity

n = velocity exponent

R = proportionality constant on semi-log scale

Exponential fit is the major strength of the model. However, erosion rates have been predicted to be affected by impingement angle

significantly and this model has an inherent weakness of not considering the impingement angle function for erosion prediction.

The empirical constants were determined through parametric trial and error method. Hence, it provides further scope to improve the model. Throughout this study, Baker Hughes-ERC-2008 erosion model is further investigated and improved.

Chapter 5

Data Analysis

Various data analysis techniques like regression, exploratory data analysis and artificial neural networks are implemented in this work. Although, complete discussion of various data analysis techniques is out of the scope of this thesis, details about the methods and algorithms implemented are presented in this chapter. MATLAB was used for all data analysis performed during this work.

5.1 Correlation Analysis

The core to data analysis for erosion modeling is to establish relationship or association between various independent parameters to erosion (which is the dependent parameter in each case). The two variables are said to be associated if the behavior of one affects the behavior of other. Correlation coefficients are measures of association. They assign a numerical value to the degree of association or strength of relationship between two variables (Gibbons, 1993). Several correlation coefficients are proposed to measure degree of correlation. Three major ones that are analyzed in this work are described below. A general

interpretation based on the values of these coefficients (ranging from -1 to 1) is as follows;

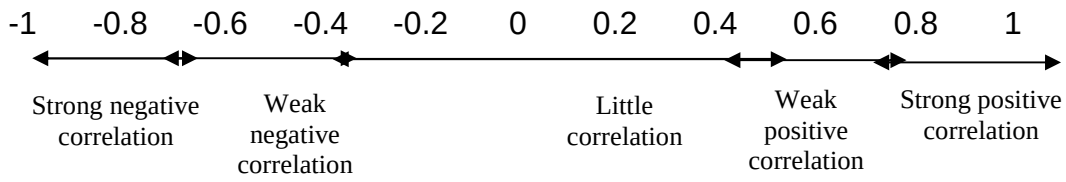

5.1.1Pearson Correlation Coefficient

This is arguably the most widely used correlation measure. It was developed by Karl Pearson in early 1900's (Pearson K., 1901) based on idea proposed by Francis Galton. (Stingler S.M., 1989) It has been widely used since then. It is many a times referred to as Pearson product-moment correlation coefficient and represented by '*r*'. It is a measure of linear correlation between two variables. It is important to mention here that linear correlation may exist even if variables having a nonlinear relation to one another. (David S., 2003) it varies from -1 to 1 where 0 means no correlation, 1 means total positive linear correlation and -1 means total negative linear correlation. For a paired x and y values in a sample, Pearson correlation coefficient *r* is given by:

$$r = \frac{\text{degree to which X and Y vary togather}}{\text{degree to which X and Y vary separaterly}}$$

$$r = \frac{\text{covariance of X and Y}}{\text{variance of X and Y}}$$

$$r = \frac{\sum (x - \bar{X})(y - \bar{Y})}{\sqrt{\left[\sum (x - \bar{X})^2\right]\left[\sum (y - \bar{Y})^2\right]}}$$

Nonlinearity and outliners are major factor that affect the value of *r* .

5.1.2Spearman's Rank Correlation Coefficient –Rho

Spearman's rank coefficient is a nonparametric measure of dependence. As most of the variables encountered in this work do not have a strong linear or parametric relation to erosion, a nonparametric approach is important to consider while performing correlation analysis. Spearman rank coefficient is calculated using following formula:

$$\rho = 1 - \frac{6 \sum d^2}{n^3 - n}$$

Where *d* is the difference in rank between the two variables

Once the data is collected, it is ranked by giving highest rank to highest value and so on. Then difference in rank of each data set is calculated and the values are plugged in the formula above. Spearman correlation can give a perfect value (1 or -1) when the two variables are related by any monotonic function in contrast to only linear function in

case of Pearson correlation. (Gibbons, 1990)(Lee Rodger J. and Nicewander W.A., 1988)

5.1.3Kendall's Rank Correlation Coefficient- Tau

Like Spearman's rho, Kendall's tau is also a nonparametric measure of correlation.. It was first introduced by Maurice Kendall in 1938 (Kendall, 1938)

The general formula for calculating the Kendall's Tau is given below:

$$\tau = \frac{(number\ of\ concordant\ pairs) - (number\ of\ discordant\ pairs)}{0.5n(n-1)}$$

For a given sample of variables x and y , both with sample size of 'n', there ${}_nC_2$ combinations possible for selecting distinct pairs (x_i., y_i) and (x_j., y_j) Now these pairs are defined as concordant if (x_i. > x_j and y_i > y_j) or (x_i. < x_j and y_i < y_j) ; discordant if (x_i. > x_j and y_i < y_j) or (x_i. < x_j and y_i > y_j) and neither if $x_i = x_j$ or $x_i = y_j$.

Then the number of concordant pairs and discordant pairs are plugged into the above formula to get a coefficient which lies between -1 to 1.

Although in many cases , as in ours, the interpretation of both Spearman's rho and Kendall's tau is much similar, Some people have argued that Kendall's tau has an advantage of very direct observation and interpretation considering agreeable (concordant) and non-agreeable(discordant) pairs.(Bolboaca S.D. and Jantschi L. ,2006)

5.1.4Bootstrap Sampling

Bootstrap resampling is one of the most controversial techniques in statistics (Kvan P.H., Vidakovic B., 2007). The bootstrap described by Efron (1979, 1982) is arguably the most popular resampling tool in statistics and specifically nonparametric statistics today. Bootstrap resampling has a great advantage of a simple and straight forward way to derive properties of estimators. It measures the properties from number of resamples created by random data sampling with replacement from the data set. The number of elements in each bootstrap sample is equal to that in original data set. It is a great tool in nonparametric statistics to reaffirm the inferences made based on a parameter value. It helps to determine how certain the conclusion made on a parameter value are. The argued disadvantage of bootstrap resampling is that as its tendency to be more optimistic in some cases due to resampling based on substitution.(Efron,1982)

5.2Curve Fitting and Regression

Various different fits, algorithms and methods are explored to find the best fit for identified CFD parameter. MATLAB curve fitting toolbox is used for the purpose (2012). For all the methods implemented, input data is first centered and scaled. This normalized the predictor (input) data. The input variables have wide difference in scale in our data set and hence normalizing the data improved the fit.

5.2.1Least-Squares Fitting

Least square method is used by MATLAB while fitting the data. A parametric model relating the response data, erosion in our case, and predictor data with various coefficients depending on the fit desired is set up. Model coefficients are then estimated by minimizing summed square of residuals. Residues are defined as the difference between response (observed output) value and fitted value:

$$r_i = y_i - \hat{y}_i$$

Response = data – fit

Then minimization function, sum of square of residues is given by:

$$Fmin = \sum_{i=1}^{n} (y_i - \hat{y}_i)^2$$

Three different least square fitting methods were implemented. Linear least square, Robust least square and nonlinear least square.

5.1.1.1Linear Least Squares:

Linear least-square method was employed when fit for a linear model (linear in the coefficients) was desired. In our case, it was used primarily when polynomial fit was desired. A detailed application of least square methods to various problems is covered by CL Lawson and RJ Hanson in their book (1974). The following example from MATLAB documentation (2013) illustrates application of liner least square fitting process:

Let us consider we have n data points and want to fit the data by first-degree polynomial:

$$y = p_1 x + p_2$$

Now we write S as a system of n simultaneous liner equation in two unknowns. The system is overdetermined if the number of equation are more than the number of unknowns.

$$S = \sum_{i=1}^{n} \left(y_i - (p_1 x_i + p_2)\right)^2$$

The coefficients can be determined by differentiating S with respect to each parameter and setting the result equal to zero as least square fitting minimized the summed square of residuals.

$$\frac{\partial S}{\partial p_1} = -2 \sum_{i=1}^{n} x_i \left(y_i - (p_1 x_i + p_2)\right) = 0$$

$$\frac{\partial S}{\partial p_2} = -2 \sum_{i=1}^{n} \left(y_i - (p_1 x_i + p_2)\right) = 0$$

Let us represent the true parameters by *b.* now substituting b1 and b2 instead of p1 and p2 the equations become:

$$\sum_{i=1}^{n} x_i \left(y_i - (p_1 x_i + p_2)\right) = 0$$

$$\sum_{i=1}^{n} \left(y_i - (p_1 x_i + p_2)\right) = 0$$

The summation runs from *i*=1 to n and normal equations can be defined as :

$$b_1 \sum x_i^2 + b_2 \sum x_i^2 = \sum x_i \, y_i$$

$$b_1 \sum x_i + n b_2 = \sum y_i$$

Now, solving for b1 and then b2

$$b_1 = \frac{n\sum x_i\, y_i - \sum x_i \sum y_i}{n\sum x_i^2 - (\sum x_i)^2}$$

$$b_2 = \frac{1}{n}\left(\sum y_i - b_1 \sum x_i\right)$$

This concept can be extended to higher degree polynomials simply by adding normal equation for each liner term added to the model.

5.1.1.2Weighted Least Square:

Weighted least square is helpful when the assumption that the response data is of equal quality is violated. It improves fit by adding a weight (scale factor) in fitting process. The minimization function in this case will be:

$$s = \sum_{i=1}^{n} w_i (y_i - \hat{y_i})^2$$

The weight determines how much the response value influences the parameter estimates i.e. a high quality data point influences the fit more than low-quality data point.

5.1.1.3Robust Least Square:

The disadvantage of least square of being highly sensitive to outliers is rectified in Robust scheme. Two methods are available in MATLAB (2013) for Robust least square fitting

1. Least absolute residuals (LAR) - To reduce the effect caused by squaring of absolute residuals of outlier, it calculates the curve that minimizes the absolute difference. This way the outliers will have less influence on the fit.
2. Bisquare weights – Weights are assigned to each data point depending on its distance from the fitted line. The points that are much farther from the line get a zero weight. Thus it minimizes the weighted sum of squares. Bisquare method is preferred most of the time as it finds the curve that fits majority of data still utilizing least-squares approach and neglects the outliers.

A robust iteratively reweighted least-square algorithm is proposed by Holland and Welsh (1977). MATLAB implements the following steps for Robust fitting with Bisquare weights. (2013)

1. Fit the model by Weighted least square
2. Compute the adjusted residuals given by:

$$r_{adj} = \frac{r_i}{\sqrt{1 - h_i}}$$

r_i is the usual least-square residuals and h_i are the leverages that adjust the weight reducing weight of data points that had huge effect on least-square fit.

3. Standardize the adjusted residues by:

$$u = \frac{r_{adj}}{K_s}$$

Where K is the tuning constant with a value 4.685 ans s is the robust variance given by:

$$S = \frac{median\ absolute\ deviation\ of\ residues}{0.6745}$$

4. Compute robust weights as a function of *u:*

$$w_i = (1 - (u_i)^2)^2 \qquad for \quad |u_i| < 1$$

$$w_i = 0 \qquad for \qquad |u_i| \geq 1$$

5. Stop if fit converges else go back to step one for next iteration.

5.1.1.4Non Linear Least Square:

A nonlinear least square method is employed to fit a model that has equation nonlinear in coefficients or is a combination of linear and nonlinear in the coefficients. Exponential and power functions fit were obtained using nonlinear methods.

The general matrix from of the model is given by:

$$y = f(X,\beta) + \varepsilon$$

where,

y is n-by-1 vector of responses

β is m-by-1 vector of coefficients

X is n-by-m design matrix for the model

And ε is n-by-1 error vector.

An iterative approach is required to solve for the coefficients in a nonlinear model. Following steps are performed by MATLAB function to solve for the coefficients in nonlinear least square regression for curve fitting (2013):

1. Estimate the value of each coefficient
2. Calculate the fitted response values given by

$$\hat{y} = f(X, b)$$

3. Adjust the coefficients following a fitting algorithm. And see if the fit improves. Two different fitting algorithms are available in MATLAB
    a. Trust-Region – This algorithm is described by More and Sorensen (1983) and Cartis et. al. (2009). It is used if the constraints on coefficients are known.
    b. Levenberg-Marquardt – it is one of the most popular algorithms employed since decades. Proposed by Levenberg (1944) and improved upon by Marquardt(1963), it has proved to give a good fit for wide range of nonlinear models.
4. Stop if the convergence criteria is reached else return to step 2 for next iteration.

A detailed discussion about development and implementation of each of the methods and algorithms is out of scope of this work but can be obtained from respective reference. Its application in MATLAB is discussed in Matlab Documentation (2013).

Chapter 6

Artificial Neural Networks

Human brain is a remarkable organ of the body. Many tasks performed by brain like reading, identifying a picture that you might have seen years ago or even recognizing a person's face, are extremely difficult for even large scale computers to do. Artificial Neural Network (henceforth referred by ANN) is a system inspired from functioning of human brain. They are based on simulated nerve cells or neurons which are connected in various ways to for a network. Much like brain, they are capable of learning, memorizing and creating relationships amongst what may seem like a random data.

Haykin, in his book "Neural Networks: a comprehensive foundation" (1994) defines ANN as "a massively parallel distributed processor that has a natural propensity for storing experiential knowledge and making it available for use". Another simple definition is presented in DARPA Neural Network study (1987) as " Neural network is a system composed of many simple processing elements operating in parallel whose function is determined by network structure, connection strengths, and the procession performed at computing elements or nodes."

Since the advances in computing power, ANNs have been increasing applied to various real world problems. McCulloch and Pitts (1943) had developed a ANN model based on their knowledge of neurology. Frank Rosenblatt can be credited for development of first simple learning algorithm called *Perceptron* (1958). It was a very simplistic model. Yet another system called *ADALINE (ADAptive Linear Element)* was developed by Widrow and Hoff in 1960. It differed from Preceptron in a way that it employed Least Mean Squares learning rule. It was in 1970's and 1980's that significant innovation in the field of ANN happened. ART(Adaptive Resonance Theory) network based on Grossberg and Carpenter's school of thought which explored resonating algorithms(1985) was developed. Klopf (1972, 1975), developed basis for learning in artificial neuron inspired from biological principle of neuronal learning called heterostasis. But arguably one of the most important contributions in learning method was that by Paul Werbos (1974, 1988) called back-propagation learning method. It is one of the most extensively used methods today in ANN. Rezaul Begg (2006) calls Back Propagation a "Perceptron with multiple layers, a different threshold function in neurons and a more robust and capable learning rule." Today, ANNs are used for classification, forecasting, modeling and pattern recognition in various fields like Business, Engineering, Science and Medicine.

ANN has been successfully developed for reservoir modeling and estimation in oil and gas industry (S Mohaghegh et. al., 1995, M Shahab et. al., 1997). They have been implemented in analysis of log data (H Eskandari et. al., 2004) and for continuous oil field optimization (L. Saputelli, 2002). Veten et al. (2000) and Zhang et al. (2003) were amongst the first ones to implement ANN in wear of polymer composites. More recently work by Suresh et al. (2009) reports successful implementation of ANN in predicting solid particle erosion in composites. Multilayer feed forward network with back propagation training algorithm has been used widely in wear prediction (Zhang et al. 2003) Bayesian regularization training algorithm was found more accurate for erosion modeling by Zhang et al. (2003), Danaher et al. (2004) as well as Suresh et al.(2009).

6.1Artificial Neural Network Design

The basic building blocks of an ANN are (1) Network Architecture, (2) Transfer Functions and (3) Training methods.

6.1.1Network Architecture

6.1.1.1Neuron Model

The most basic element of human brain is neurons. They help us to recall process and apply previous experiences to our actions. Basic components and function of each component is presented in figure below:

Figure 15 Single Neuron (Klerfors, 1998)

Similarly the basic unit of ANN is called artificial neurons. These neurons simulate the four basic functions of natural neurons. A basic artificial neurons is shown in figure below:

Figure 16 Artificial Neuron (Klerfors, 1998)

Various inputs are represented by x(n). These inputs are then multiplied by connection weight represented by w(n). In a simple case shown in the figure, these products are summed, fed through transfer function to generate result and then output.

A neuron represented by terminology used in MATLAB Neural Network user guide (Demuth and Beale,1993) is shown below:

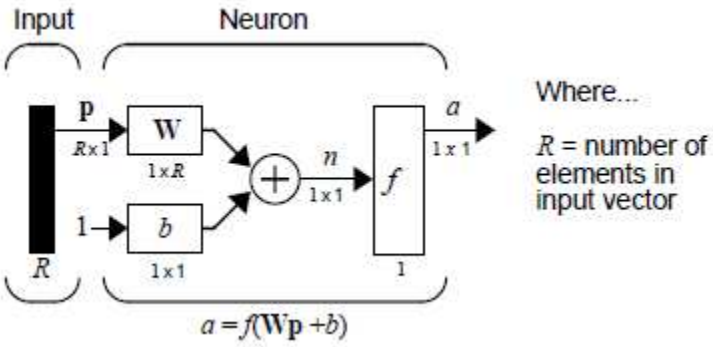

Figure 17 Single Neuron with Vector input (Demuth and Beale, 1993)

Input vector is represented by ‘p’ with dimension shown in the bottom. The input to the transfer function f is n, sum of bias b and the product ‘Wp’. Where ‘W’ is the weight function. It is passed to transfer function to get output from the neuron. It should be noted that if there were more than one neuron, the output would be a vector rather than a scalar.

6.1.1.2Multiple Layered Network

A Network can be of multiple layers with different weight and biases for each layer. Each layer may have different network architecture. The layer that produces the final output of the network is called Output layer. Rests of the layers are usually called hidden layers. A simple three layer network with on input layer, one hidden layer and one output layer is depicted below:

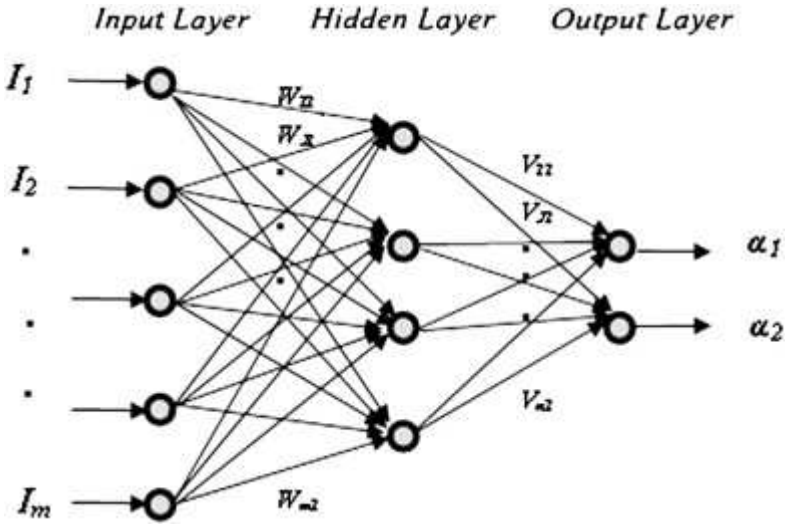

Figure 18 Schematic of a typical multilayer neural network model (Hagan et al., 1996)

A similar multilayer model with three hidden layers in MATLAB notations is shown in figure below:

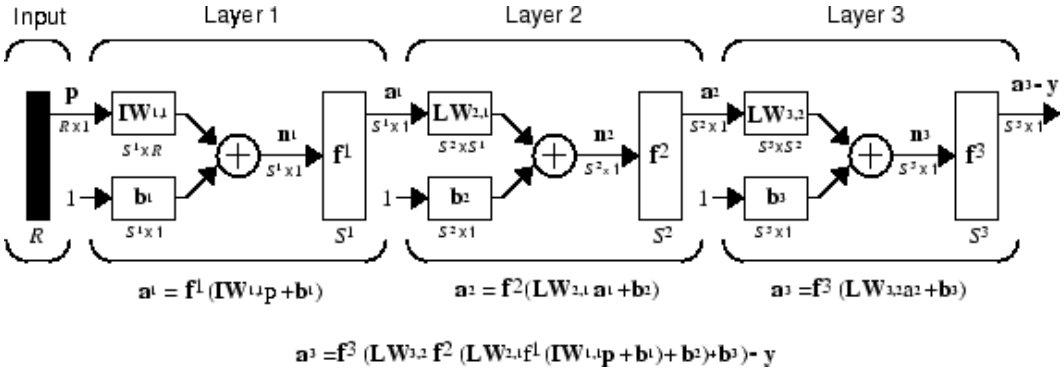

Figure 19 Multilayer neural network (Demuth and Beale, 1993)

6.1.2Transfer Functions

Various different transfer functions have been employed in different ANNs. Discussion of each of them is beyond the scope of this document. However, two of most commonly employed transfer functions that were utilized in this work are discussed in this section.

6.1.2.1Linear Transfer Function

As the name suggests, it is an identity function given by:

$$F(x) = x;\ for\ all\ x$$

Following is the picture of the graph and MATLAB notation associated with it.

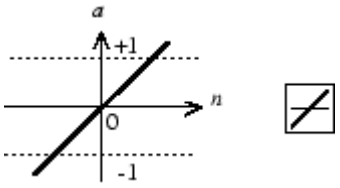

Figure 20 Linear Transfer Function (Demuth and Beale, 1993)

6.1.2.2Hyperbolic Tangent Sigmoid Function

Advantage of implementing Sigmoidal functions to accelerate convergence in back-propagation algorithms (discussed later in detail) have been discussed by Vogl et al. (1988) and Harrington (1993). The functional representation is

$$F(x) = \frac{2}{1 + \exp(-2 * x)} - 1 = \tanh(x)$$

Function shape and MATLAB symbol is presented in figure below:

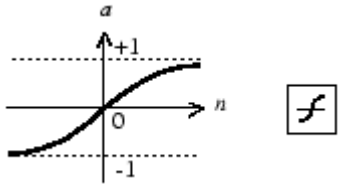

Figure 21 Tan-Sigmoid Transfer Function (Demuth and Beale, 1993)

6.1.3Learning

The method of setting weights in an ANN enables the process of learning. Training is generally referred to as the process of modifying the weights in the connection between network layers to achieve expected output (Shivanandam at el., 2006) The process that takes place while network is trained is called learning. Generally there are three different types of training.

6.1.3.1Supervised Training

Supervised training or training with a teacher is a process in which network is provided a series of sample inputs and the outputs are compared with expected responses. The network training continues till satisfactory output is obtained. There are target output vectors for sequence of input training input vectors. The weight are adjusted

according to different algorithms employed. Hebb's net, Backpropagation network, counter propagation net, etc. are example of some supervised training algorithms.

6.1.3.2Unsupervised Training

If there are no target vectors for the training input vectors, the training is called unsupervised training. The weights are adjusted in such a way that most similar input vector is assigned to same output. They are more complex and difficult to implement. Binary Adaptive Resonance Theory(ART1), Competitive learning, Self-organizing maps and topology preserving maps (SOM/TPM) are some examples of unsupervised training.

6.1.3.3Reinforcement Training

It can be termed as a type of supervised training, where teacher is present to guide the direction but outputs are not presented. The network is presented with indication of whether it is successful or whether it failed is provided. It tries to maximize a performance index called reinforcement signal through trial and error. The system would know if the outputs are correct or not but not the exact outputs.

There are various learning laws and algorithms that cannot be covered in this document. Books by Sivanandam et al.(2006), Hagen et al.

(1996), Begg and Palaniswami (2006), Mehrotra et al. (1997) and Haykin(1994) discuss in depth various training algorithms and more complex neural networks.

Various combinations of network architecture and training algorithm are developed and successfully applied to different problems. All of them are impossible to cover in this text. A Multilayer feedforward network with backpropagation was modeled in this study and is explained in the next section.

6.2Multilayer Feedforward Network with Backpropagation Algorithm

Feedforward network with backpropagation algorithm (Rumelhart and McClelland, 1986) is one of the most commonly used networks. It means that neurons are organized in layer and send their signals “forward”. The errors are then propagated backwards. The backpropagation algorithm falls under supervised learning category. The central idea for backpropagation algorithm is that of minimizing the error till the network is trained. As in many other networks, random weights are assigned at the beginning of training and they are adjusted till minimization criteria for error is reached. Hagan and Menhaj (1994) first demonstrated the development of Levenberg-Marquardt algorithm for neural networks. It’s reported to train the neural network 10 to 100 times

faster than then popular gradient descent backpropagation method. Bayesian regularization algorithm to avoid over fitting of data is introduced to Levenberg-Marquardt algorithm. Detail explanation about the method are available in MacKay(1992) as well as Foresee and Hagan(1997).

A detailed derivation of any of the methods is easily available in literature mentioned and will not be discussed here. However, a top level overview of the steps involved in it is presented.

6.2.1Backpropagation

The steps of backpropagation for a connection between hidden layer neuron A and output neuron B are simply explained below (MacLeod, 2013):

1. Initialize random weights, apply inputs and calculate the outputs
2. Calculate the error for neuron B. Remember that the transfer function is sigmoid function, hence error is:

$$ErrorB = OutputB\,(1 - OutputB)(TargetB - OutputB)$$

3. Update the weights by following equation

$$W_{AB}^{+} = W_{AB} + (ErrorB \times OutputA)$$

4. Calculate the error for the hidden layer neuron by back propagating them form output layer. It is done by taking error form output neuron and running them back through the weight to get hidden layer errors. If neuron is connected to two output neuron B and C then:

   $ErrorA = Output\ A\ (1 - Output\ A)(ErrorB\ W_{AB} + ErrorC\ W_{AC})$

5. Go back to 3 to update the weight of hidden layer on the left

   A simple calculation for this procedure on a network with 2 input , 2 output and 3 hidden layer neurons is show in figure below:

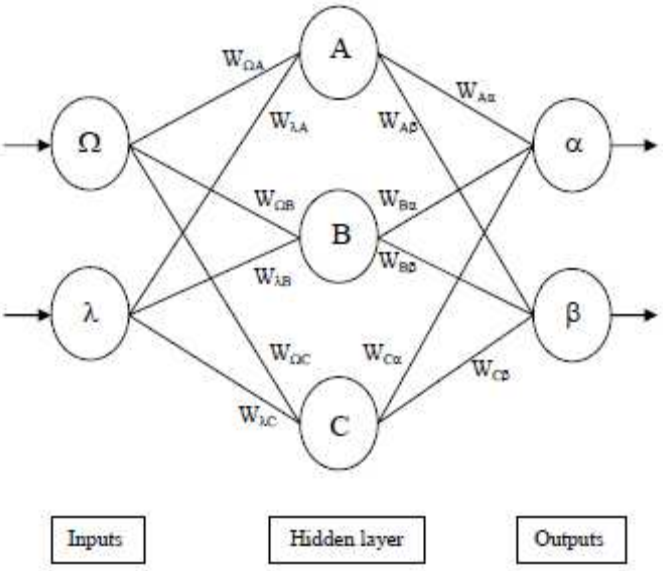

1. Calculate errors of output neurons

$$\delta_\alpha = out_\alpha\,(1 - out_\alpha)\,(Target_\alpha - out_\alpha)$$
$$\delta_\beta = out_\beta\,(1 - out_\beta)\,(Target_\beta - out_\beta)$$

2. Change output layer weights

$$W^+_{A\alpha} = W_{A\alpha} + \eta\delta_\alpha\,out_A \qquad W^+_{A\beta} = W_{A\beta} + \eta\delta_\beta\,out_A$$
$$W^+_{B\alpha} = W_{B\alpha} + \eta\delta_\alpha\,out_B \qquad W^+_{B\beta} = W_{B\beta} + \eta\delta_\beta\,out_B$$
$$W^+_{C\alpha} = W_{C\alpha} + \eta\delta_\alpha\,out_C \qquad W^+_{C\beta} = W_{C\beta} + \eta\delta_\beta\,out_C$$

3. Calculate (back-propagate) hidden layer errors

$$\delta_A = out_A\,(1 - out_A)\,(\delta_\alpha W_{A\alpha} + \delta_\beta W_{A\beta})$$
$$\delta_B = out_B\,(1 - out_B)\,(\delta_\alpha W_{B\alpha} + \delta_\beta W_{B\beta})$$
$$\delta_C = out_C\,(1 - out_C)\,(\delta_\alpha W_{C\alpha} + \delta_\beta W_{C\beta})$$

4. Change hidden layer weights

$$W^+_{\lambda A} = W_{\lambda A} + \eta\delta_A\,in_\lambda \qquad W^+_{\Omega A} = W^+_{\Omega A} + \eta\delta_A\,in_\Omega$$
$$W^+_{\lambda B} = W_{\lambda B} + \eta\delta_B\,in_\lambda \qquad W^+_{\Omega B} = W^+_{\Omega B} + \eta\delta_B\,in_\Omega$$
$$W^+_{\lambda C} = W_{\lambda C} + \eta\delta_C\,in_\lambda \qquad W^+_{\Omega C} = W^+_{\Omega C} + \eta\delta_C\,in_\Omega$$

The constant η (called the learning rate, and nominally equal to one) is put in to speed up or slow down the learning if required.

Figure 22 Calculation of Reverse pass for Backpropogation

(MacLeod,2013)

6.2.2Levenberg-Marquardt Training

The training process for Lavenberg-Marquardt algorithm is described in following steps (Yu and Wilamowski, 2012):

1. With the initial weights (randomly generated), evaluate the total error (SSE).
2. Perform the update as directed by Levenberg-Marquardt update rule to adjust weights with the new weights, evaluate the total error.

$$w_{k+1} = w_k - (H)^{-1} J_k e_k$$

$where\ w\ are\ weight\ at\ respective\ levels\ H\ is\ the\ Hessian\ matrix\ J^T J + \mu I$

$I\ is\ identity\ matrix, \mu\ is\ positive\ combination\ coefficient\ and\ e\ is\ error$

3. If the current total error is increased as a result of the update, then retract the step (such as reset the weight vector to the precious value) and increase combination coefficient μ by a factor of 10 or by some other factors. Then go to step ii and try an update again.
4. If the current total error is decreased as a result of the update, then accept the step (such as keep the new weight

vector as the current one) and decrease the combination coefficient μ by a factor of 10 or by the same factor as step 4

5. Go to step 2 with the new weights until the current total error is smaller than the required value

A Block diagram for it is presented in figure below:

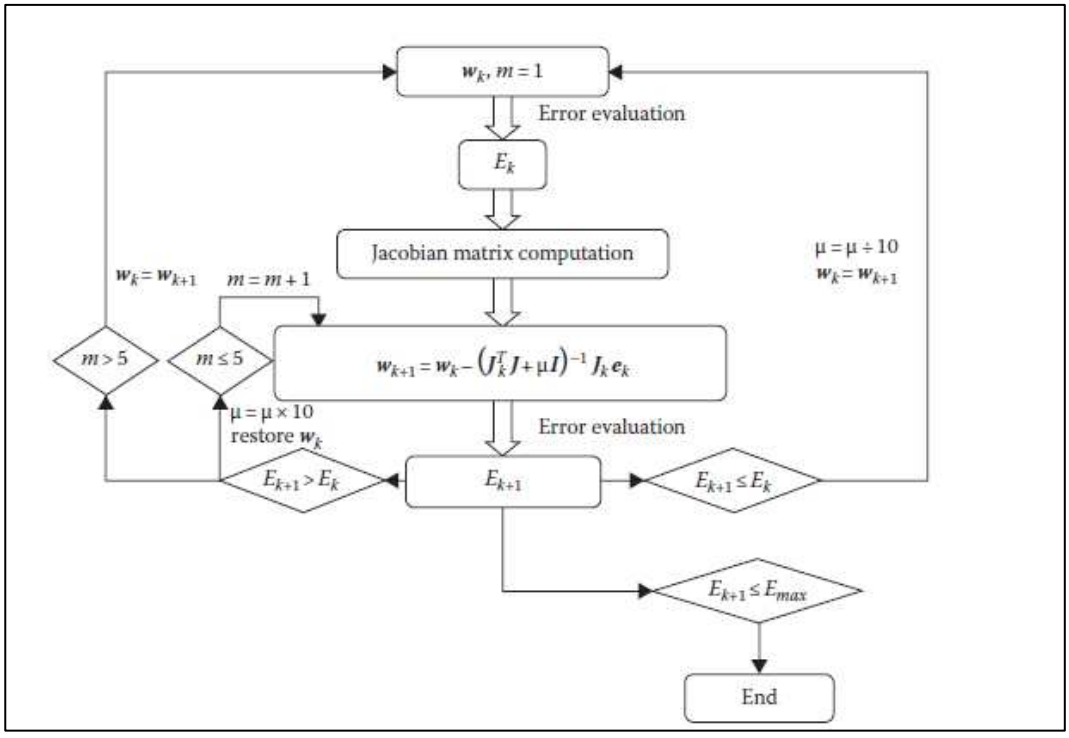

Figure 23 Levenberg - Marquardt algorithm (Yu and Wilamowski, 2012)

6.2.3Bayesian Regularization

Bayesian regularization is implemented in Levenberg-Marquardt algorithm to minimize a liner combination of squared errors and weights. It is one of the approaches to stop over fitting a problem. It also reduced the need to test different number of hidden neuron for a problem.

The typical performance function for feedforward network is mean sum of squares of the errors.

$$F = mse = \frac{1}{N}\sum_{i-1}^{N}(e_i)^2$$

A term consisting of mean sum of squares of the network weights is added to performance to improve generalization

$$F = \beta E_d + \alpha E_w$$

Where α and β are parameters optimized in Bayesian framework (MacKay,1992).This results in smaller weight and forces a smooth response. In this framework the weights are assumed to be random variable with specified distribution. The regularization parameters are associated with variance of these distributions. The parameters are then estimated by statistical techniques.

An expanded Levenberg-Marquardt Algorithm with Bayesian regularization is presented below (Souza, 2009):

1. Compute the Jacobian

2. Compute the error gradient

$$g = J^T E$$

3. Approximate the Hessian matrix

$$H = J^T J$$

4. Calculate the performance function

$$F = \beta E_d + \alpha E_w$$

5. Solve $(H - \lambda I)\delta = g$ to find δ
6. Update the weights w using δ
7. Recalculate performance function using updated weights
8. If the value has decreased
    a. Discard the new weights, increase λ using γ and go to step 5
    b. Else , decrease λ using γ
9. Upgrade the Bayesian hyperparameter using MacKay's formulae
    a. $\gamma = W - (\alpha \times tr(H^{-1}))$ where W is number of network parameter (weights and biases) and tr= trace of the matrix

b. $\beta = {(N - \gamma)}/{(2.0 \times E_d)}$ where N is the number of entries in training set

c. $\alpha = {\gamma}/{(2.0 \times E_w)}$

More details, proof and derivation of the algorithms can be obtained in MacKay(1992) and Foresee and Hagan (1997)

Chapter 7

Results And Discussion

7.1Performance Measures

Before we jump into the results obtained by implementing various erosion prediction models, it is important to discuss the parameters used throughout results to measure efficiency and effectiveness of the models. Following are quantities measured and their implications are related to results in this work.

7.1.1 Performance Measure for CFD Based Models

7.1.1.1Percentage Error

The most frequently used quantity to measure the quantitative performance of the model throughout this work is Percentage error defined by equation below:

$$Percentage\ Error = \frac{Predicted\ value - Experimental\ value}{Experimental\ value} \times 100$$

Lower the percentage error, better the model.

7.1.1.2Value Ratio

Ratio of the predicted value to experimental value is a good measure to visualize the results when plotted. An Ideal situation would be when this value is 1, which would mean that predicted value and experimental values are the same.

$$Value\ Ratio = \frac{Predicted\ value}{Experimental\ value}$$

7.1.2 Goodness of Fit Measure for Statistical Models

7.1.2.1Sum of Squares Due to Error

Denoted by SSE, sum of squres due to error, measures the total deviation of the predicted value form the experimental value. It is also sometimes called as sum squared of residues.

$$SSE = \sum_{i=1}^{n} (experimental\ value - predicted\ value)^2$$

Value closer to 0 means that the model has smaller random error and is a better fit

7.1.2.2R-Square

This measure is the most widely used measure to determine quality of fit for statistical models like regression or neural network. It measure how well the model is explains the variation in data. It is called coefficient of determination.

R-square is defined as ratio of sum of squares of regression (SSR) and the total sum of squares (SST) is following way:

$$SSR = \sum_{i=1}^{n} (Predicted\ value - mean\ value)^2$$

$$SST = \sum_{i=1}^{n} (Experimental\ value - mean\ value)^2$$

Also, SST= SSR+SSE

Hence,

$$R - Square = \frac{SSR}{SST} = 1 - \frac{SSE}{SST}$$

Value closer to 1 means a better fit

7.1.2.3Root Mean Squared Error

It is commonly called standard error of fit or standard error of regression. It is a measure of estimation of standard deviation of random component in the data:

$$RSME = \sqrt{\frac{1}{n}\sum_{i=1}^{n}(predicted\ values - experimental\ values)^2}$$

Lower value characterizes a better model

7.2CFD Best Practice and Analysis of Present Model

In this section of results, we will compare the current Baker Hughes erosion model with Oka et al. model which is used widely in the industry. As all the models are based on CFD modeling, CFD best practices to improve quantitative prediction capability of current model is established. An exhaustive grid study is performed to examine the effect of grid on erosion prediction parameters.

7.2.1CFD Simulation Results and Convergence Studies

CFD-based erosion modeling steps discussed in previous section were employed on elbow. For preliminary study, symmetry of the model was exploited and only half model was used for simulation. A full model

was further developed mainly to have more number of data point for further model development and check for any physics that is not captured in assuming symmetry. Both half model and full model capture the flow physics in similar manner as will be seen from following results. Although, 4 different cases as described in table below were simulated, only Test 1 case results are presented here to avoid repetitive results.

Table 1 - Test parameters simulated

Test 1: 256 micron sand, 50 ft/s
Test 2: 53 micron sand, 50 ft/s
Test 3: 53 micron sand, 85.785 ft/s
Test 4: 256 micron sand, 85.785 ft/s

The geometry for both full and half model is presented in Figure 24 below:

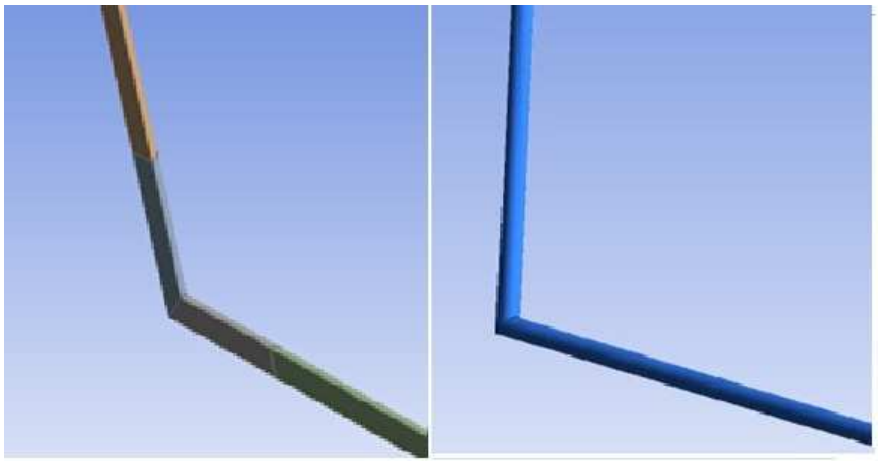

Figure 24 Geometry of CFD model (Half model on left and Full on right)

Various different grids were used to perform grid dependency study which will be addressed in separate section.

7.2.1.1Convergence Studies

Convergence studies were preformed considering two different criteria for fluid flow modeling. Static pressure drop was monitored for various grids. Normalized values for pressure considering experimental value as a basis for normalization is presented below:

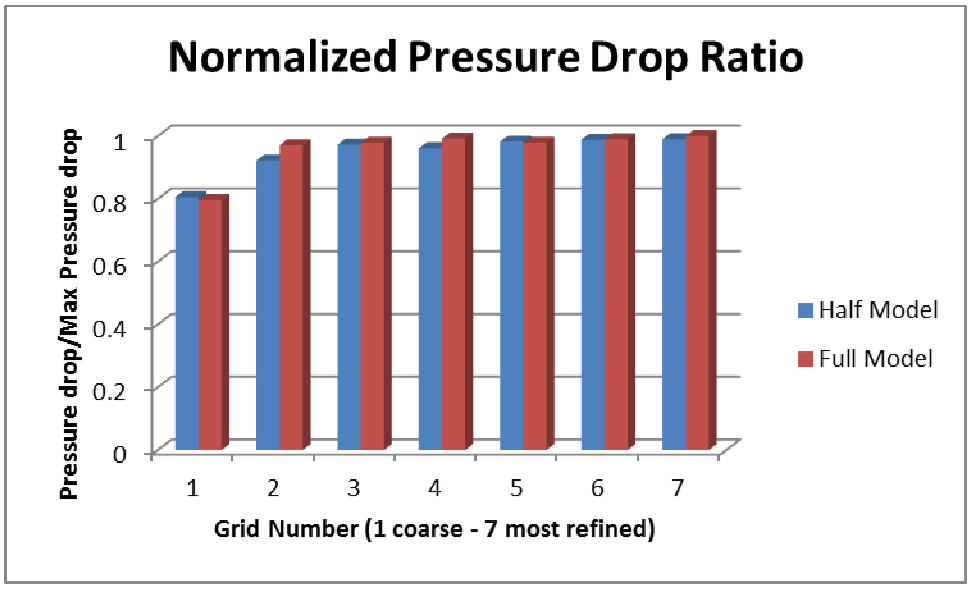

Figure 25 Pressure convergence

It can be observed from Figure 25 that all the grids except grid 1 predict pressure close to maximum pressure obtained. Also, half model and full model predict pressure within 2% error margin.

As experimental velocities are not available, a law of wall plot for fully developed turbulent flow is considered as basis for monitoring velocity convergence. A law of wall plot for both half model and full model is presented below.

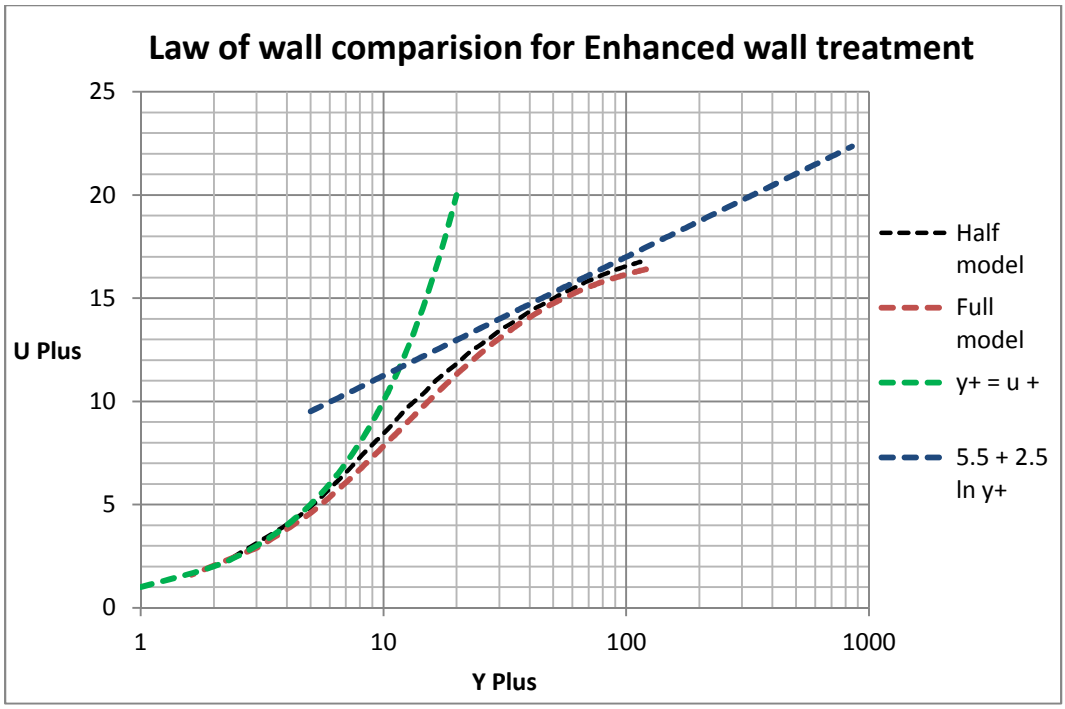

Figure 26 Law of wall comparison for wall integration approach (low y+ values)

While employing wall function approach, specifically scalable wall function approach in FLUENT, the solver ensures that y+ is always greater than 11.225. Comparison for such a case is presented below.

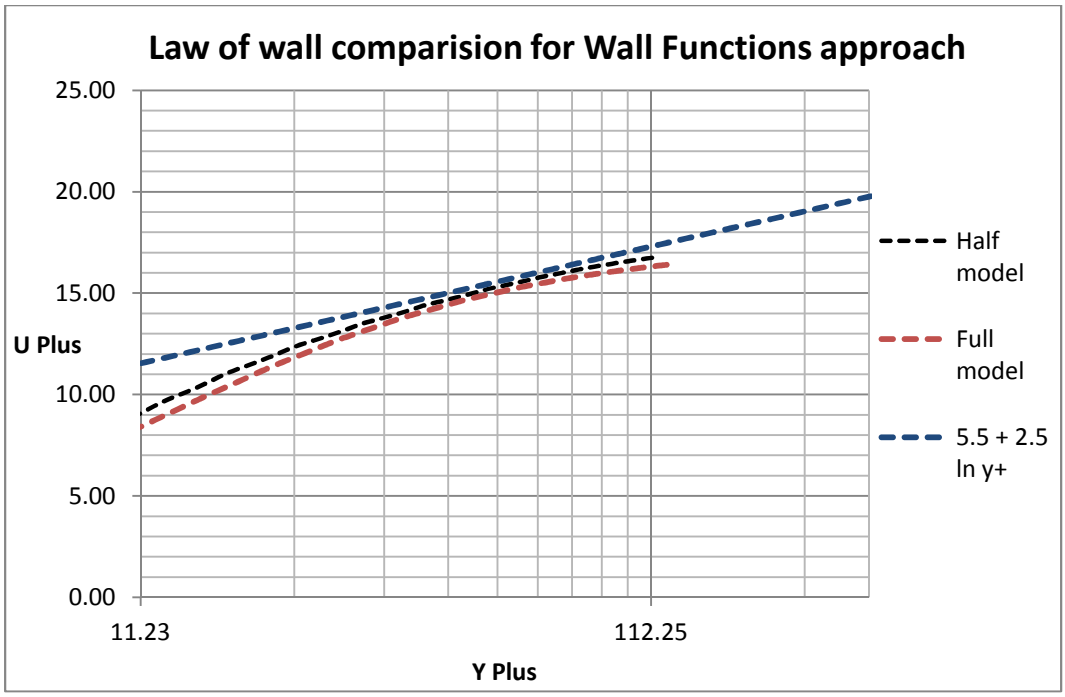

Figure 27 Law of wall comparison for wall function approach (y + <11.225)

It can be seen in this comparison as well that both half model and full model simulate the fully developed flow profile very accurately. Also, both the models predict similar values with less than 1% error in this case.

Convergence studies for DPM model is also very important in this case as erosion rate measurements are influenced highly by DPM concentration. In our studies, only spherical surface injections were considered. However, a tracking parameter of number of steps is critical in predicting exact DPM rate. A convergence study for number of steps for

particles was performed and its effect on highest DPM concentration is observed. Again, normalized values are presented here considering highest DPM concentration as the basis. It should be noted that these results are for single mesh as DPM concentration is highly sensitive to mesh density. It will be discussed in details in further sections. Also, these results are for Test 1 but similar studies for each test were conducted with comparable results.

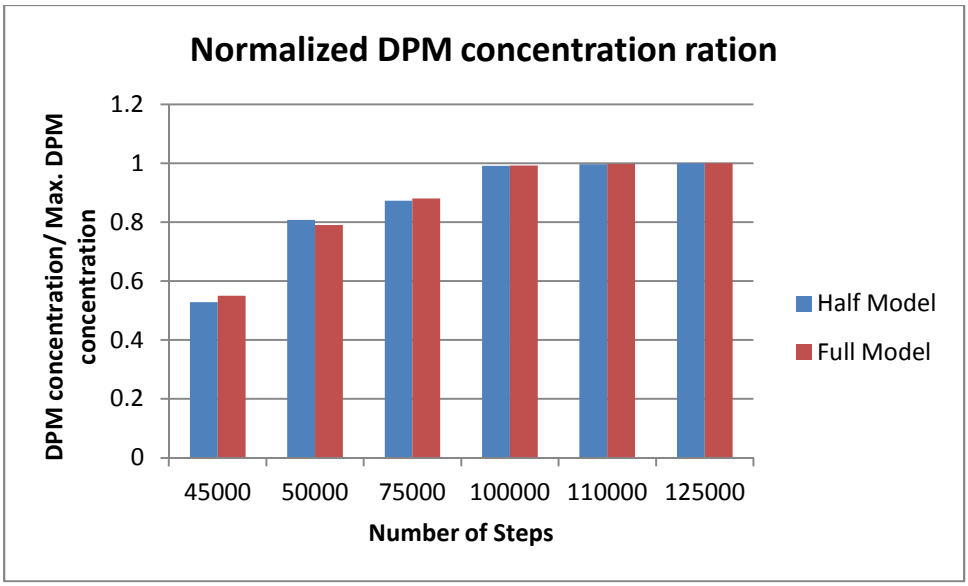

Figure 28 Convergence monitoring for number of steps in DPM

It is clearly observed that for our case, number of steps of around 110 thousand is optimum. All the further studies were carried out considering 110 numbers of steps in tracking parameter for DPM modeling.

7.2.1.2Comparison of Half Model and Full Model

A symmetric half model was simulated for preliminary results. The results from full model compared very well with half model. The major reason for performing full model simulations is to have more number of data points for development of new erosion models as well as for improvement of current model. Contour plots of velocity, pressure, DPM concentration and impact angle are compared here for wall y+ value of 30-200 for half model as well as full model. All the results show comparable results quantitatively (as seen in section above) as well as qualitatively (seen from contours below). All contours are plotted on same range of values. Values are not presented to maintain confidentiality.

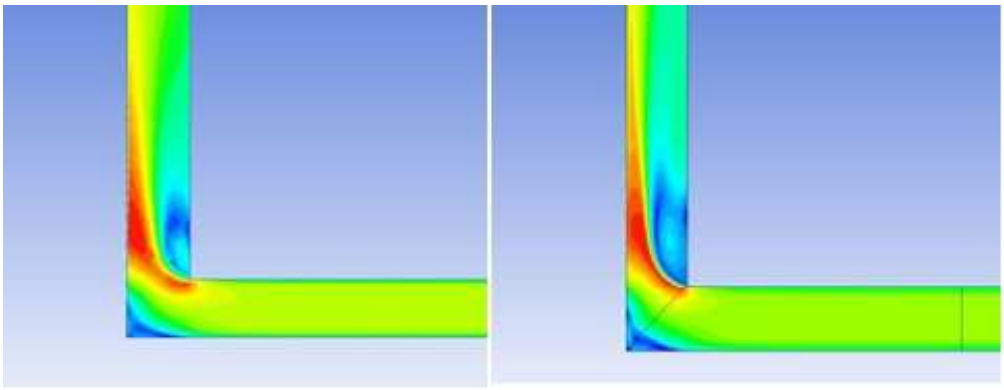

Figure 29 Velocity contour at mid-section for Full model (Left) and Symmetry plane for Half model (right)

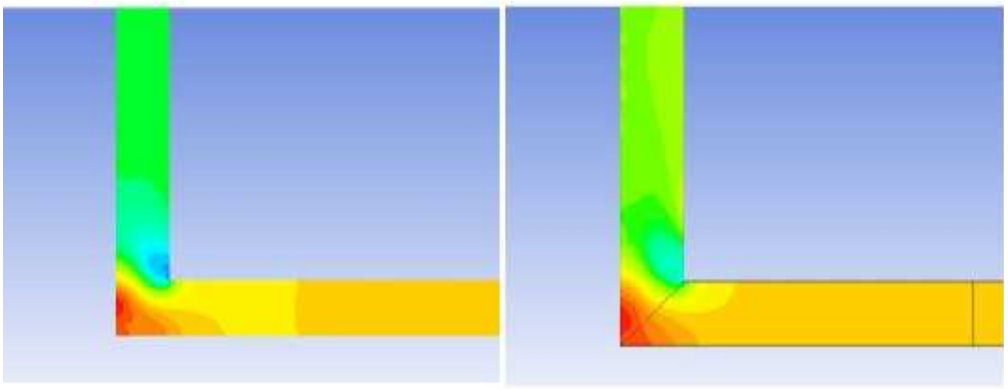

Figure 30 Pressure contour at mid-section for Full model (Left) and Symmetry plane for Half model (right)

It is established by results in this section as well as previous section that half model and full model results are in agreement with less that 1%

error margin. It is important to establish this fact as the results from both will be used interchangeably where ever necessary.

7.2.2Evaluation of Present Model

In this section, current Baker Hughes model is evaluated and compared with model presented by Oka et. al.,. A quantitative comparison is made. Both the models do a great job in identifying the regions of erosion.

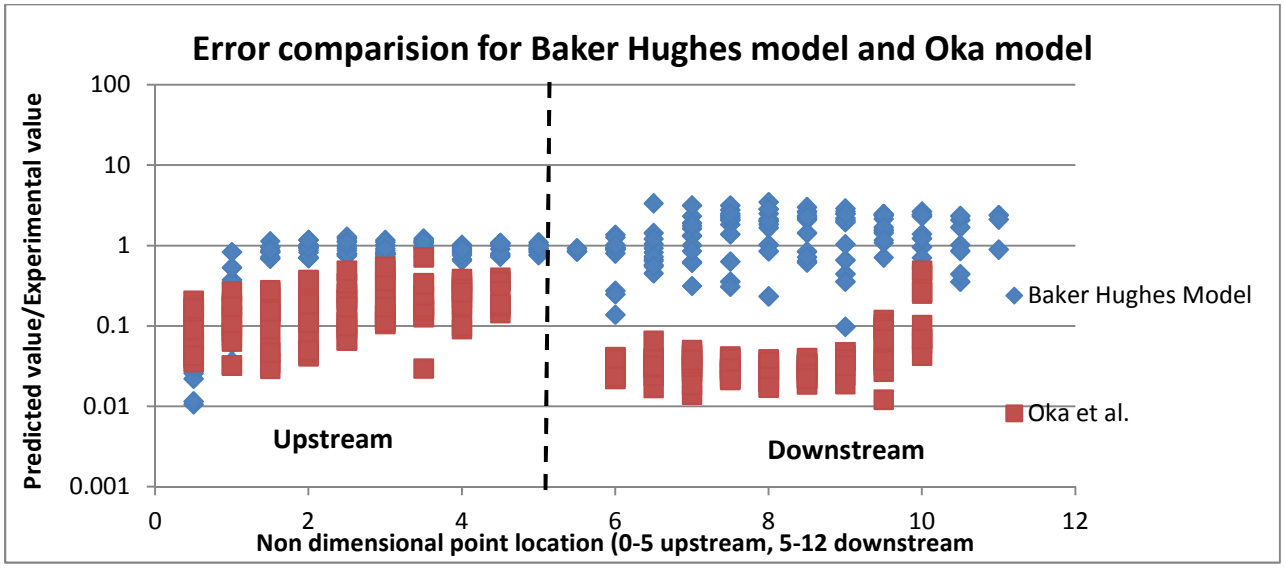

Figure 31 Error comparison between Baker Hughes model and Oka et al. model

It is clearly observed from the graphs that Baker Hughes model does a better job at prediction erosion rates. Mean percentage error in Baker Hughes model is 57% compared to 93% for Oka Model.

An effort is made to improve the efficiency of current model. The results are presented in following sections.

7.3Grid Dependency Study

A significant amount of time was spent to perform grid dependency studies. From initial results on half model, it was observed that grid size and wall y + values affect erosion prediction significantly. An exhaustive study of grid dependency was performed with more than 30 iterations of different grid being evaluated. This section present the primary results on symmetric half model and then the results on full model are presented.

7.3.1Preliminary Results on Symmetric Half Model

As observed in previous sections, both half model and full model produce similar results. Hence, to reduce computational time and manual time, an in-depth grid dependency study was performed on half model. The results were then utilized to simulate more efficient full model whose output parameters will be further explored in statistical analysis.

Seven different mesh iterations were identified for post processing. Results for 4 different ones are presented below. The mesh 1 and 2 are quad meshes with no boundary layers whereas all the others are tetrahedral with boundary layer. The most refined Mesh 7 has wall y+ of 1-7 with wall integration approach applied for solution.

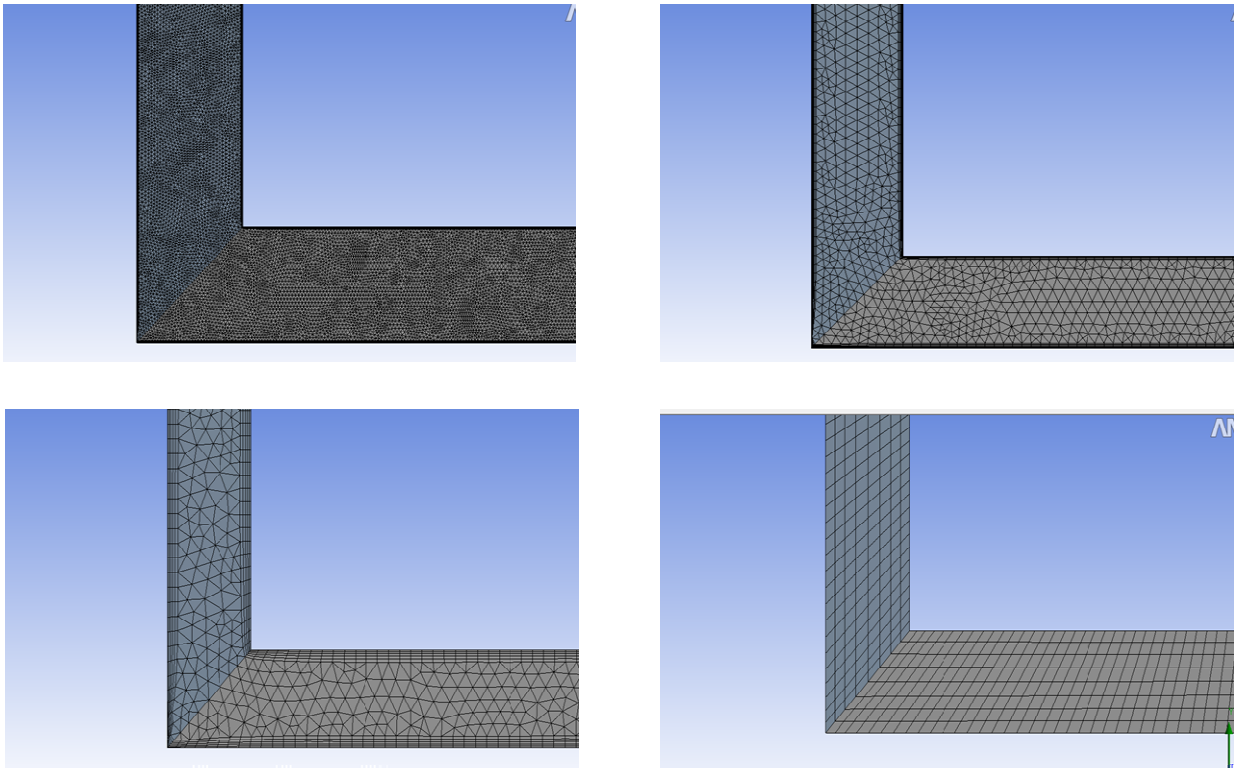

Figure 32 Mesh (top-left – 7, top –right – 5, bottom-left - 4, bottom-right - 2)

Table 2 Elbow- Mesh information

Grid Number	Elements	Max. skewness	Max. Aspect Ratio	Y+
1	17K	0.74	4	>2000
2	41K	0.67	4	1000-2000
3	125 K	0.84	72	650-750
4 (baseline)	151 K	0.82	17	350-600
5	389K	0.87	117	100-200
6	795 K	0.87	45	60-110
7	1 M	0.84	60	1-7

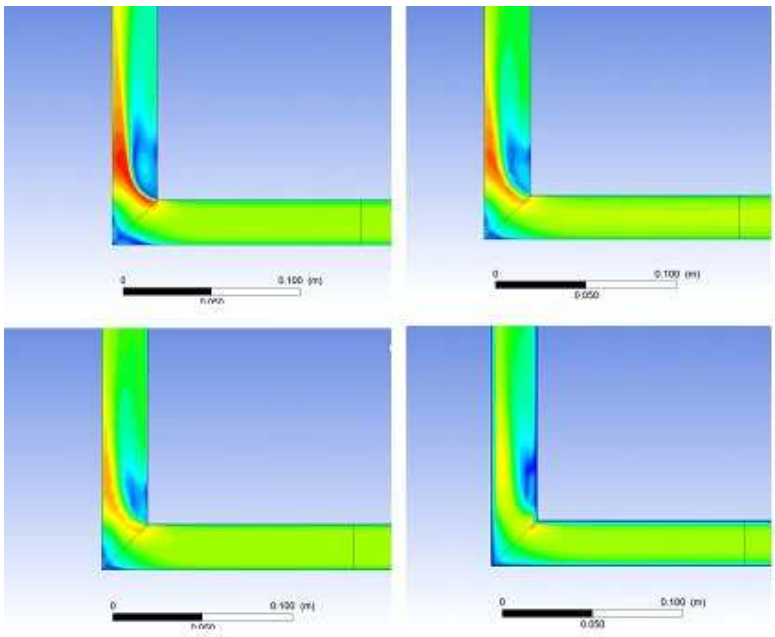

Figure 33 Velocity contours at longitudinal section (top-left – 7, top –right – 5, bottom-left - 4, bottom-right - 2)

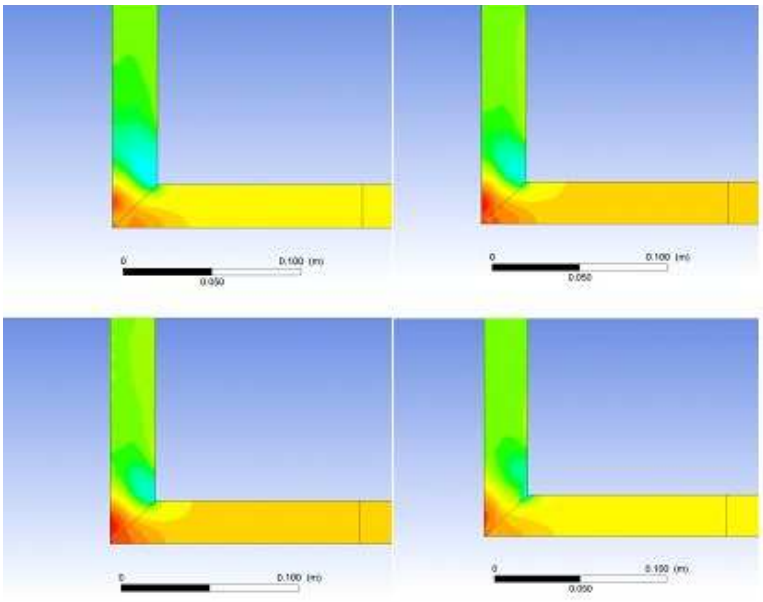

Figure 34 Pressure contours at longitudinal section (top-left – 7, top –right – 5, bottom-left - 4, bottom-right - 2)

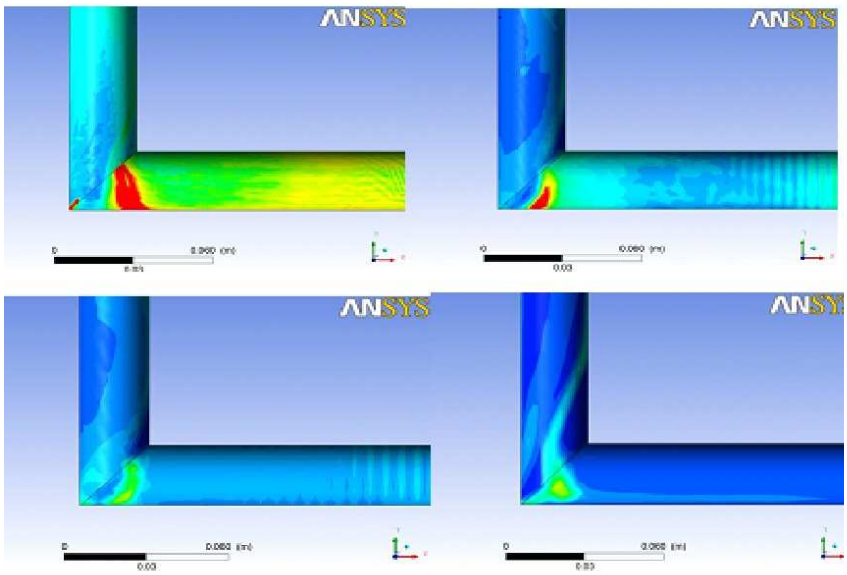

Figure 35 DPM Concentration –Clipped to range (top-left – 7, top –right – 5, bottom-left - 4, bottom-right - 2)

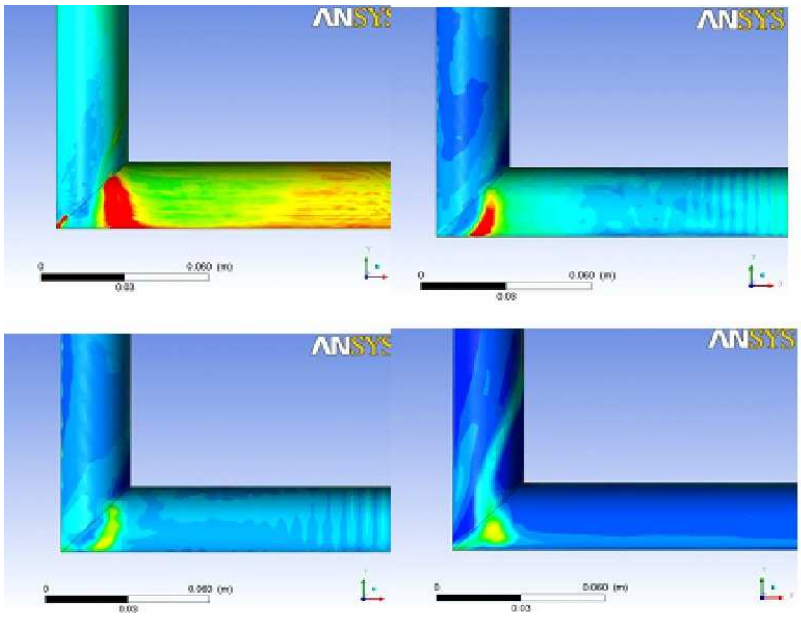

Figure 36 Erosion contours –Clipped to range (top-left – 7, top –right – 5, bottom-left - 4, bottom-right - 2)

Erosion rate is computed at 230 locations on the elbow and compared to experimental data. Error analysis is then performed. The following figure explains what points are referred to as located in upstream and downstream

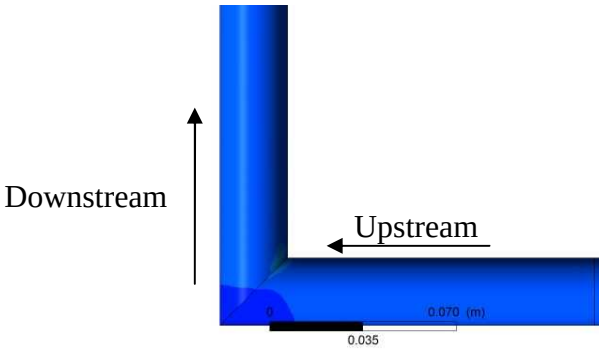

Figure 37 Location of points

As a first step of quantitative comparison, the total mean and median error for all 107 points was calculated and plotted. From those results it was found out that the coarse grid has less error as show in following graphs.

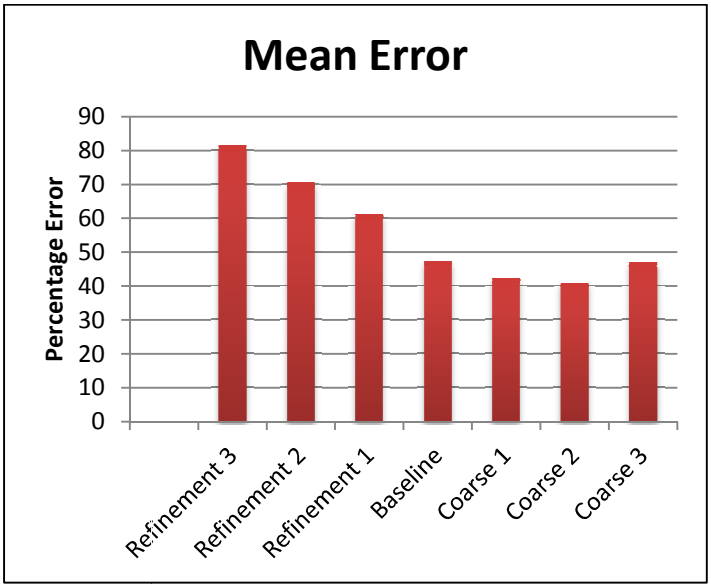

Figure 38 Mean error for all 107 points

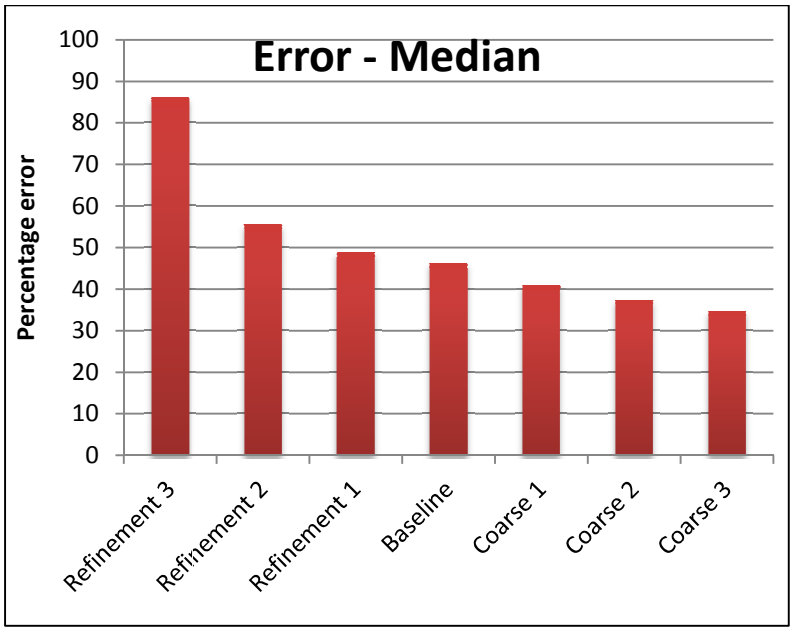

Figure 39 Median Error for all 107 points

To further investigate the nature of error. Line graph for all the grids comparing erosion rate at each point individually was plotted as shown in following Figure 40

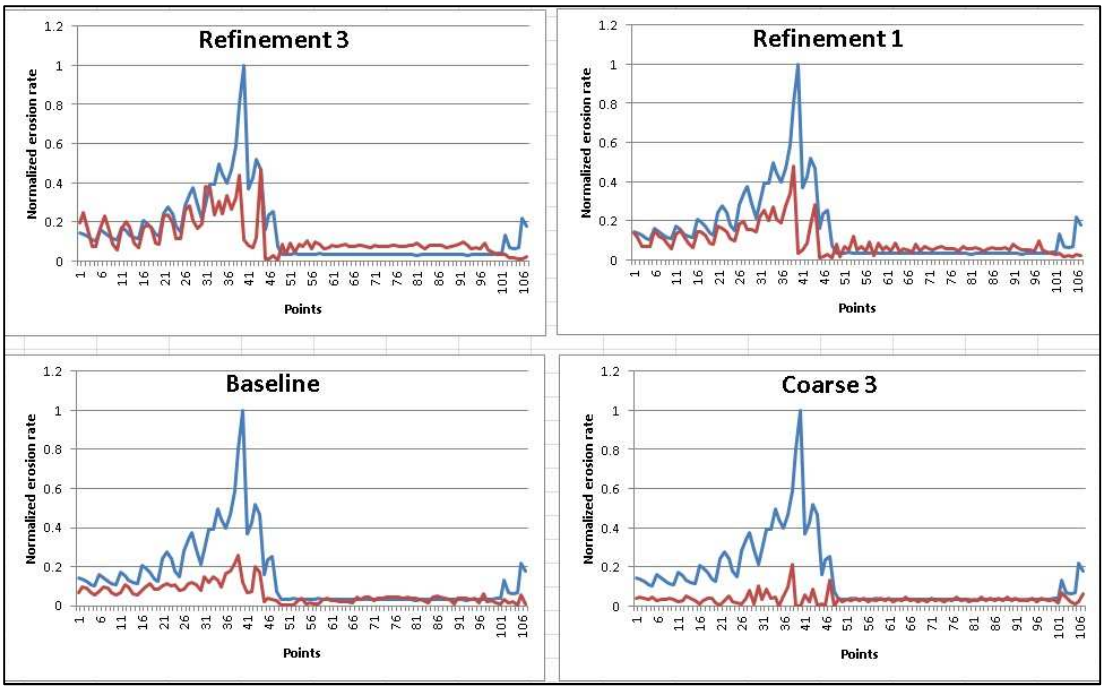

Figure 40 One on one comparison of erosion rates in (in/hr) for all 107 points

CFD Results

Experimental Results

Figure 40 show that the fine grid does a better job at predicting erosion rate in the critical regions. DPM concentration increases with grid refinement while keeping all other parameters constant. This is due to the fact that Ansys Fluent calculated DPM concentration as follows:

$$\text{DPM Concentration} = \frac{(Avg.particle\ mass\ in\ cell\ \times Particle\ residence\ time\ \times strength\ of\ particle)}{cell\ volume}$$

$$Strength\ of\ particle = \frac{total\ particle\ flow\ rate}{mass\ of\ single\ particle\ in\ the\ stream}$$

A wall integrated boundary layer approach gives more accurate boundary layer velocity results that contribute to the erosion calculation.

While considering all points, the major source of RMS error were points in low erosion regions as seen on the right side of the graph. It is also to be noted that the coarse grid may have small error but it does follow the exact pattern to that of experimental data in higher erosion rate region.

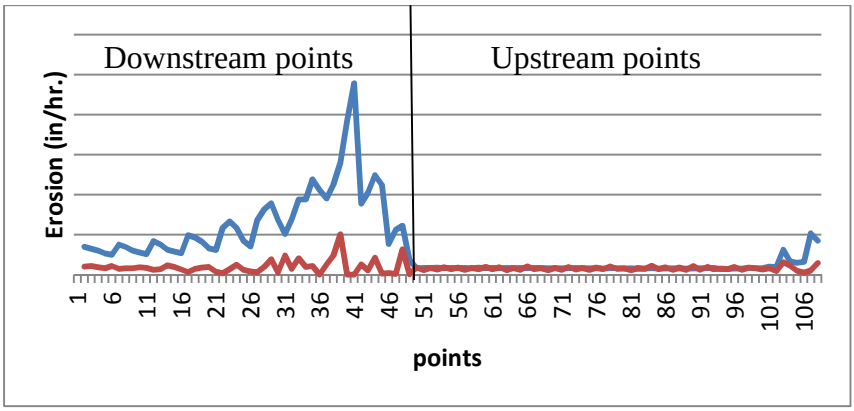

Figure 41 Points distribution as can be seen from line graph

Hence, so further calculations were performed considering two set of points :

Upstream points – Less erosion (pts. 52-107)

Downstream points – High erosion (pts. 1-51)

A correlation plot explaining the error was plotted for two different set of points. It is clearly observed that as the mesh becomes finer, the

correlation points seem to move towards the center line suggesting less error for downstream (Figure 42) and they seem to move away from 45^0 line for upstream points (Figure 43). This reinforces our conclusion that fine grid reduces error for calculating erosion rate in critical regions with higher erosion rate.

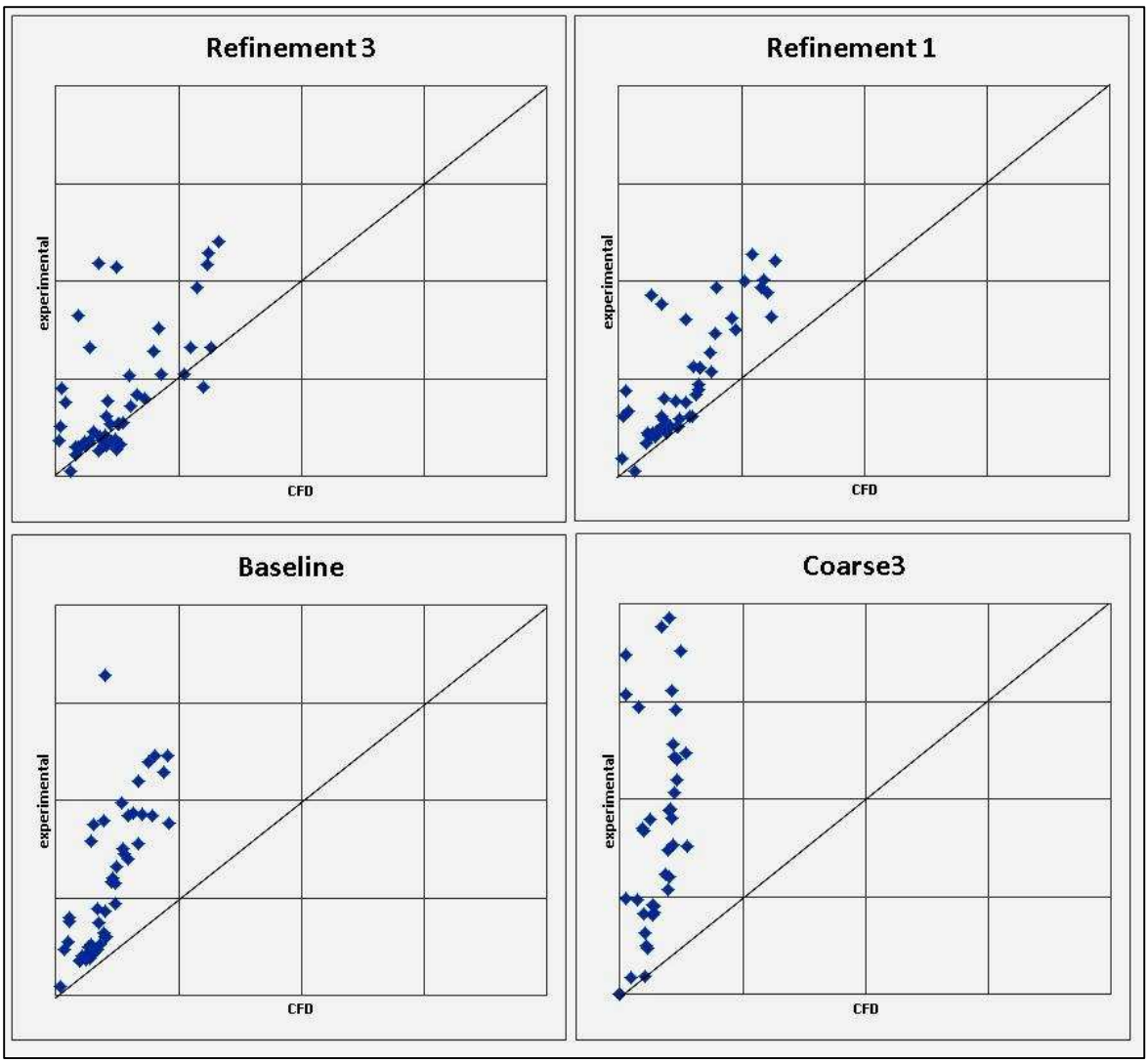

Figure 42 Error Correlation for downstream points (1-51) (CFD results on x axis vs. experimental results on y axis)

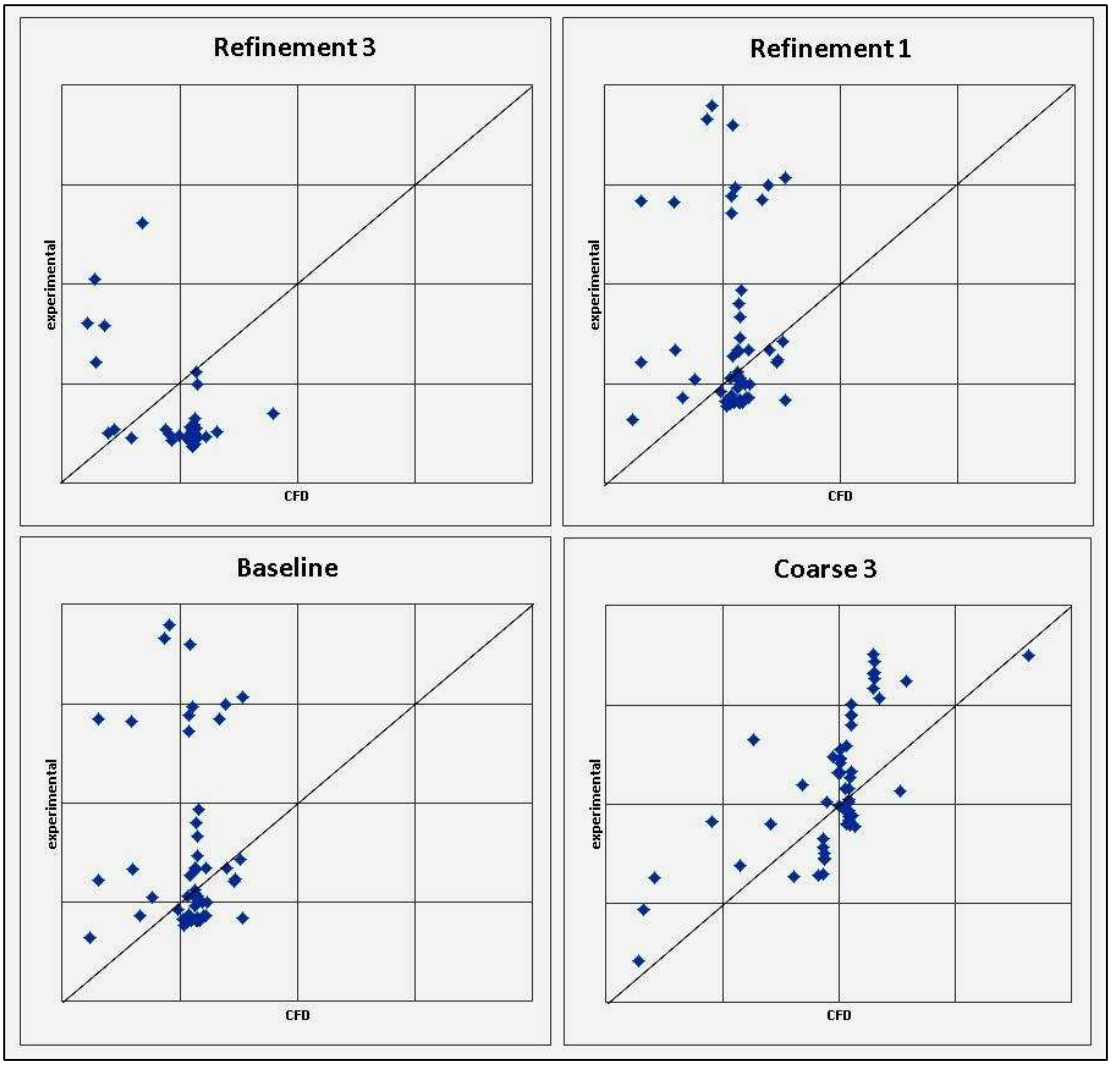

Figure 43 Error Correlation for upstream points (52-107) (CFD results on x axis vs. experimental results on y axis)

Hence, if the mean error bars are plotted for upstream and downstream points separately, they show an exact opposite nature (Figure 44,Figure 45)

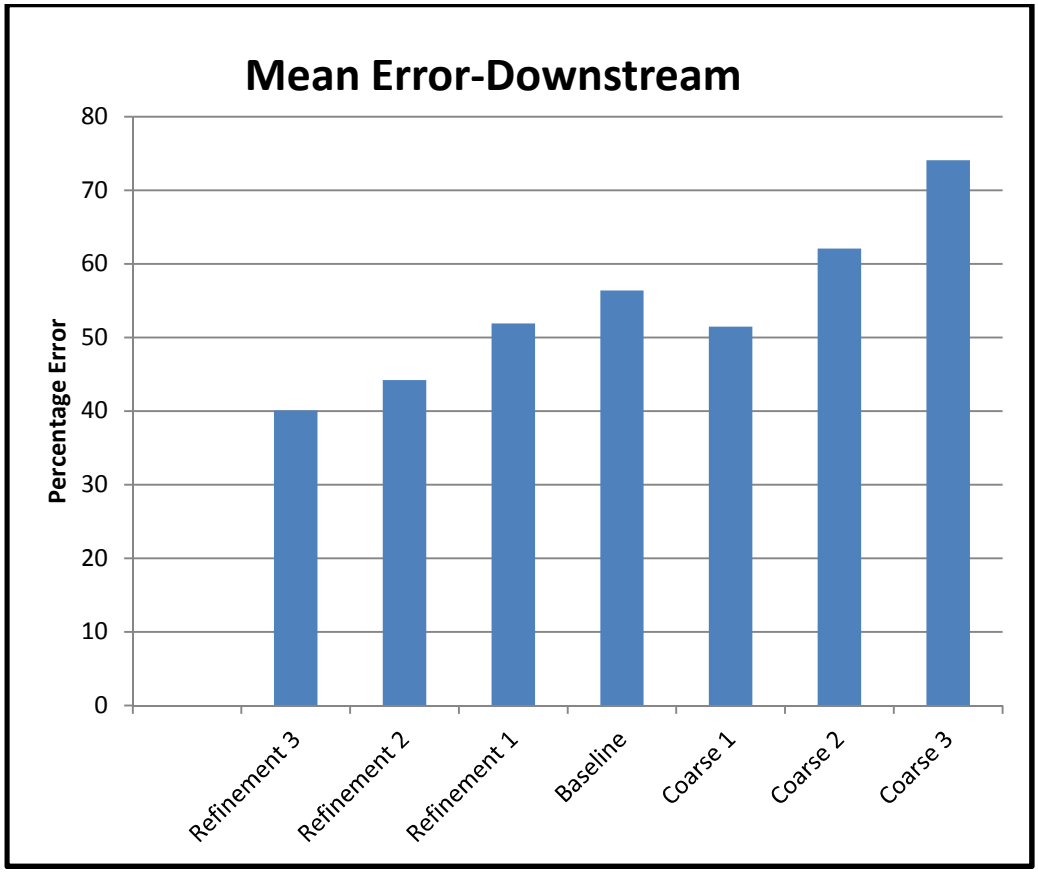

Figure 44 Mean percentage error for downstream points

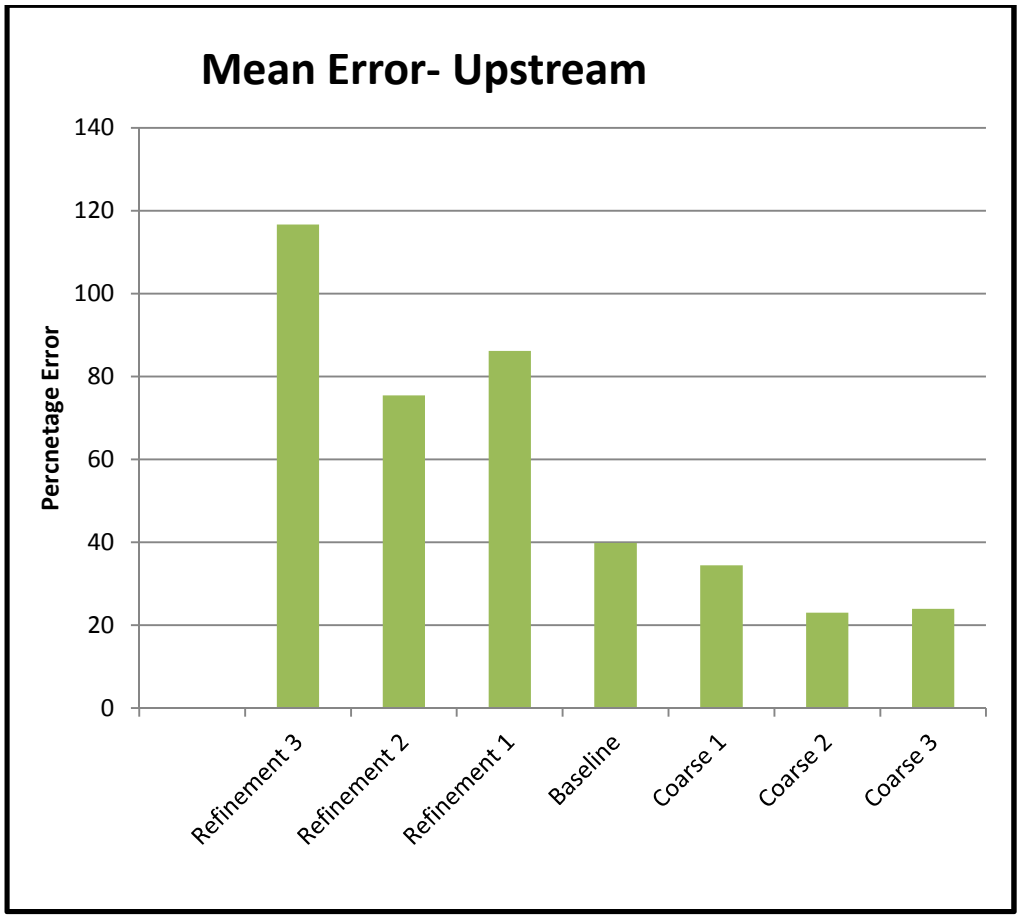

Figure 45 Mean percentage error for upstream points

The following Figure 46 and Figure 47 represent the velocity vs. erosion rate / DPM concentration for a coarse grid and a fine grid. It can be seen that fine grid does a great job at prediction erosion for a wider range of velocity compared to coarse grid.

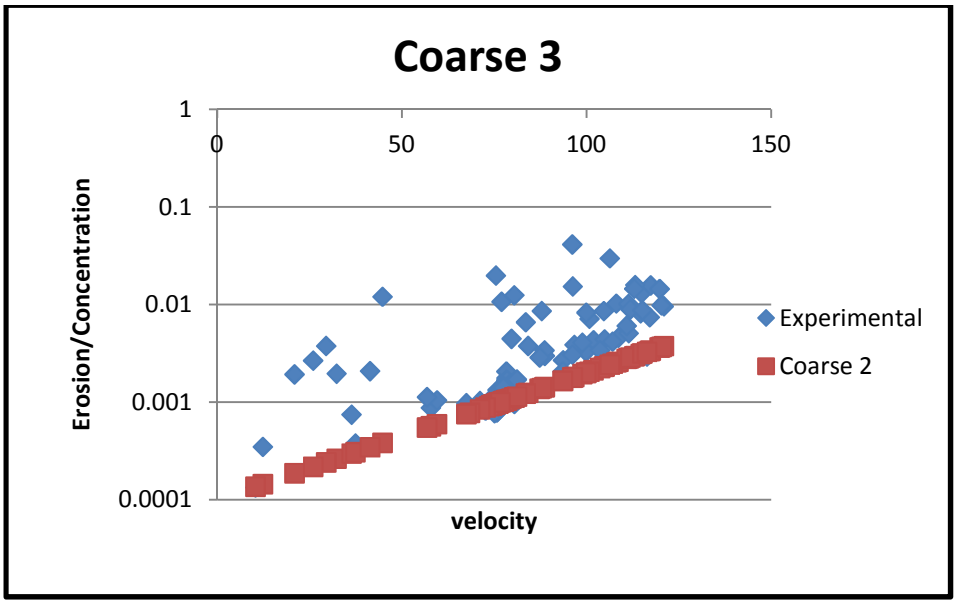

Figure 46 Velocity vs. E/C for Coarse Grid

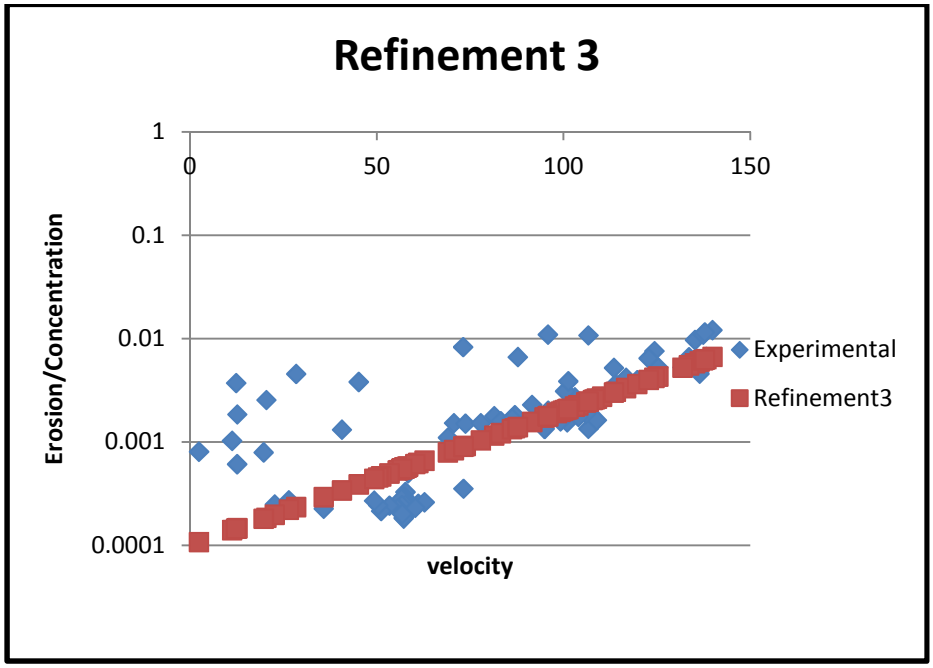

Figure 47 Velocity vs. E/C for Fine Grid

7.3.2Full Model Results

A refined grid does better job at predicting erosion rate in critical regions and also for larger velocity range. But it is very difficult to understand how much refinement is required. Also, what might be higher erosion rate region for this application may not be so for other applications? Hence, a full model analysis considering both upstream and downstream regions is performed and a relation between a non-dimensional length unit wall y+ and erosion rate prediction is established.

Description for again 7 different grids is presented in Table 3 below. Now onwards, rather than saying coarse or refined, grids are addressed by their respective wall y+ values.

Table 3 Grid description for Full model

Grid Number	Surface Y + range	Near wall approach
1	800-1100	Standard Wall Functions
2	400-700	Standard Wall Functions
3	300-650	Standard Wall Functions
4	50-270	Scalable Wall Functions
5	30-200	Scalable Wall Functions
6	≈1	Wall integration – Enhanced wall functions
7	<1	Wall integration – Enhanced wall functions

Comparison results, experimental vs. predicted regression plot and error ratio plot for each Test and three different grids are presented next. All regression plots are plotted with experimental values on x axis and predicted values on y axis. For comparison plots, data point number are plotted on x axis and normalized erosion rate on y axis.

Table 4 Mesh and y+ information

Grid Name	Wall Y + Value
Mesh B	<30 (wall integration approach)
Mesh B1	90-250 (wall functions approach)
Mesh B2	30-90 (Wall functions approach)

7.3.2.1Test 1

Following Figure 48 and Figure 49 present comparison plots, regression plot and finally error ration plot for all the three grids considering 50ft/s inlet velocity and 256 micron particle size.

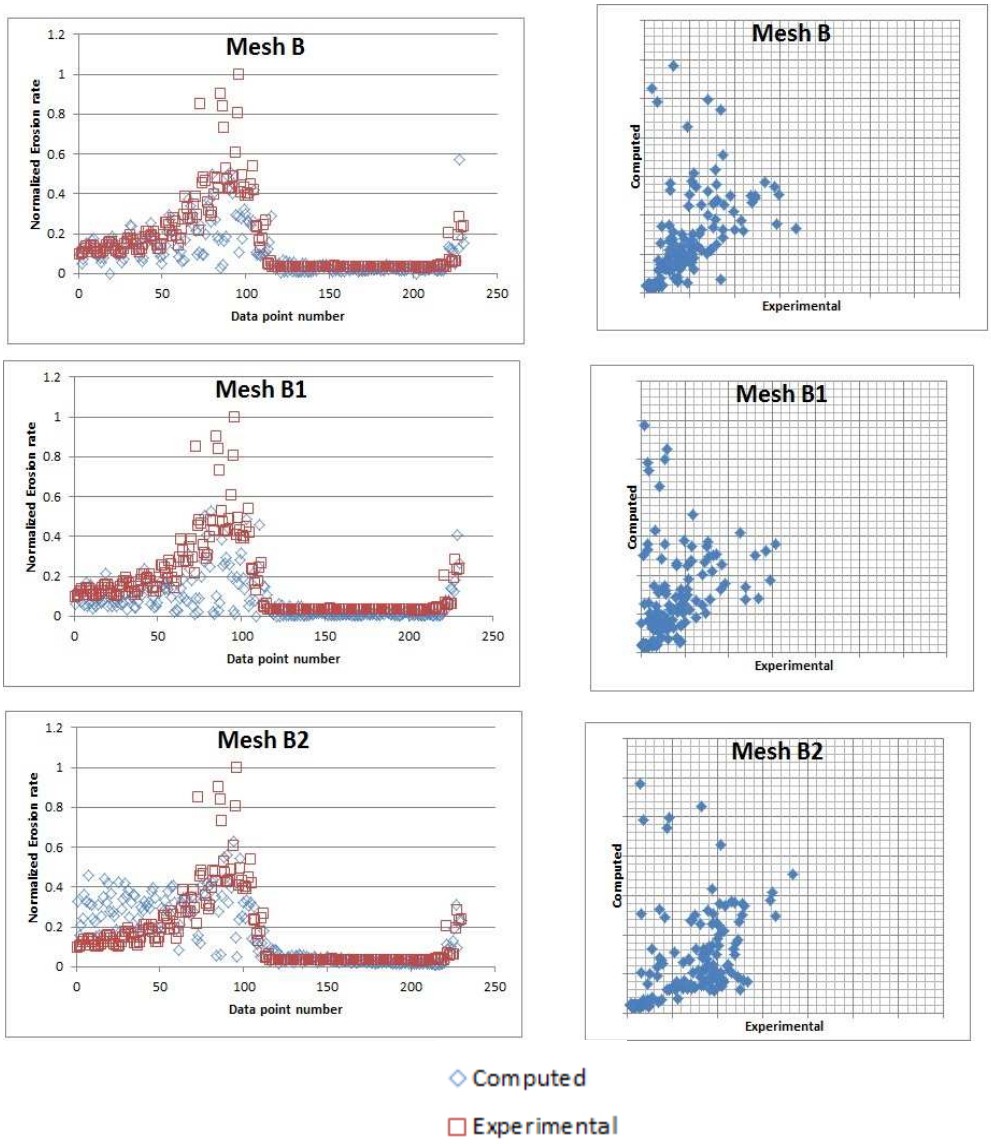

Figure 48 Comparison plot (top) and regression plot(bottom) for Test 1

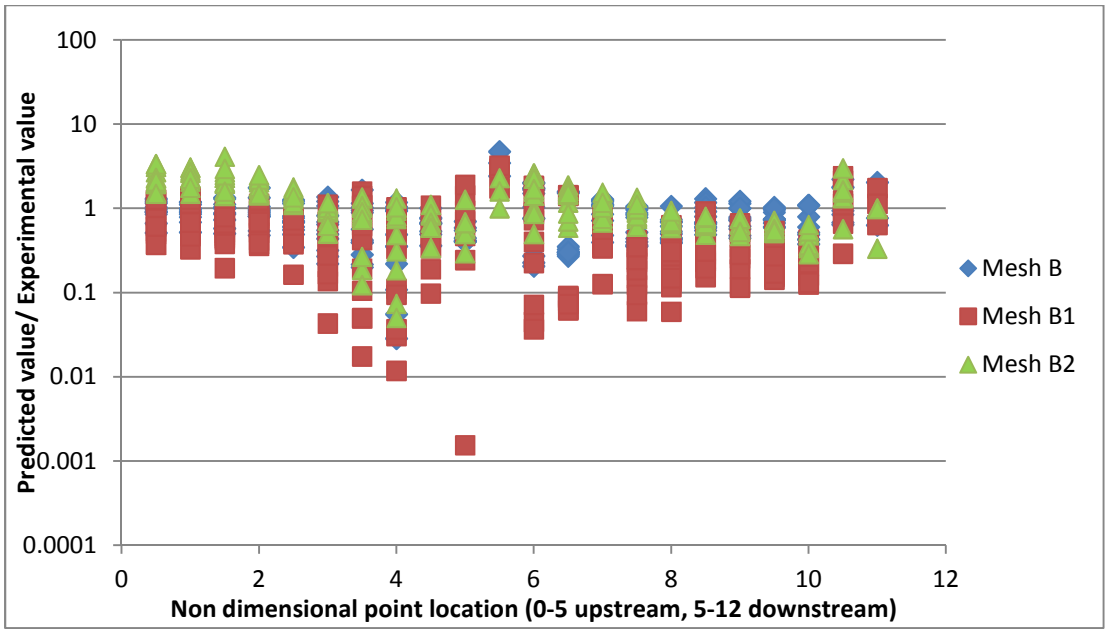

Figure 49 Error ratio plot for Test 1

Mesh B2 with y+ values of 30-90 predicts erosion more accurately for Test 1

7.3.2.2Test 2

Figure 50 gives comparison plot and regression plot whereas Figure 51 gives error ratio plot for 50 ft/s inlet velocity and 53 micron particle size.

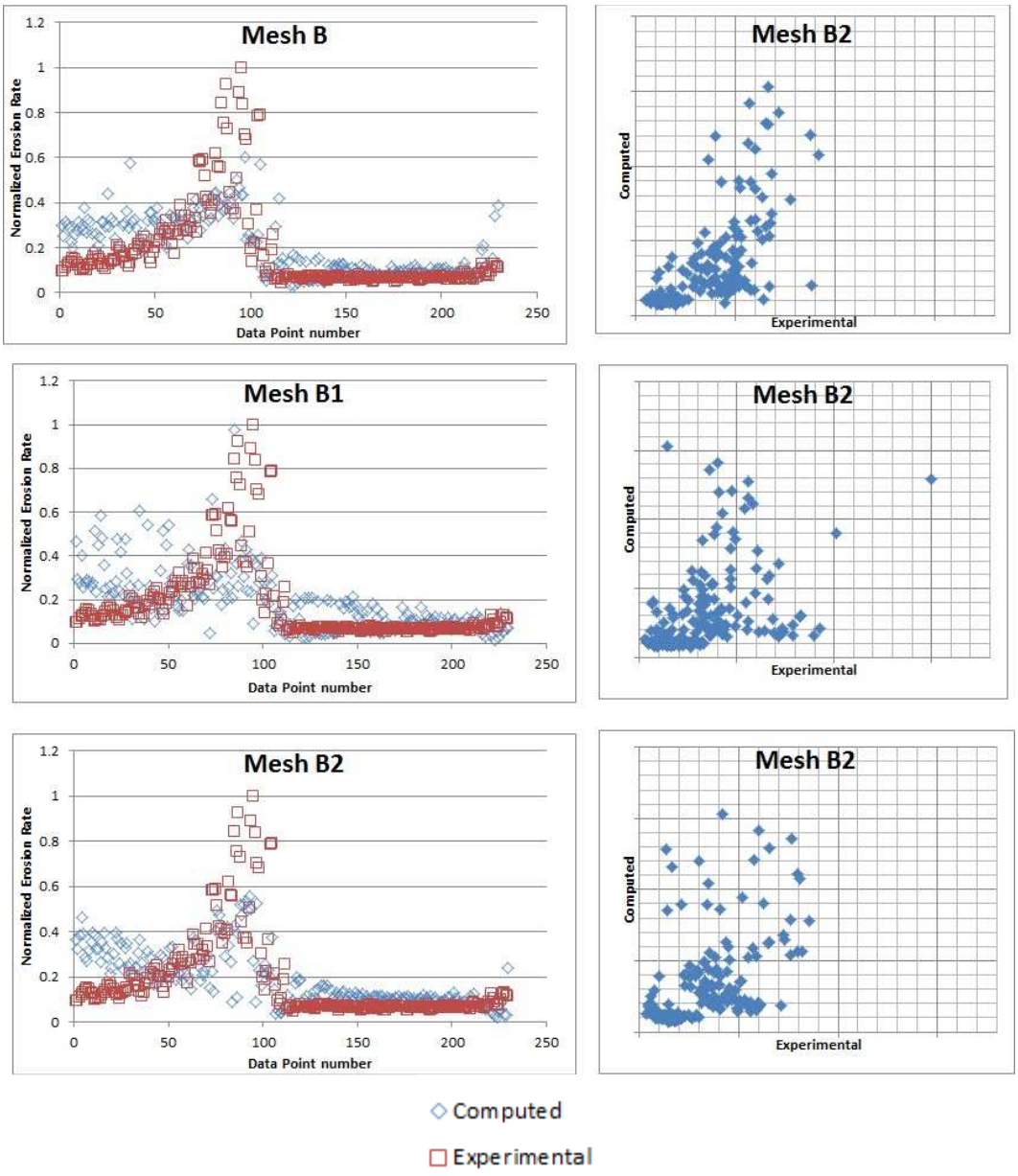

Figure 50 Comparison plot (top) and regression plot(bottom) for Test 2

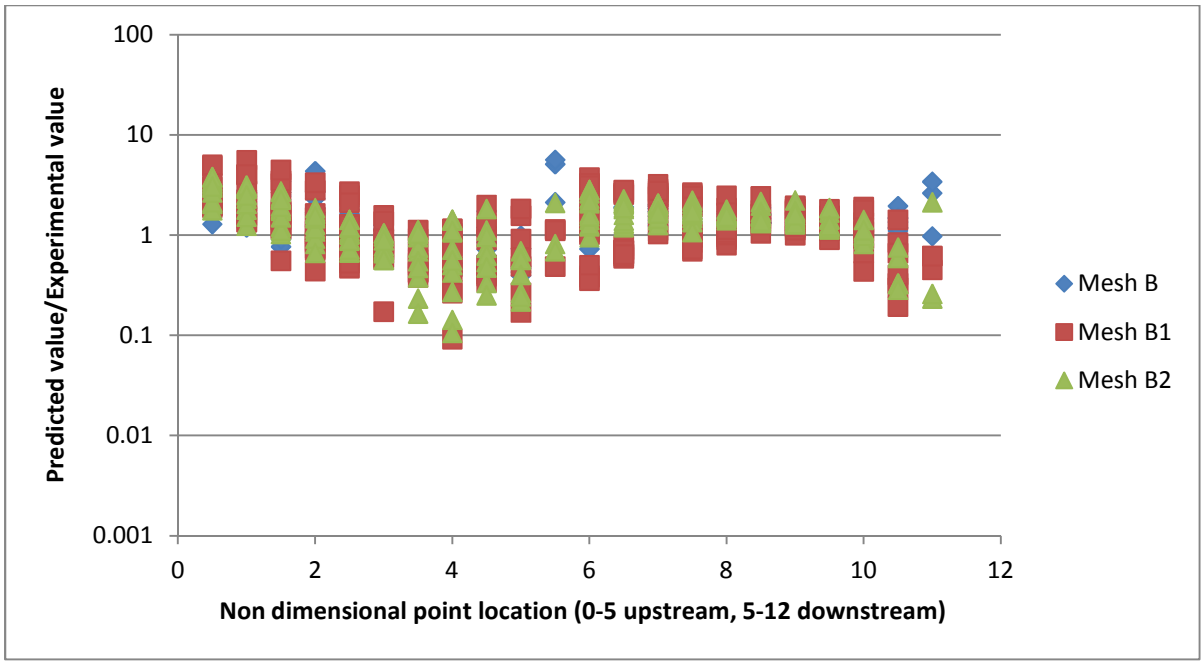

Figure 51 Error ratio plot for Test 2

All the grids seem to give similar results. Mesh B2 give slightly better results compared to other two grids.

7.3.2.3Test 3

For inlet velocity of 85.78 ft/s and 53 micron particle size , Figure 52 presents comparison plot and regression plot and

Figure 53 presents error ration plots

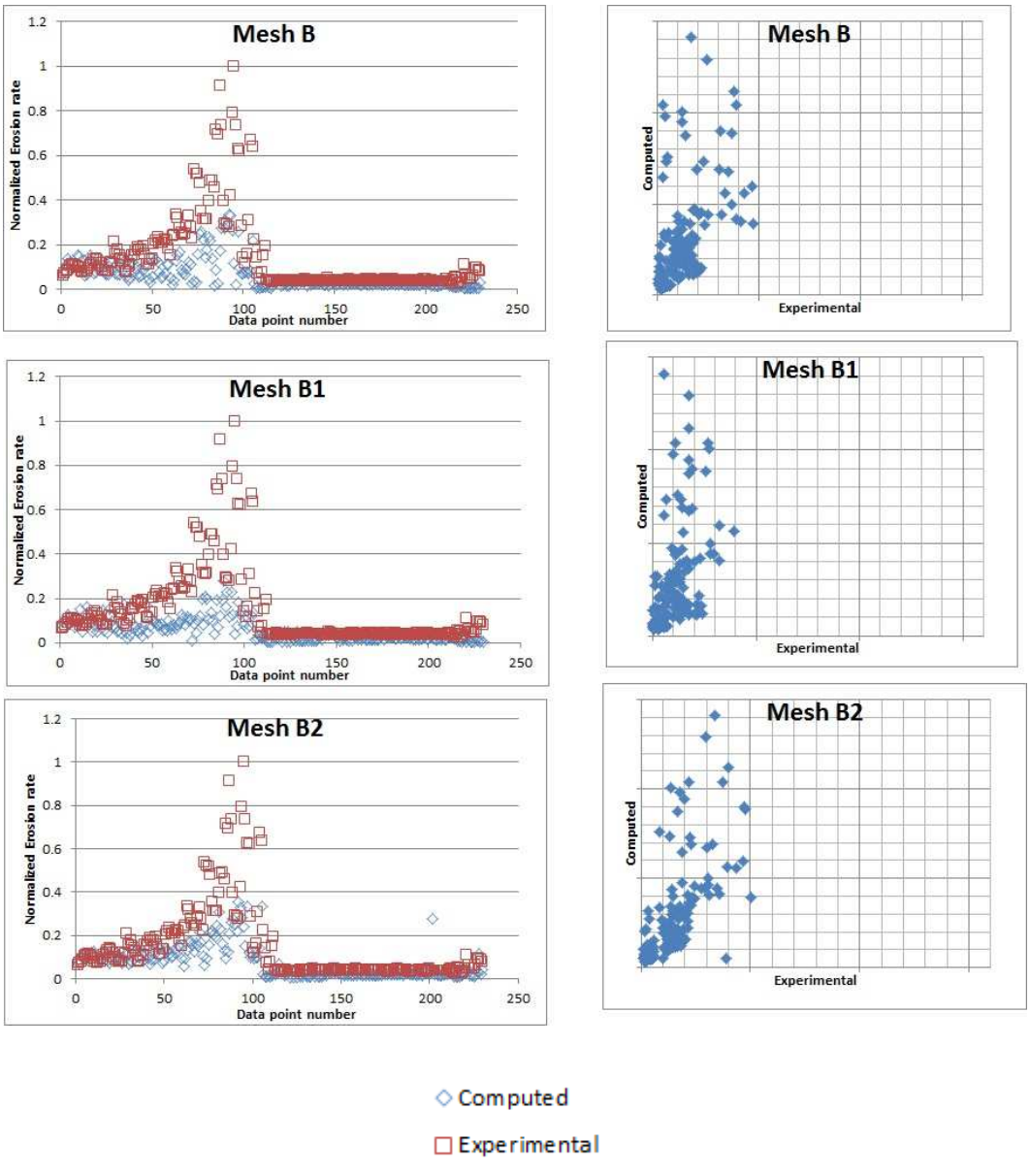

Figure 52 Comparison plot (top) and regression plot(bottom) for Test 3

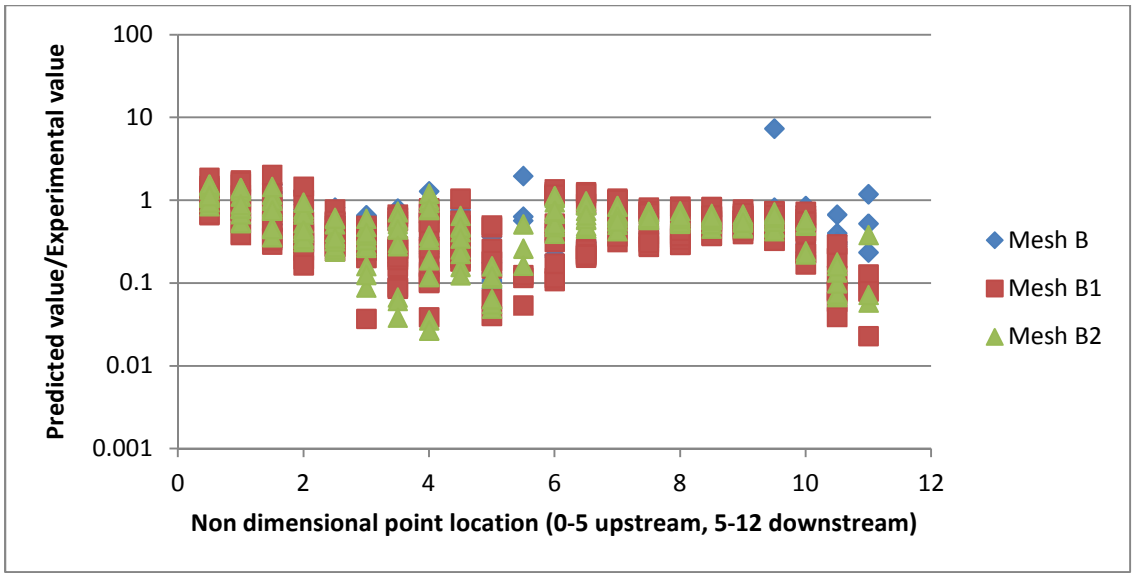

Figure 53 Error ratio plot for Test 3

Again for Test 3, each grid has almost equivalent performance. A slightly better performance from mesh B2 is seen. But it need to be quantified to be sure.

7.3.2.4Test 4

Figure 54 below presents Comparison plot and regression plot for 256 microns particle size and 85.78 ft/s inlet velocity. Error ratio plots are presented in Figure 55

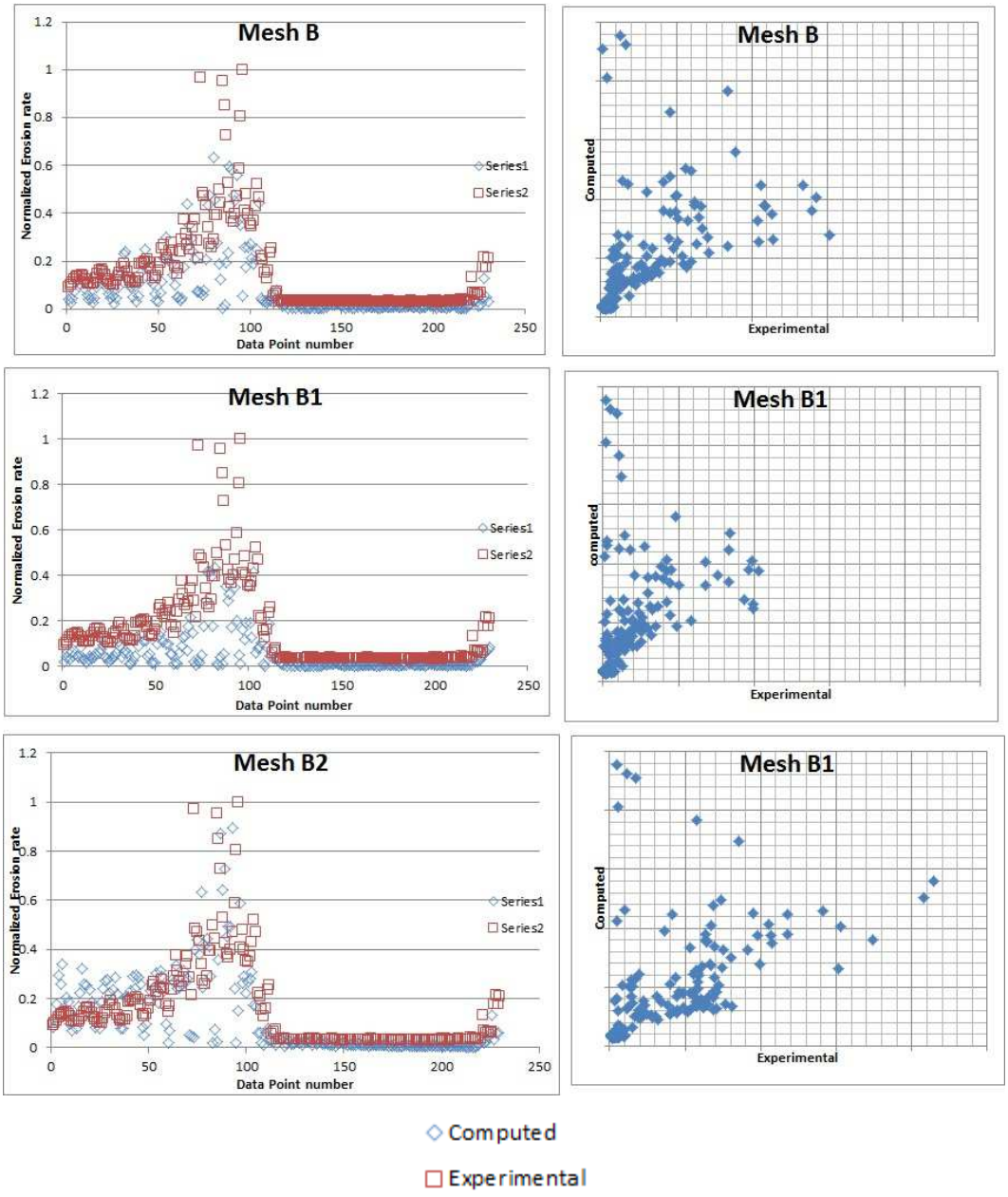

Figure 54 Comparison plot (top) and regression plot(bottom) for Test 4

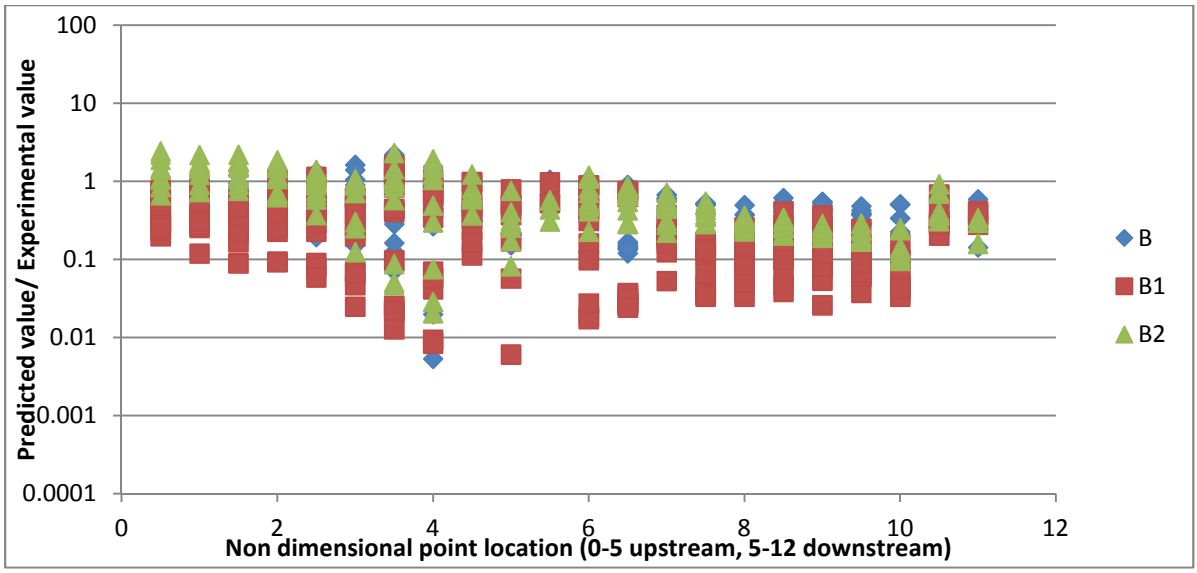

Figure 55 Error ration plot for Test 4

In this case, it is clearly observed that again Mesh B2 is more accurate compared to other two meshes in terms of quantitative prediction.

7.3.2.5 Results in Quantifiable Terms

For particle size of 256 microns, it is clearly observed that mesh B2 is more accurate whereas for 53 microns particle size, it is very close call. Hence, the results in terms of quantifiable parameter minimization function are presented here.

Minimization function is defined as :

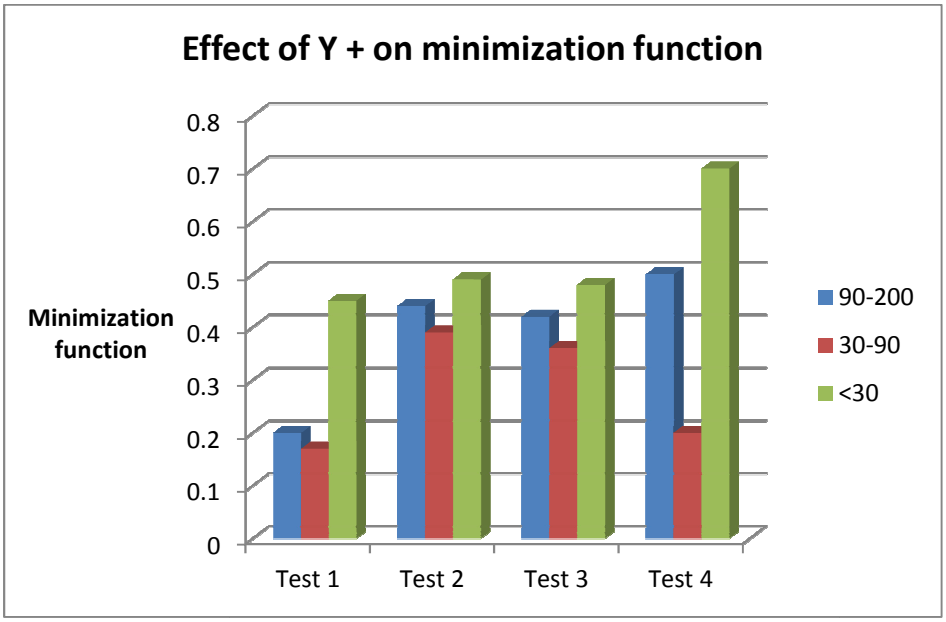

Figure 56 Minimization function comparision

Also, percentage error for all seven mesh in consideration is presented in figure below. X axis represents mesh number as described in Table 3.

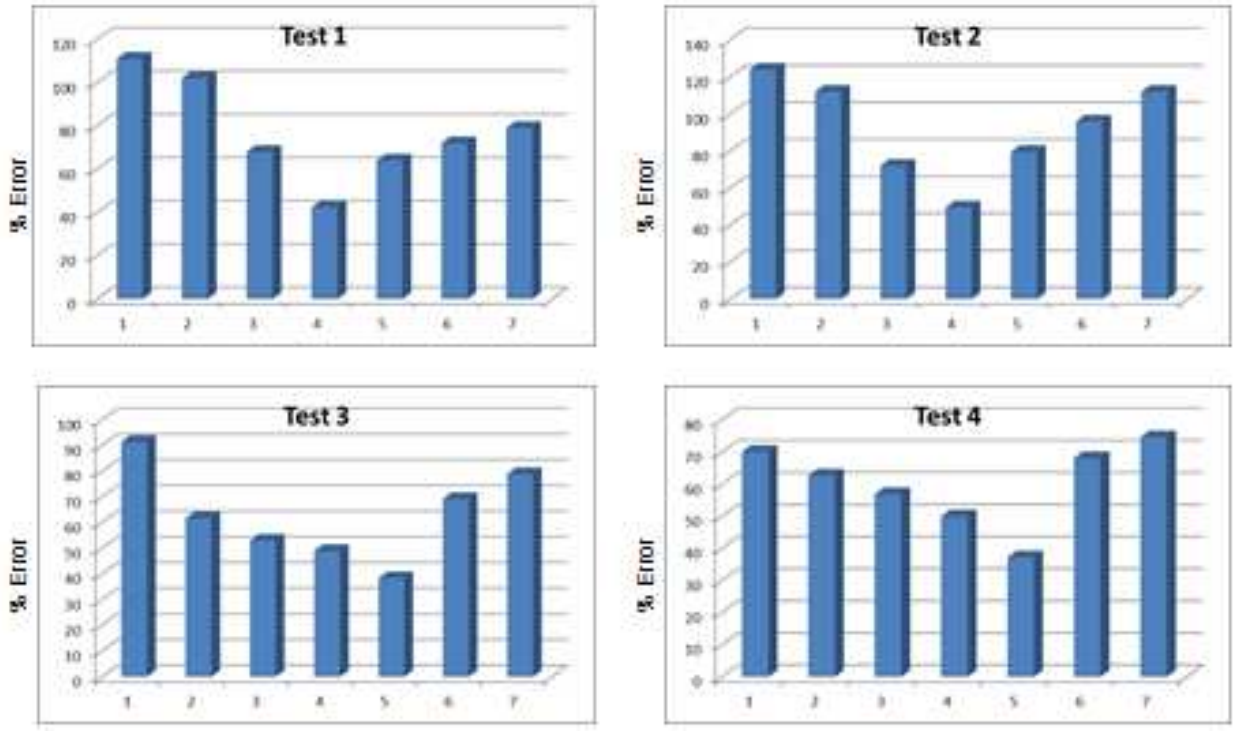

Figure 57 Percentage error for different mesh for full model

Both percentage error graphs and minimization function graphs clearly depict that mesh 4 or 5 which correspond to wall y+ values of 30-300 predict erosion rates most accurately. A error ratio comparison for present Baker Hughes model and improved CFD modeling is represent in figure below. The percentage error is reduced from 57% to 39% . This depicts a 31.5 % improvement in overall predictions by just by implementation of appropriate CFD modeling techniques.

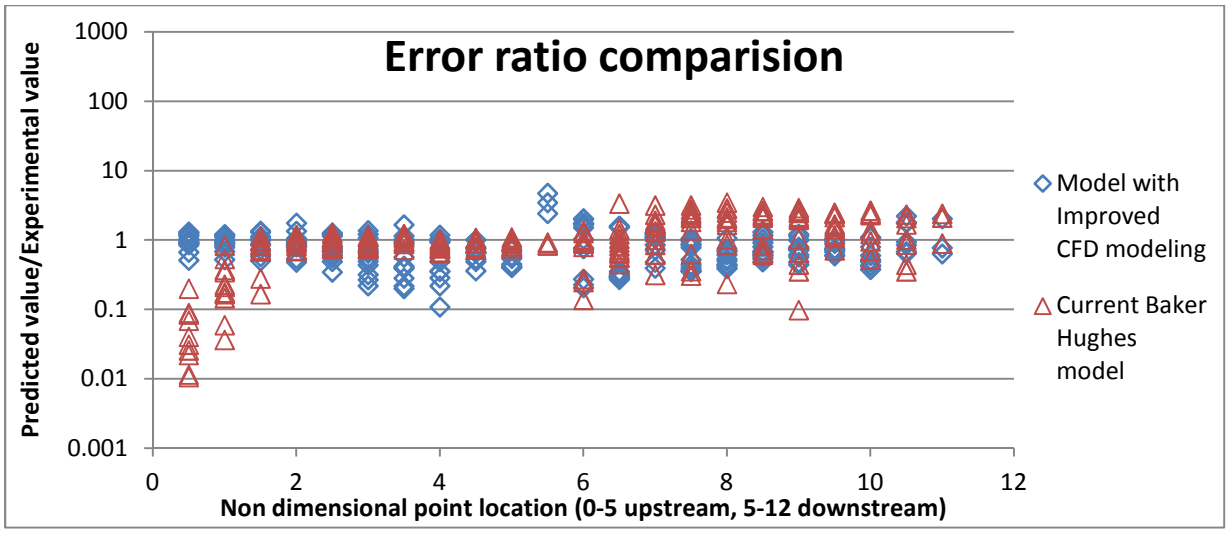

Figure 58 Error ratio comparison for current model before and after improved CFD modeling technique

7.4Development of New Models

Various new models are developed by performing regression analysis and curve fitting. Models and algorithms used in this analysis are discussed in details in previous chapters.

7.4.1Statistical and Correlation Analysis

It was clearly observed that type of grid has great effect on erosion rate prediction. Effect of mesh on DPM concentration, Velocity, Shear stress and Turbulent Kinetic Energy is studies by analyzing standard deviation for each parameter for 7 different mesh sizes.

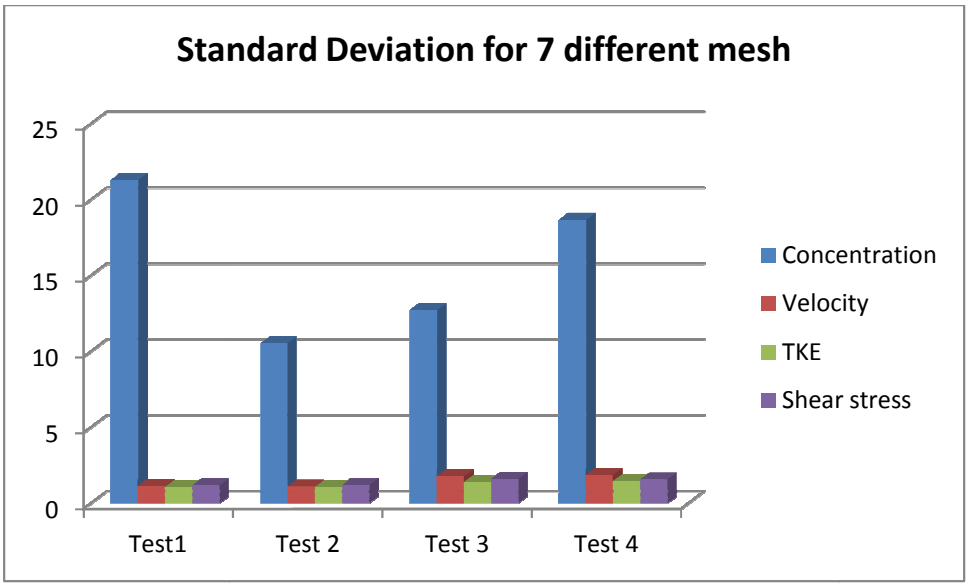

Figure 59 Standard deviation of critical parameters for different mesh sizes

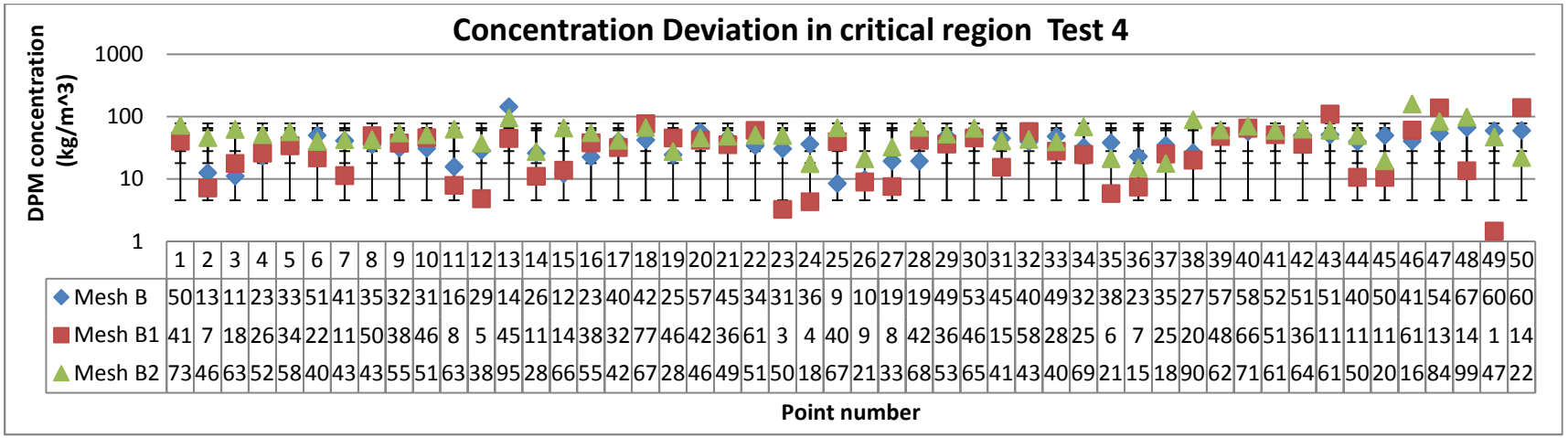

	1	2	3	4	5	6	7	8	9	10	11	12	13	14	15	16	17	18	19	20	21	22	23	24	25	26	27	28	29	30	31	32	33	34	35	36	37	38	39	40	41	42	43	44	45	46	47	48	49	50
Mesh B	50	13	11	23	33	51	41	35	32	31	16	29	14	26	12	23	40	42	25	57	45	34	31	36	9	10	19	19	49	53	45	40	49	32	38	23	35	27	57	58	52	51	51	40	50	41	54	67	60	60
Mesh B1	41	7	18	26	34	22	11	50	38	46	8	5	45	11	14	38	32	77	46	42	36	61	3	4	40	9	8	42	36	46	15	58	28	25	6	7	25	20	48	66	51	36	11	11	11	61	13	14	1	14
Mesh B2	73	46	63	52	58	40	43	43	55	51	63	38	95	28	66	55	42	67	28	46	49	51	50	18	67	21	33	68	53	65	41	43	40	69	21	15	18	90	62	71	61	64	61	50	20	16	84	99	47	22

Figure 60 Deviation of DPM concentration in critical region

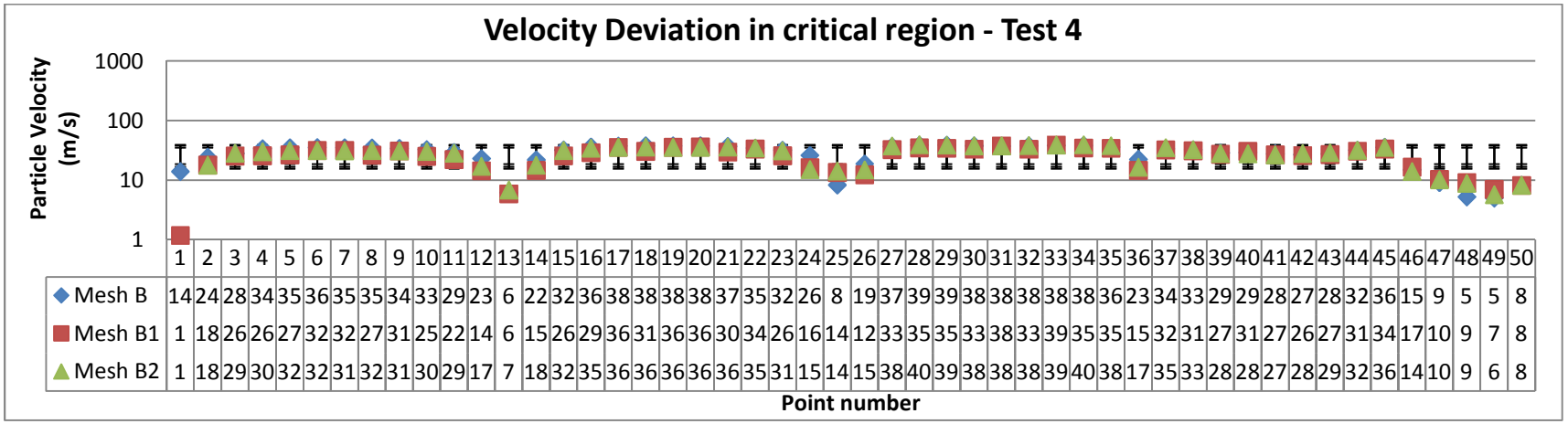

	1	2	3	4	5	6	7	8	9	10	11	12	13	14	15	16	17	18	19	20	21	22	23	24	25	26	27	28	29	30	31	32	33	34	35	36	37	38	39	40	41	42	43	44	45	46	47	48	49	50
Mesh B	14	24	28	34	35	36	35	35	34	33	29	23	6	22	32	36	38	38	38	38	37	35	32	26	8	19	37	39	39	38	38	38	38	38	36	23	34	33	29	29	28	27	28	32	36	15	9	5	5	8
Mesh B1	1	18	26	26	27	32	32	27	31	25	22	14	6	15	26	29	36	31	36	36	30	34	26	16	14	12	33	35	35	33	38	33	39	35	35	15	32	31	27	31	27	26	27	31	34	17	10	9	7	8
Mesh B2	1	18	29	30	32	32	31	32	31	30	29	17	7	18	32	35	36	36	36	36	36	35	31	15	14	15	38	40	39	38	38	38	39	40	38	17	35	33	28	28	27	28	29	32	36	14	10	9	6	8

Figure 61 Deviation of Velocity in critical region

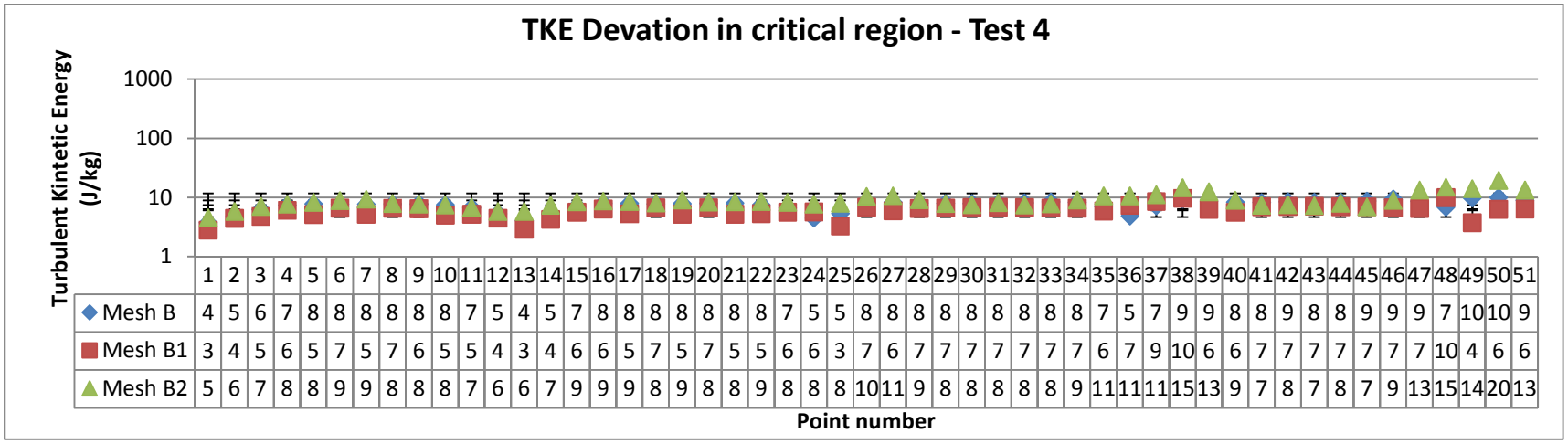

	1	2	3	4	5	6	7	8	9	10	11	12	13	14	15	16	17	18	19	20	21	22	23	24	25	26	27	28	29	30	31	32	33	34	35	36	37	38	39	40	41	42	43	44	45	46	47	48	49	50	51
Mesh B	4	5	6	7	8	8	8	8	8	8	7	5	4	5	7	8	8	8	8	8	8	8	7	5	5	8	8	8	8	8	8	8	8	8	7	5	7	9	9	8	8	9	8	8	9	9	9	7	10	10	9
Mesh B1	3	4	5	6	5	7	5	7	6	5	5	4	3	4	6	6	5	7	5	7	5	5	6	6	3	7	6	7	7	7	7	7	7	7	6	7	9	10	6	6	7	7	7	7	7	7	7	10	4	6	6
Mesh B2	5	6	7	8	8	9	9	8	8	8	7	6	6	7	9	9	9	8	9	8	8	9	8	8	8	10	11	9	8	8	8	8	8	9	11	11	11	15	13	9	7	8	7	8	7	9	13	15	14	20	13

Figure 62 Deviation of Turbulent Kinetic Energy in critical region

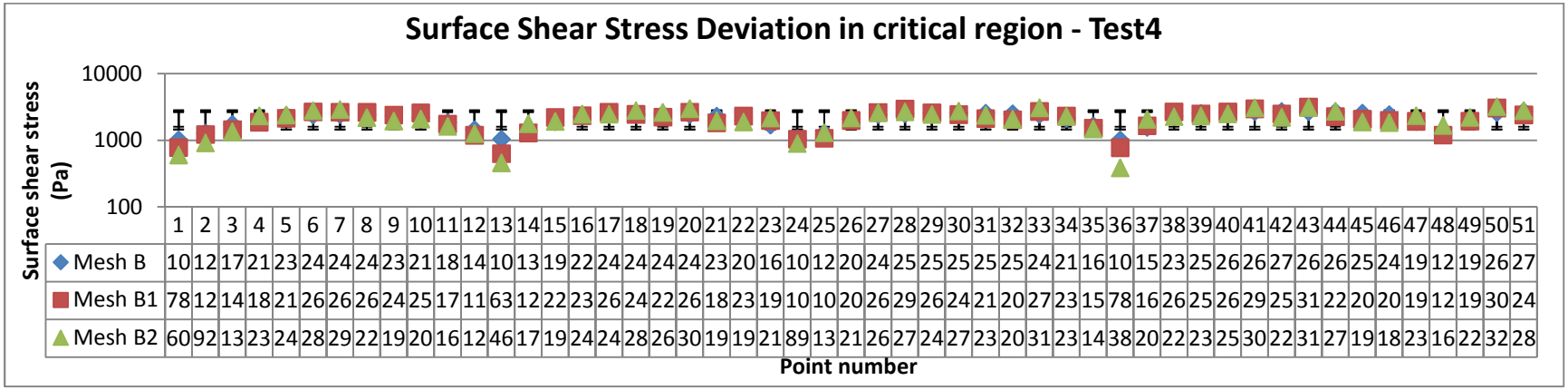

	1	2	3	4	5	6	7	8	9	10	11	12	13	14	15	16	17	18	19	20	21	22	23	24	25	26	27	28	29	30	31	32	33	34	35	36	37	38	39	40	41	42	43	44	45	46	47	48	49	50	51
Mesh B	10	12	17	21	23	24	24	24	23	21	18	14	10	13	19	22	24	24	24	24	23	20	16	10	12	20	24	25	25	25	25	25	24	21	16	10	15	23	25	26	26	27	26	26	25	24	19	12	19	26	27
Mesh B1	78	12	14	18	21	26	26	26	24	25	17	11	63	12	22	23	26	24	22	26	18	23	19	10	10	20	26	29	26	24	21	20	27	23	15	78	16	26	25	26	29	25	31	22	20	20	19	12	19	30	24
Mesh B2	60	92	13	23	24	28	29	22	19	20	16	12	46	17	19	24	24	28	26	30	19	19	21	89	13	21	26	27	24	27	23	20	31	23	14	38	20	22	23	25	30	22	31	27	19	18	23	16	22	32	28

Figure 63 Deviation of Surface Shear Stress in critical region

Figure 60 to Figure 63 show deviation of DPM concentration, Velocity, Turbulent kinetic energy and Surface shear stress for test 4 in critical region . It is clearly observed from above figures as well as from standard deviation bar chart, that DPM concentration is highly effected by Mesh size. As discussed in sections earlier, this is primarily due to the way Fluent calculates DPM concentration. Thus, models that do not incorporate DPM concentration for erosion rate predictions are more robust and less prone to error due to meshing strategy employed.

7.4.2 Correlation Analysis

Correlation analysis is performed to identify parameters that affect erosion rate the most. This analysis is performed on 920 data points obtained from CFD analysis of all four test cases. Aim is to develop more robust erosion rate prediction model. Three different correlation coefficients are calculated. Pearson coefficient 'R' is most commonly used correlation coefficient. However, it evaluates linear correlation between parameters (Note: a linear correlation between parameters with nonlinear relationship is possible). Hence, Kendal's 'tau' and spearman's 'rho', both of which is rank correlations are also calculated. Values closer to one depict strong correlations. Figure 64 shows correlation coefficient for various parameters. To avoid statistical error, a boot strap analysis with 100 sample data set for correlation coefficient is also performed. It is a procedure to be absolutely sure about statistical parameter value obtained. Figure 65 presents bootstrap analysis results. The results agree well with correlation analysis performed. It can be observed that turbulent kinetic energy is identified as most influential parameter followed by Surface shear stress, velocity and concentration.

Impact angle does not have any conclusive correlation with erosion rate prediction. It is also verified when overall performance of ANN was degraded by including impact angle as an input variable in the model.

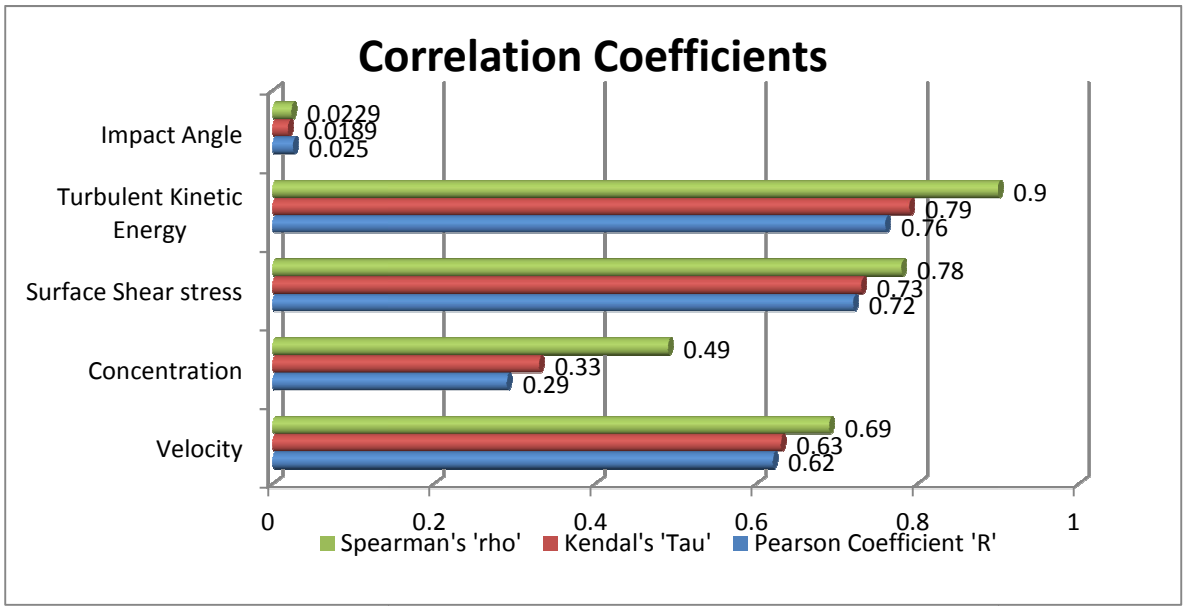

Figure 64 Correlation Coefficients

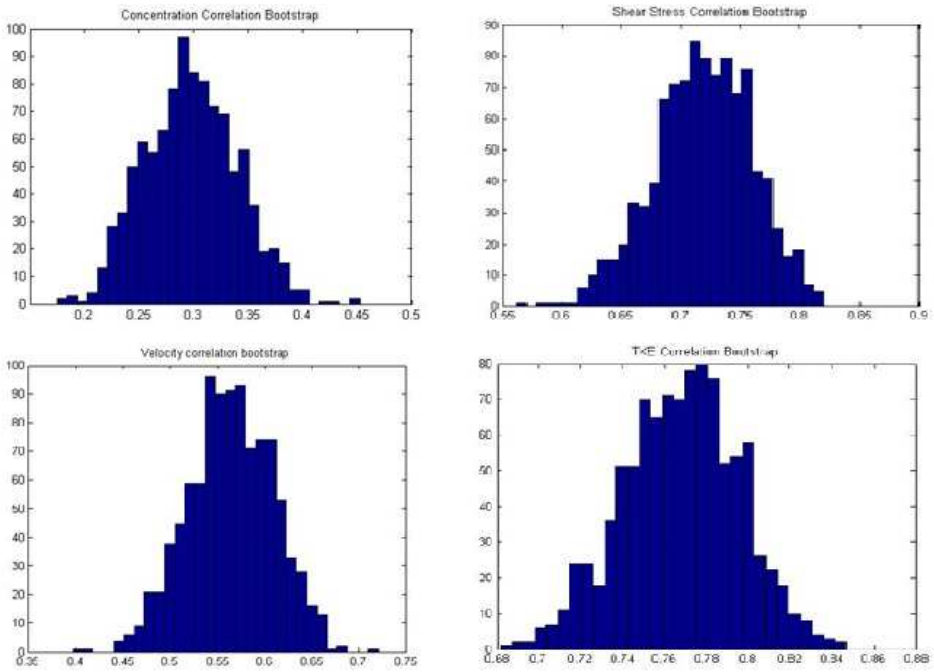

Figure 65 Correlation coefficient bootstrap results

Concentration has some positive correlation with erosion rate. An analysis is done to check if it DPM concentration can be used as a conditioning parameter in velocity based erosion models. A co-plot for Velocity, concentration and Erosion rate presented in Figure 66 shows that for every range of concentration, a similar trend line is observed. Hence, use of DPM concentration as conditioning parameter in present model is validated.

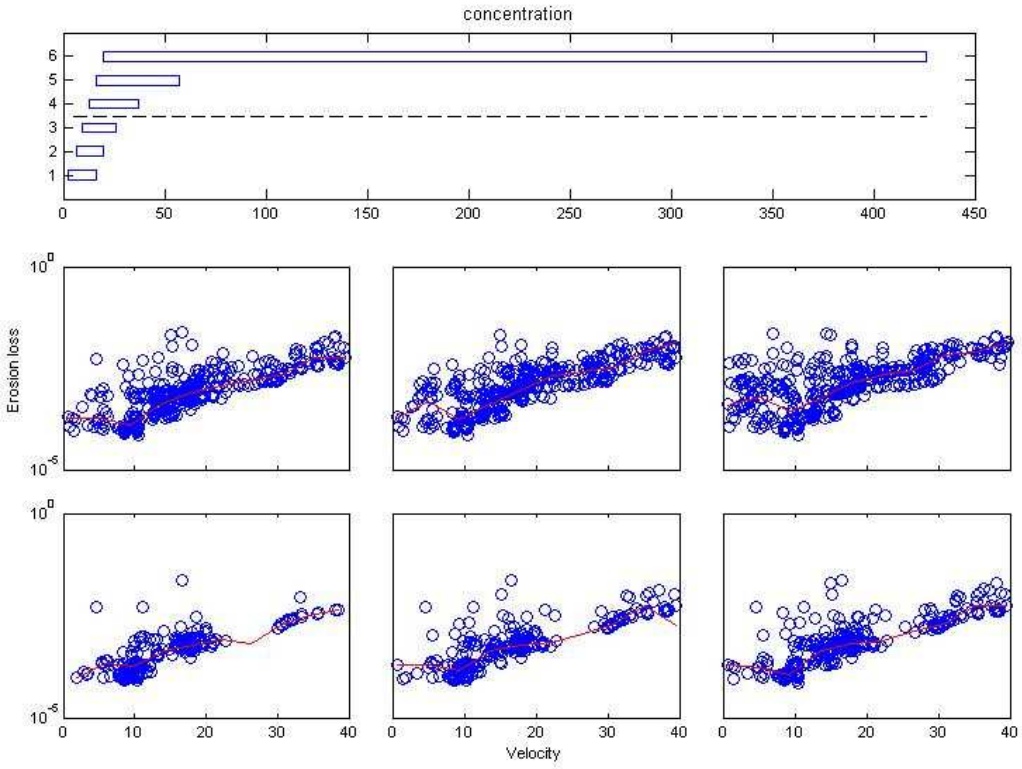

Figure 66 Velocity, Concentration, Erosion rate Co-Plot

7.4.3Models Based on Different y+ Values

As seen from previous section, mesh size has a great impact on erosion rate prediction. Different mesh may predict different value of erosion rate. It is therefore beneficial to develop models specific to y+ range obtained from CFD simulations. Current Baker Hughes model is refitted and new parameters in the model are obtained by curvefitting of combined data of all four test cases. Parameters for 3 different y+ range are obtained i.e. current model is personalized with new parameters depending on y+ range.

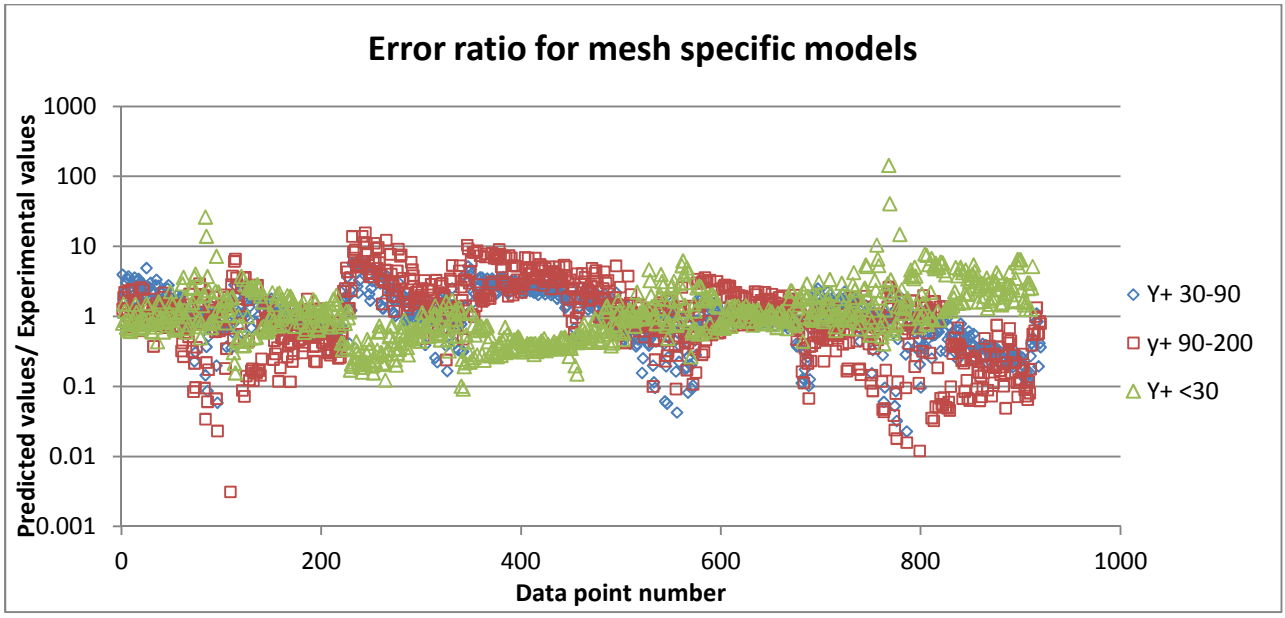

Figure 67 Error ratio plot for three different mesh specific model paramete

Goodness of fit parameter SSE, R-square, RSME and percentage error are presented below:

Table 5 Goodness of fit parameter for mesh specific models

	SSE	R -square	RSME	Percentage error
y+ 90-200	1.71E-07	0.992	3.70E-05	37
Y+ 30-90	5.70E-07	0.9957	2.50E-05	34
Y+ < 30	1.12E-07	0.9927	1.10E-05	31

A slight improvement in erosion rate prediction in terms of mean percentage error is observed in each model. Also, all three models have close performance measures. Thus depending upon the Y+ range necessary for CFD analysis, model with corresponding parameters can be utilized to predict erosion rate. (E/C =erosion rate/DPM concentration)

Curve fit for each model are presented below:

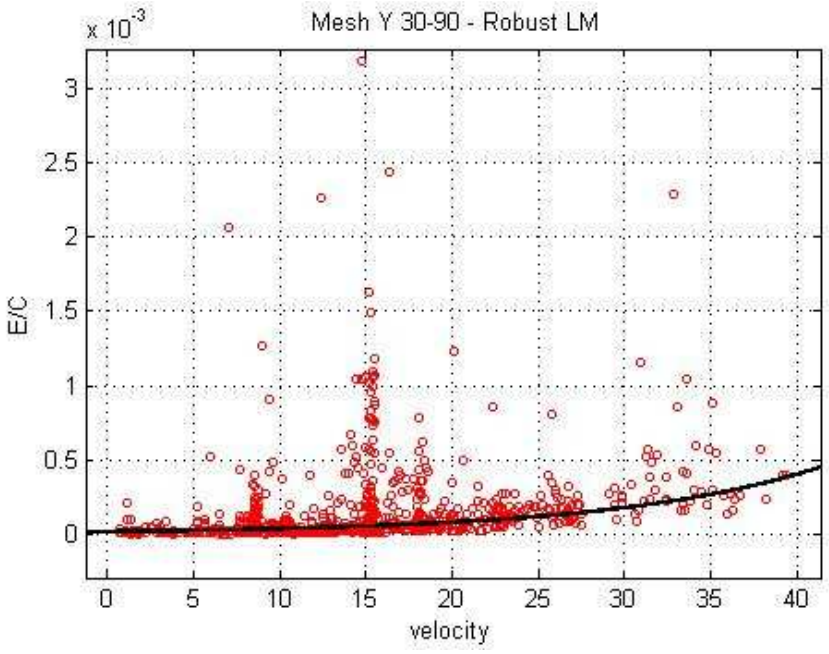

Figure 68 Curve fit for Y+ 30-90 model

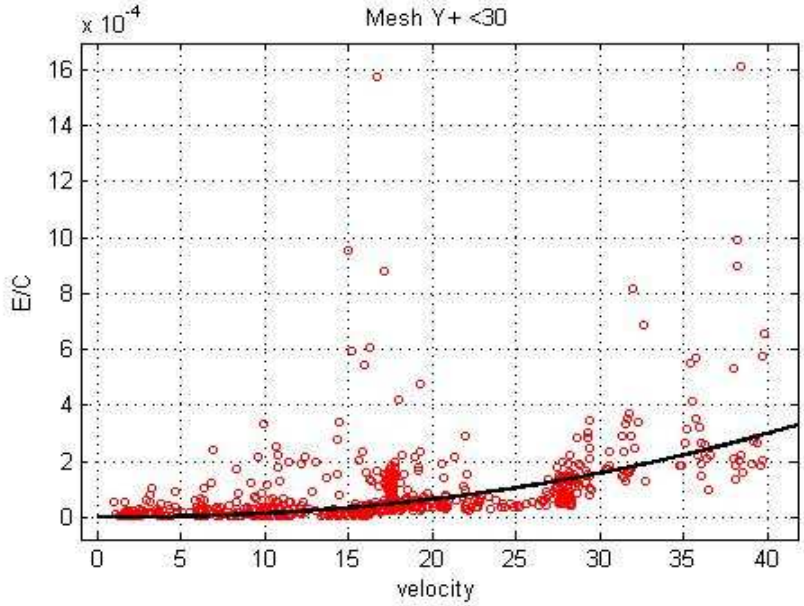

Figure 69 Curve fit for Y+ <30

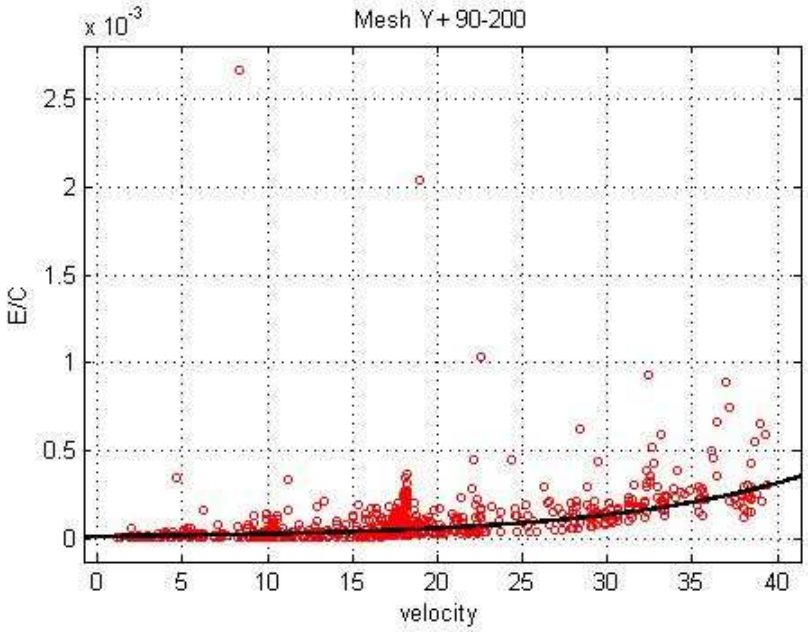

Figure 70 Curve fit for Y+ 90-200

7.4.4Surface Fit Models

Two different surface fit models were developed, Erosion rate- Concentration-Velocity model, and Erosion rate-TKE-Shear stress model. The surface fit for each is show in figures below. TKE-Shear stress based model showed better results compared to other.

Table 6 Surface fit models - goodness of fit parameters

	SSE	R -square	RSME	Percentage error
Erosion rate-Velocity-Concentration model	7.52E-05	0.9619	1.32E-03	52
Erosion rate-TKE-Shear stress model	2.43E-05	0.9867	3.46E-04	48

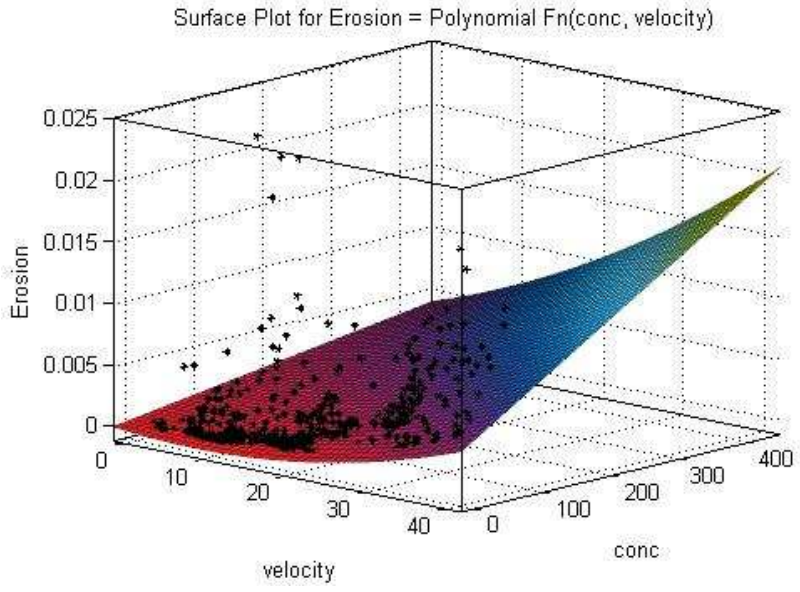

Figure 71 Erosion rate-Concentration – Velocity surface fit

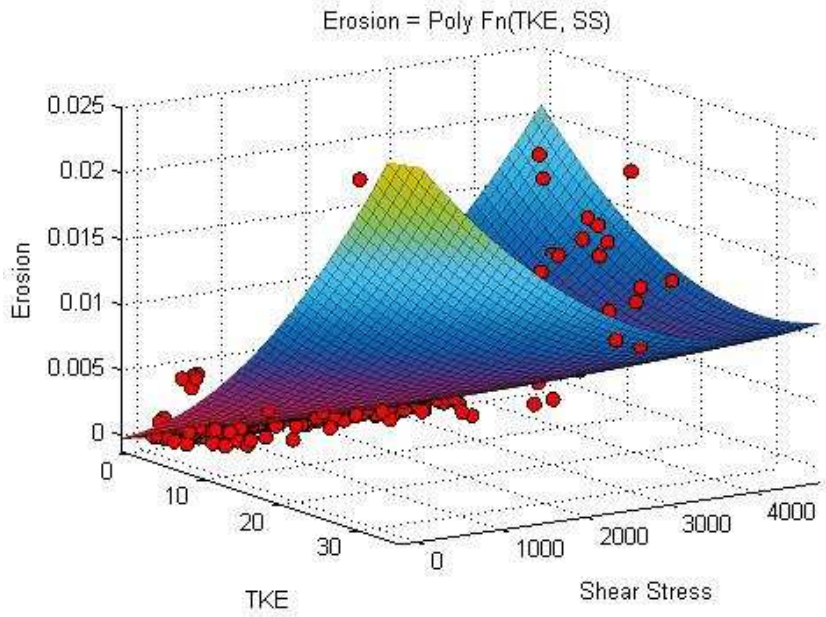

Figure 72 Erosion rate- TKE -Shear Stress model surface fit

7.4.5Surface Shear Stress Model

Surface shear stress has a strong positive correlation with erosion rate and hence curve fitting through regression is performed to develop an erosion model as a function of Surface shear stress. Two different models are developed, polynomial model and exponential model. Results for which are presented below. Exponential fit has lesser percentage error of 42 % mean error. Regression plots for exponential plot is shown

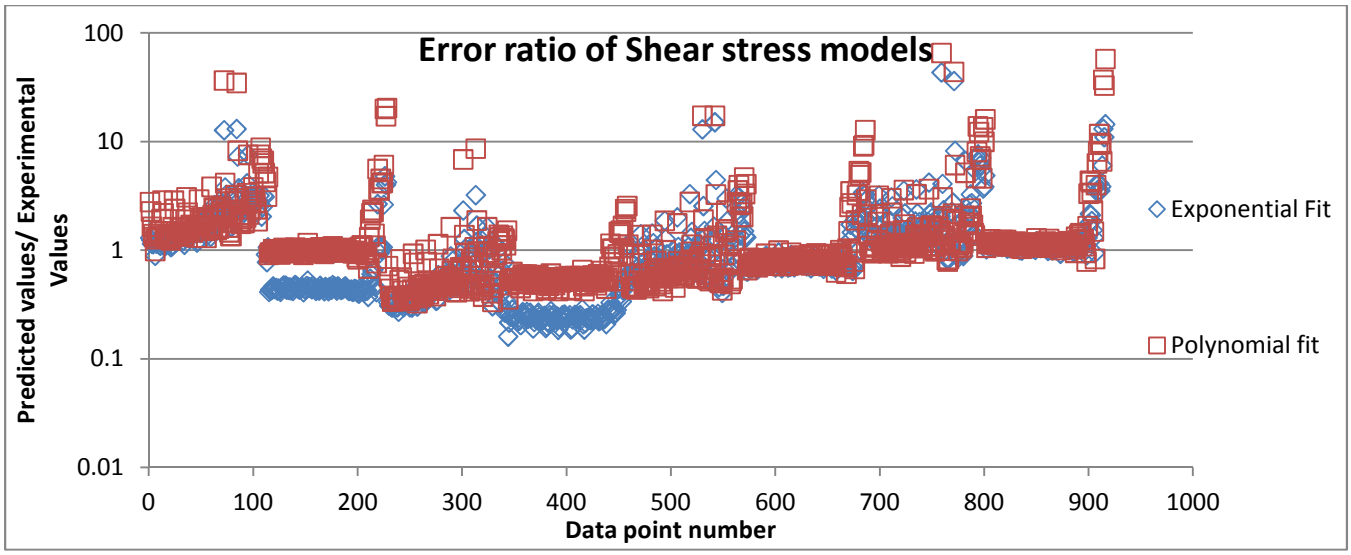

Figure 73 Surface Shear stress models -Error ratio

Table 7 Shear stress model - Goodness of fit parameters

	SSE	R -square	RSME	Percentage error
Polynomial fit	5.94E-05	0.9919	2.55E-04	47
Exponential fit	2.43E-05	0.9967	1.63E-04	42

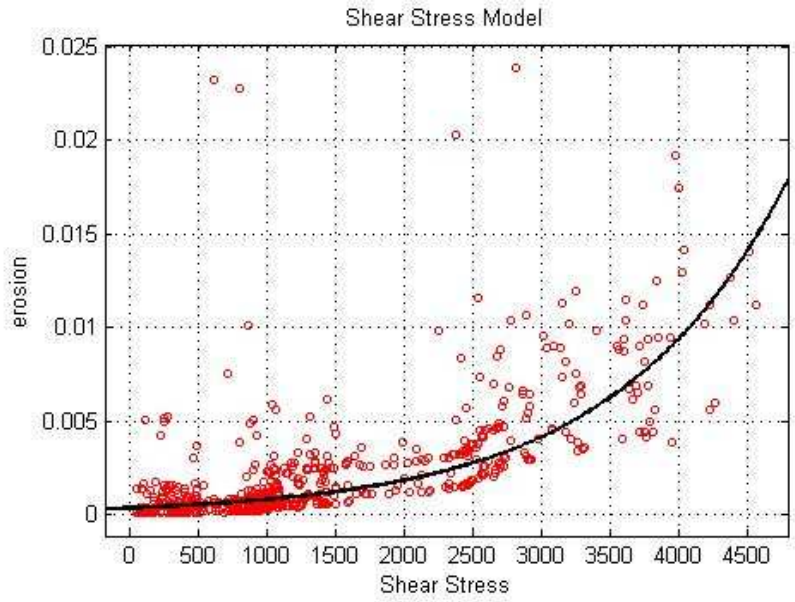

Figure 74 Exponential curve fit for Surface Shear stress model

7.4.6Turbulent Kinetic Energy (TKE) Models

Pearson's rank correlation coefficient showed a very strong positive correlation between TKE and erosion rate. Thus, as expected, TKE based model proved to be very efficient. Following Figure 75 shows Error ration plots and Table 8 presents goodness of fit data for TKE based models. Three different models were developed linear fit, 5th degree polynomial fit and an exponential fit. Only polynomial fit and exponential fit , which showed great results , are presented below;

Table 8 TKE models - Goodness of fit parameters

	SSE	R -square	RSME	Percentage error
5th degree polynomial	2.10E-07	0.9801	1.52E-05	31
Exponential	4.60E-08	0.9935	7.10E-06	29

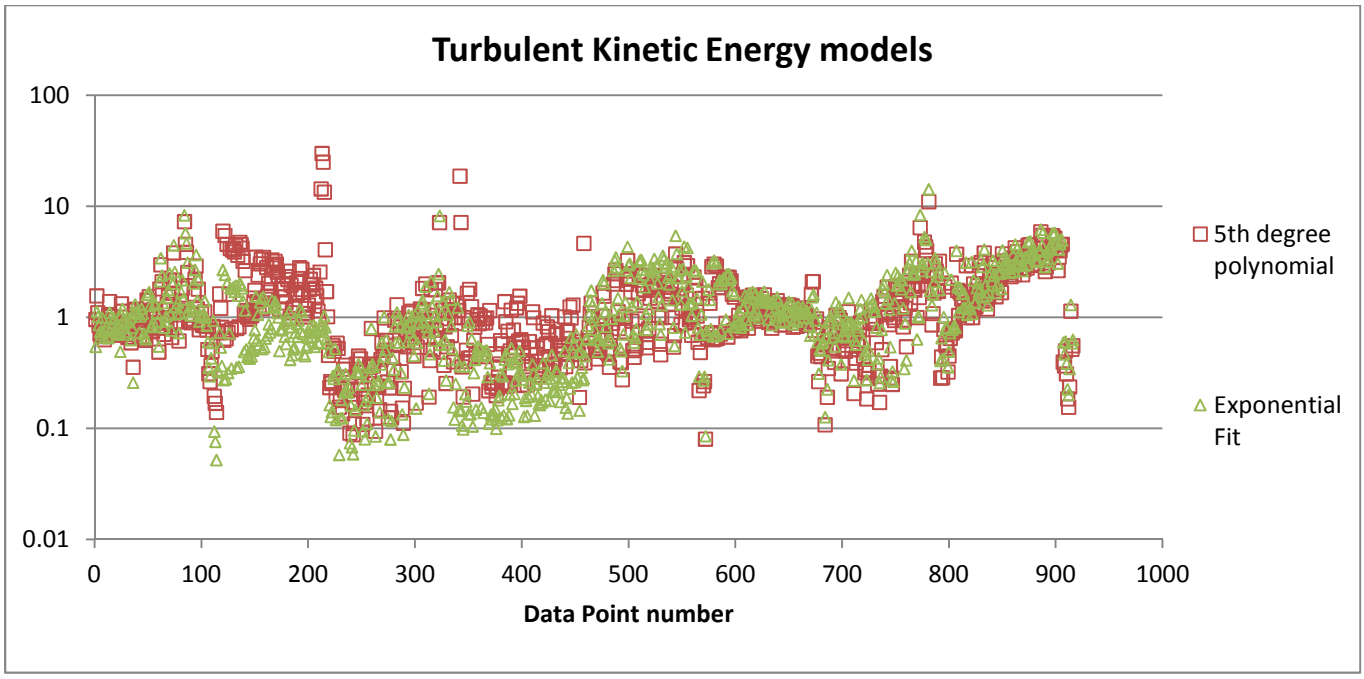

Figure 75 Error ratio for TKE based models

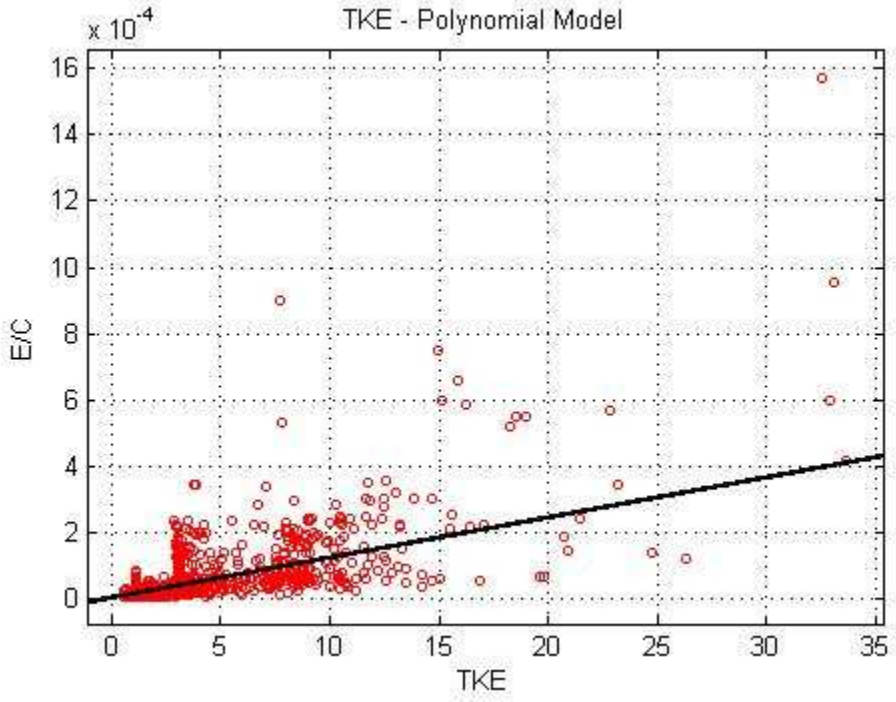

Figure 76 TKE liner polynomial model curve fit

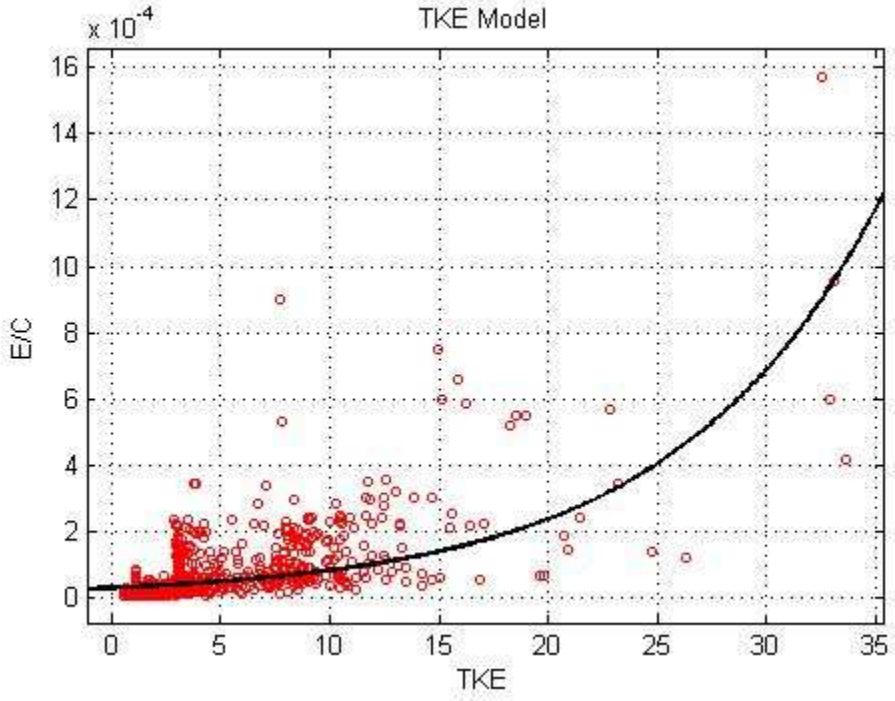

Figure 77 TKE model exponential curve fit

Exponential fit for TKE vs. Erosion rate gives the best predictions. It also shows excellent goodness of fit parameter values. The R-squared value if 0.9972 which is one of the best seen so far. Also mean percentage error is 29% which is great. It should also be observed that TKE model provides a better fit for large range as well as seen from Figure 77 above.

7.5Artificial Neural Network (ANN) Based Erosion Model

ANN model is developed as a black box to predict erosion rate. Four most influential parameters, Velocity, Concentration, TKE and surface shear stress were taken as input parameter to the ANN and Erosion rate was considered target variable. A multilayer feedforward- backpropogation algorithm with Lavernberg-Marquardt training

is implemented. A Bayesian regularization on Training algorithm give best results. More than 45 different networks were modeled and analyzed. Description and Goodness of fit parameters for 11 different ANN models is presented in table below:

Table 9 ANN model description and goodness of fit parameters

Model Number	Model	R-Square value	RSME
1	4-[20]-1	0.8757	7.2e-6
2	4-[35]-1	0.8987	6.3e-6
3	4-[50]-1	0.9224	2.4e-6
4	4-[10-10]-1	0.9654	1.1e-6
5	4-[20-20]-1	0.9845	1.8e-6
6	4-[10-20]-1	0.9799	5.1e-6
7	4-[40-40]-1	0.9523	6.9e-6
8	4-[10-10-10]-1	0.9664	2.7e-7
9	4-[15-10-15]-1	0.9767	4.2e-7
10	4-[25-10-25]-1	0.9814	6.8e-7
11	5-[10-10-10]-1	0.667	8.3e-4

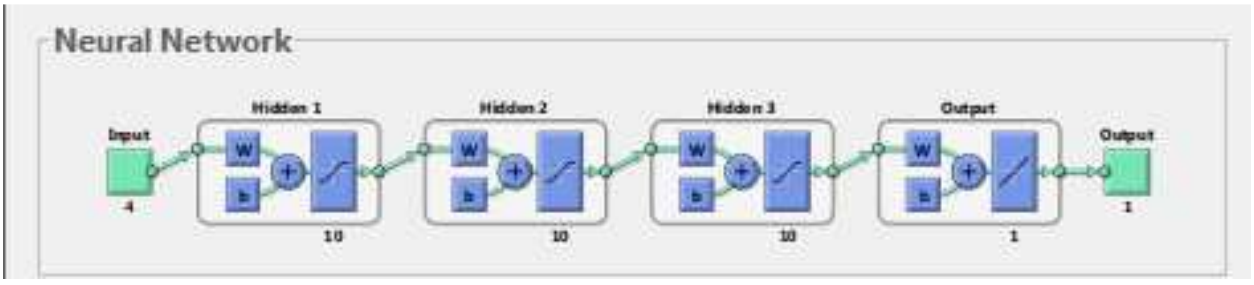

Figure 78 Neural network representation for 4-[10-10-10]-1

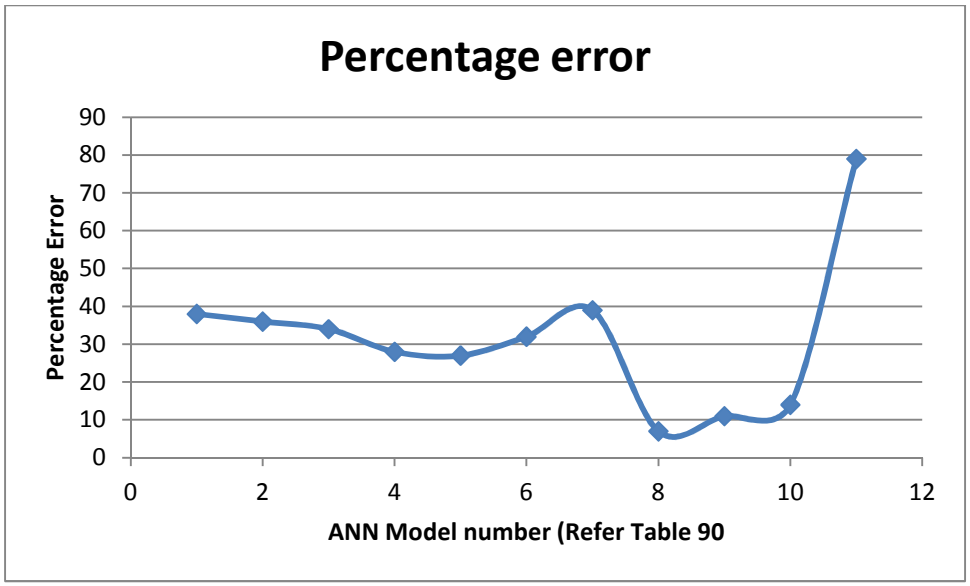

Figure 79 Error percentage for ANN models

Input parameter for 4-[10-10-10]-1 is Velocity, DPM concentration, Surface shear stress and Turbulent kinetic energy and target is experimentally observed erosion rates. Regression plot for ANN with three hidden layer and structure 4-[15-10-15]-1 with and without Bayesian regularization is presented next. Bayesian regularization avoid over fitting of the model and improved results significantly hence it is important to appreciate the comparison. A clearly visible better fit is obtained by Byesian Regularization. The mean percentage error is reduced from 27 % to as low as 7 % after regularization is forced on Lavernberg-Marquardt training algorithm. The 5-[10-10-10]-1 network represents inclusion of impact angle as an input parameter. But it is observed that it has negative effect on performance of the network.

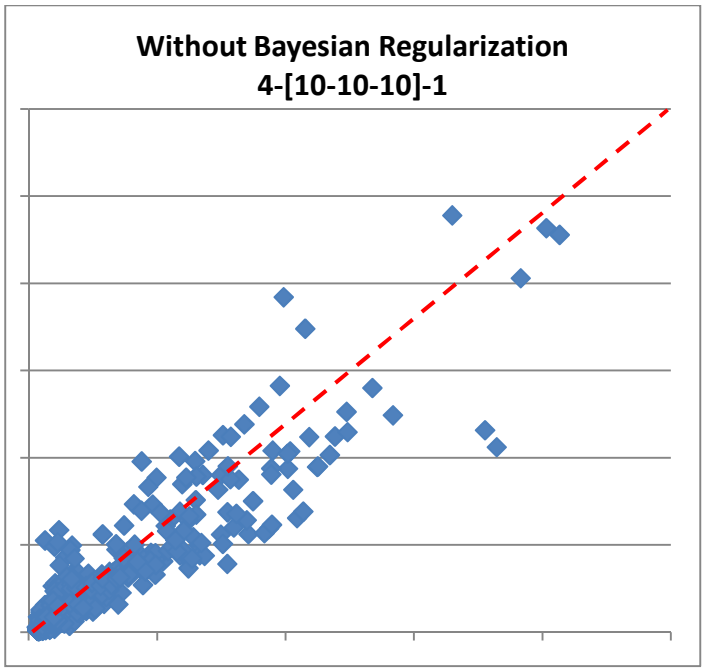

Figure 80 - ANN model without Bayesian Regularization

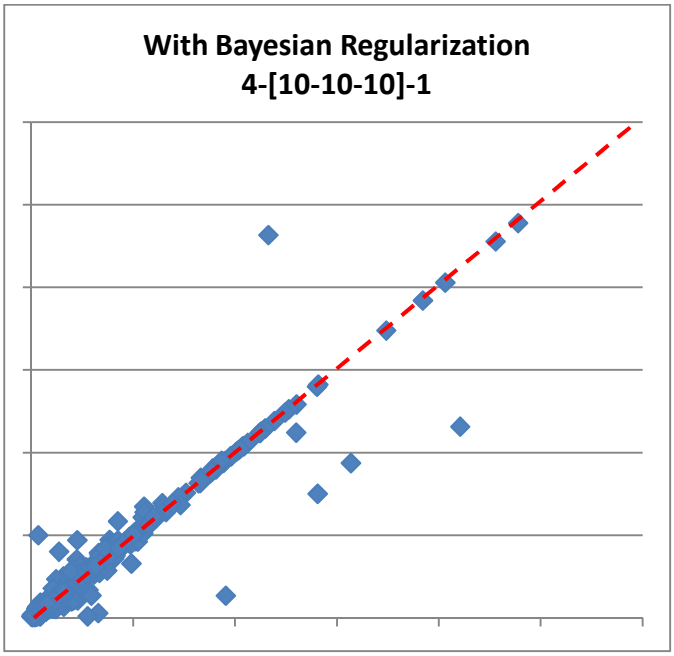

Figure 81 ANN model with Bayesian Regularization

Below is presented a graph plotting measured and predicted values for all the points.

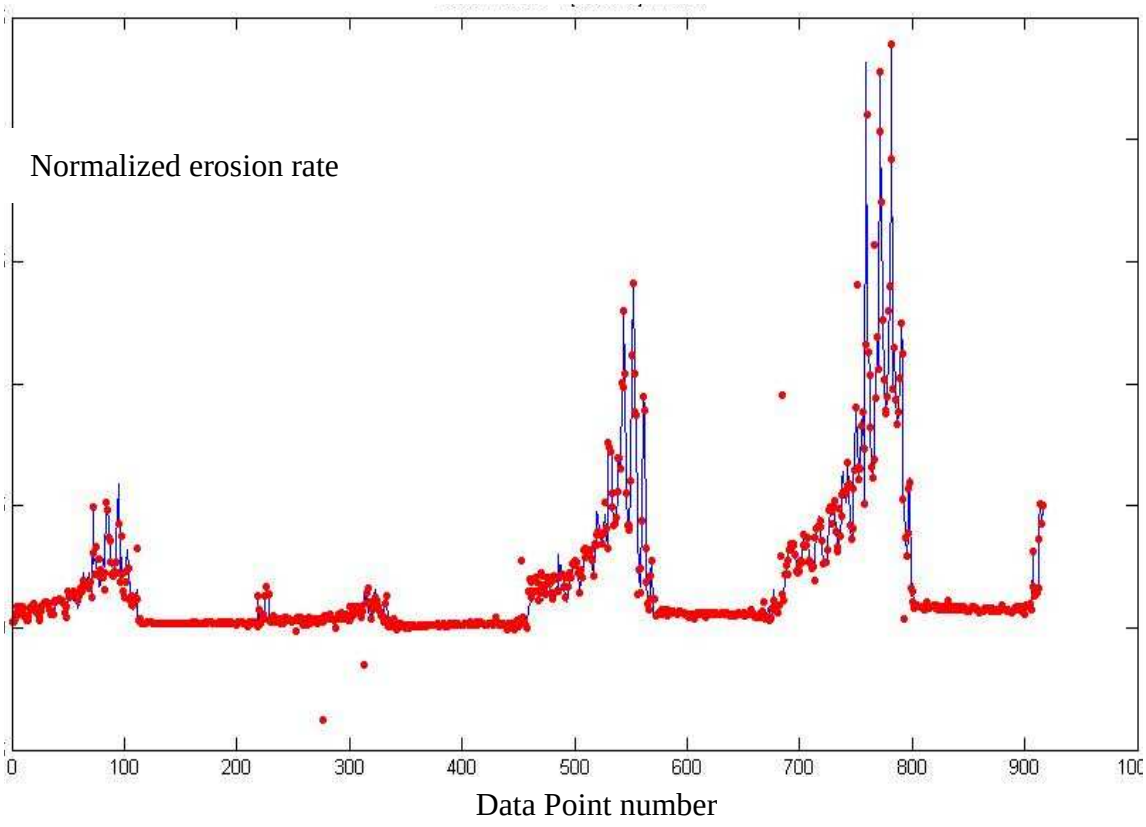

Figure 82 ANN best model fit

Reproducibility of the results by ANN has been questioned by few researchers and hence a bootstrap sampling on input parameter is performed. 100 sample input were created from current data set. Mean percentage error is presented in following histogram.

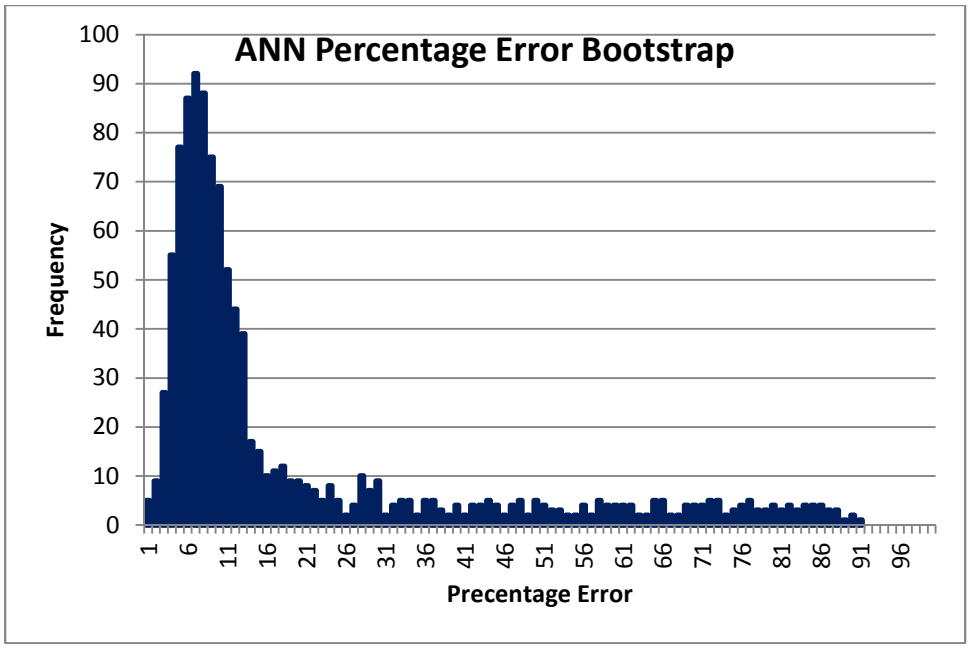

Figure 83 ANN mean percentage error bootstrap check

7.6 All Models Comparisons

Best of each model is selected and their prediction capability is compared in terms of percentage error and Error ratio in this section.

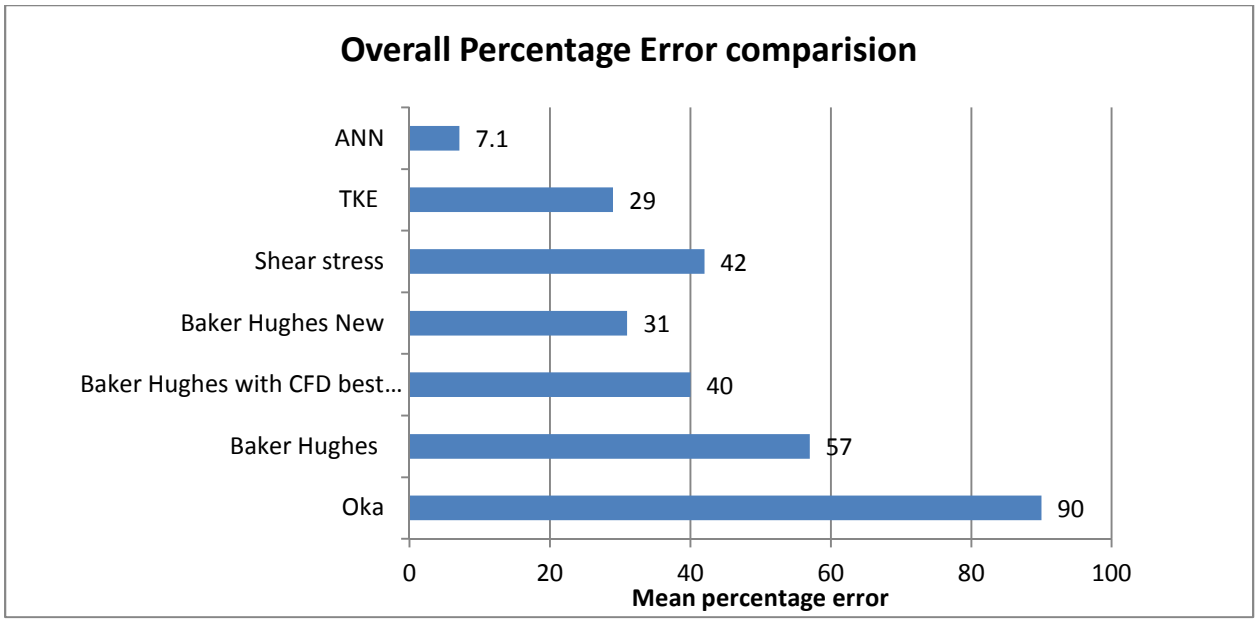

Figure 84 Percentage error comparison

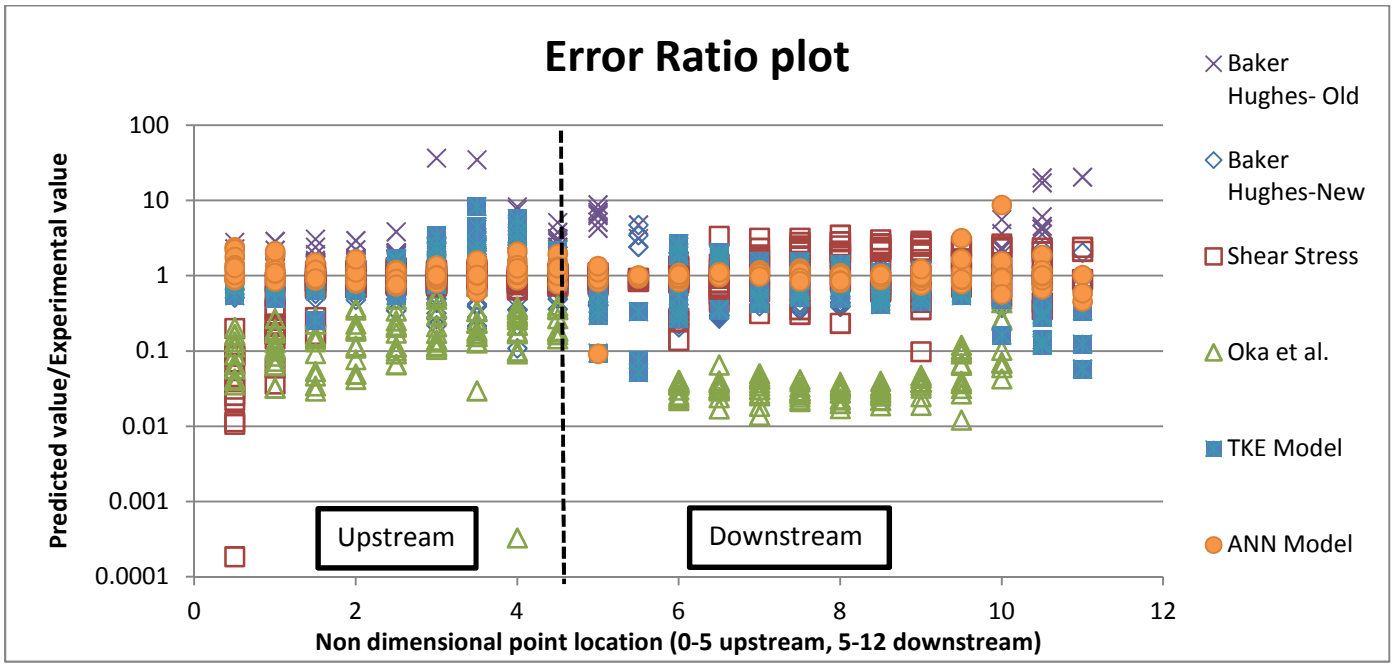

Figure 85 Error ratio plot

7.7Verification

All the models are developed based on experimental results of an elbow case. Two different sand concentration and velocities were tested but it was still the same elbow case. Hence, there was no change in geometry. Verification is necessary with different geometric case. Experimental results for test on a completion tool are compared with the models developed. Due to proprietary data restrictions, the geometry of the tool is not presented here. But to give a comparative idea, flow conditions will be discussed. The erosion rate on tool is measured for 2% sand loading with 53 micron sand size and 66.47 ft/s inlet velocity. Erosion rate at 243 points is measured and compared with simulated results from New Baker Hughes Model, Shear Stress model, Turbulent Kinetic Energy model and ANN model. Regression results are presented below.

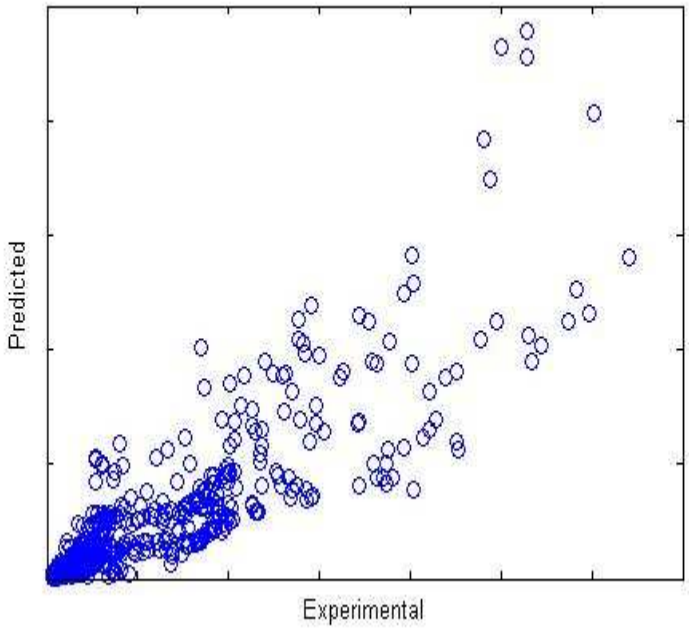

Figure 86 Baker Hughes Model – Verification

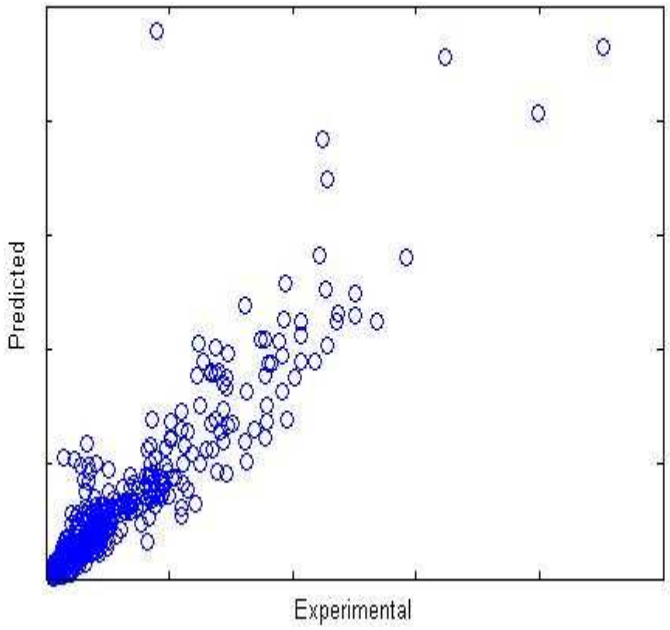

Figure 87 Shear Stress model verification

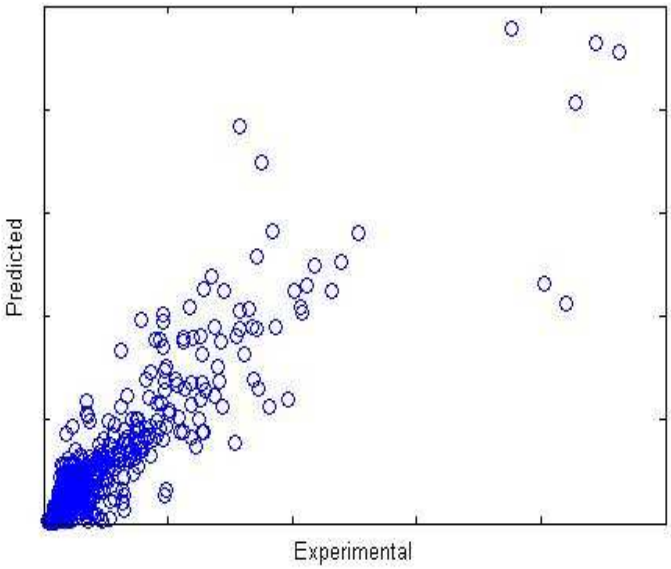

Figure 88 TKE model Verification

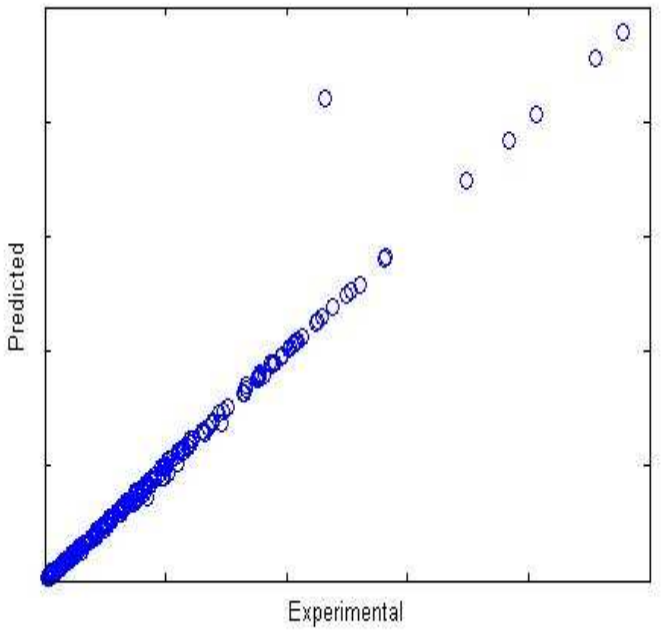

Figure 89 ANN model verification

Mean percentage errors are represented in graph below.

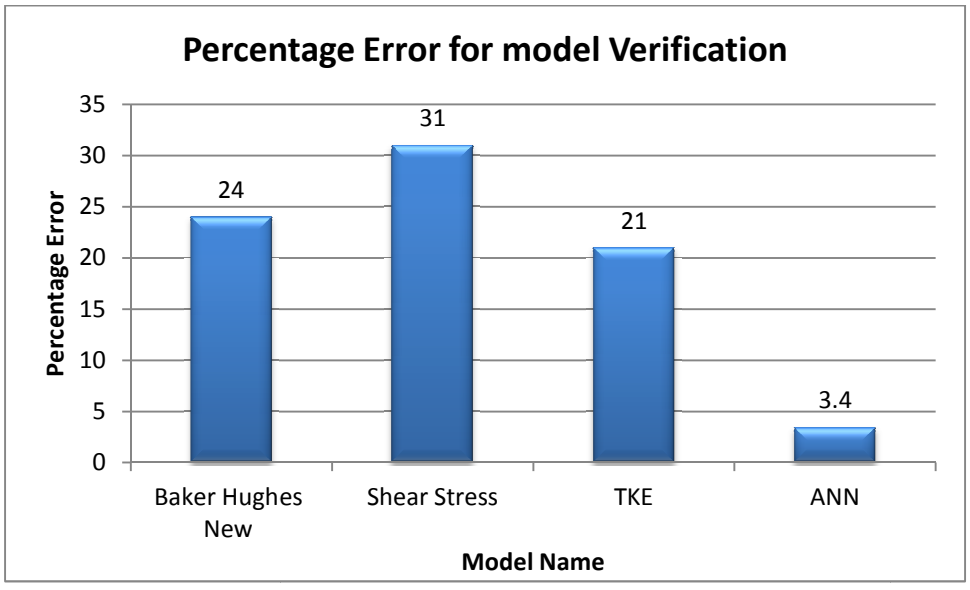

Figure 90 Mean Percentage Error Verification

It can be observed that in the verification case, each model performs better in comparison to elbow erosion rate prediction. This can be attributed to the fact that , geometry of verification model does not have major variations in terms of flow path. It has pretty much undisturbed streamline flow and is more comparable to upstream points in case of elbow. Even in elbow, mean error for upstream points is much lower compared to downstream where complex flow structures like vortices are generated.

Chapter 8

Conclusion

Following conclusions were made from the studies performed in this work.

- Current erosion models predict erosion region accurately but are many a times off by an order of magnitude when quantitative comparison is made. The mean percentage error in case of elbow was as high as 90% with more than 150% error at some points.
- Current Baker Hughes model was developed by data from a comparatively coarse grid and no significant study was performed to see the effect of CFD modeling parameters. Still it performed better than Oka et al. model quantitatively with 57% improvement in predicting erosion rate.
- An exhaustive grid study was performed on elbow case and the current model parameters were adjusted accordingly. More than 30 grid iterations were carried out with grid size ranging from few thousand elements to more than a million elements. Erosion region were predicted well with each grid but erosion rates varied drastically. Less effect was seen on upstream region of the elbow as compared to downstream. Grid refinements show different effect on error prediction in upstream and downstream regions. This can be attributed to the fact that erosion rate on downstream region is much larger compared to upstream region. Also, downstream region has complex flow vortices contributing to recirculation of particles in certain areas and causing more erosion.

- Convergence studies on number of particles to be injected in Discrete Phase model was also carried out. Solution converged at about hundred thousand particles
- As erosion rate predictions were found very sensitive to grid size, three separate models for different wall Y+ range were developed by regression. All there models now had comparable mean percentage error in the range around 35%. This is a 60% improvement from current baker hughes model.
- Correlation analysis and bootstrap analysis was performed on 8 different CFD output parameters to identify parameters effecting erosion rate. Velocity, Surface shear stress, DPM concentration and Turbulent Kinetic Energy were found to have the greatest effect.
- A new Shear stress based erosion rate prediction model was developed by implementing robust least square curve fitting. Both Least absolute residual and Bisquare weights method were explored. The new shear stress based model has average percentage error of 42 %. A turbulent kinetic energy based erosion model was also developed and it exhibited an error of 29% which is an improvement of about 20% from previous model.
- Artificial neural network models were developed and analyzed to act as a black box where CFD output was taken as input parameter and erosion was the output. More than 45 different networks with different number of neurons in hidden layers as well as different number of hidden layers were

modeled. A multilayer feed forward network with backpropogation algorithm was implemented for each of the models. Training algorithms like Scaled Conjugate gradient and Levenberg-Marquardt were implemented. A Bayesian regularization was implemented on Levenberg-Marquardt to avoid overfitting while training .This gave us the best results. The results from ANN model were excellent with mean percentage error of 7% which is a further improvement of more than 20% points and 300% from Shear stress or TKE model. Overall, it brings down error from 57 percent to 7 percent. This proved that ANN has a great potential to be developed further as a tool to predict erosion rate.

- A CFD analysis was performed on a completion tool to verify the models developed. All the models showed improvement in predicting erosion rates when compared to elbow case. This is a little counter intuitive but the verification model has very simple flow path with no circulation regions. It can be compared to just upstream data points of the elbow where erosion rate prediction capabilities were found to be more accurate as compared to downstream points. Hence, the models were successfully verified on a different geometry.

Chapter 9

Future Recommendation

It was observed that Baker Hughes models were highly sensitive to grid size hence a study was performed to quantify this effect. Percentage change in DPM concentration and Velocity was measure for all four test cases considering a point 2 mm from the wall as reference. Results are presented below;

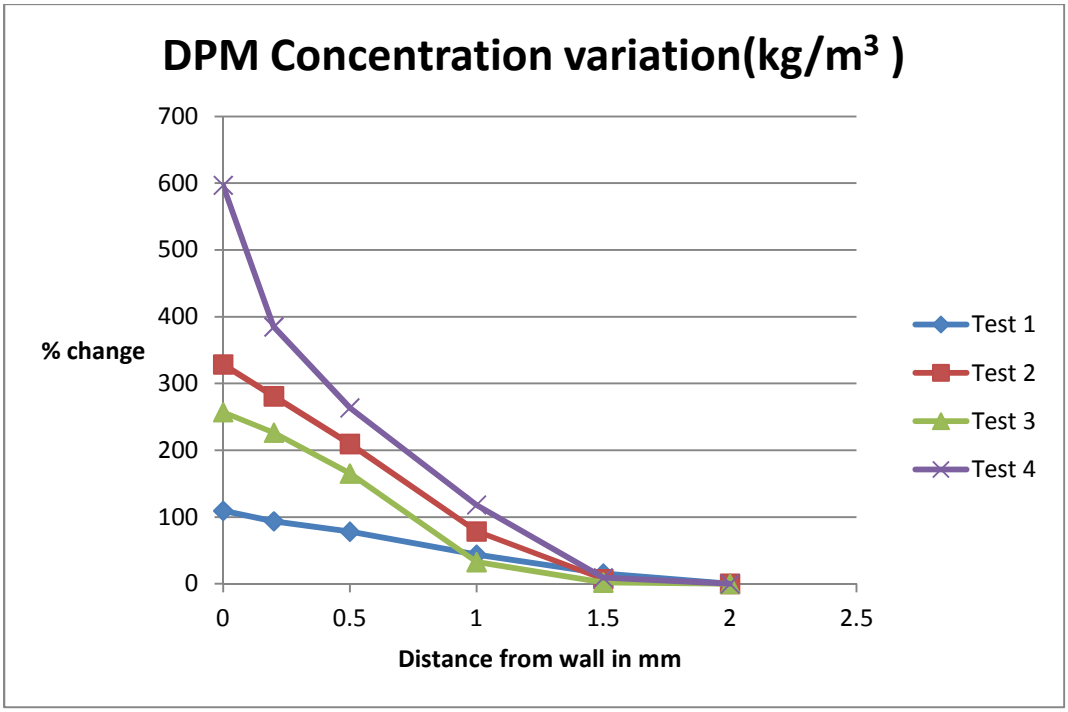

Figure 91 DPM concentration variation with wall distance

It can be clearly observed that DPM concentration is highly sensitive to wall distance. As Concentration is a conditioning parameter in Baker Hughes. Grid size as well as distance of point from wall where it is measured, has a great impact on erosion rate prediction.

To eliminate this dependence, a case with eulerian modeling approach was simulated and similar study was performed:

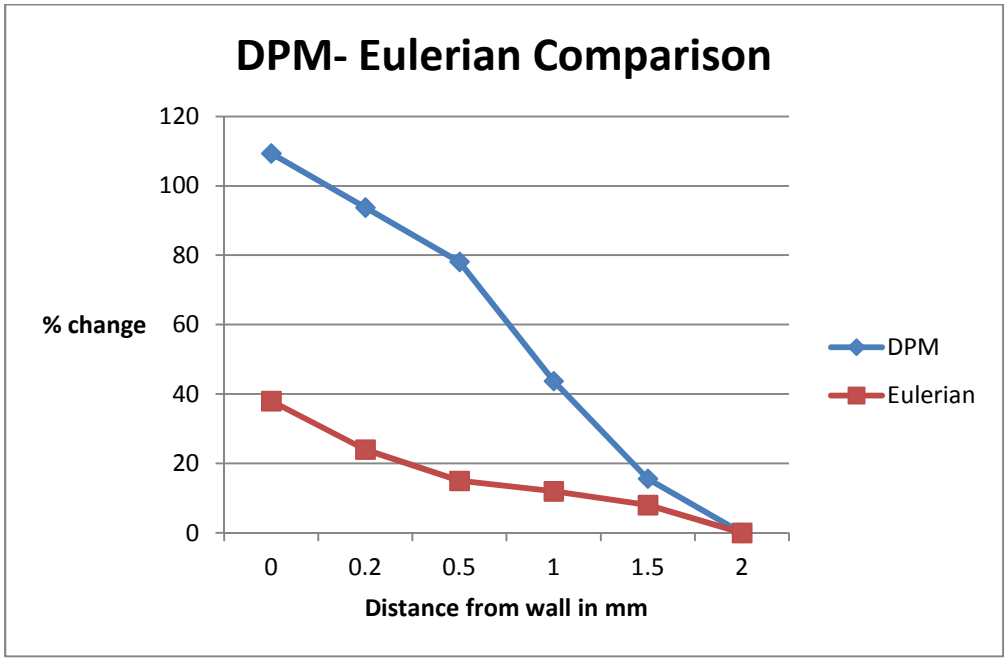

Figure 92 Concentration change comparision

Eulerian model is found to be less sensitive to location of measurement. As a future work, it is highly advised to develop a model that is based on eulerial approach and compare it with present models. It has a great potential of being more robust in terms of erosion rate prediction with minor change in location of a point where CFD parameters are calculated.

All the models were developed based on experimentation on elbow. This is just one case and hence care should be taken to generalize it. Experimentation on more complex tools that are used in oil and gas industry and that face erosion problems day in and day out should be performed. This will help in development of a better model

For any statistical model, more data points mean better model. And this can be achieved by more experimentation.

Material properties of the tool are believed to have great effect on erosion rate. Dependence of erosion rate on material properties like hardness or tensile strength should be explored.

Lastly, although our studies show no significant effect of impact angle, may other experimental studies have found it to be a significant parameter affecting erosion. (Finnie et al. 1992, Sheldon 1970). More efforts should be made to implement a custom impact angle function into erosion models.

References

Ahlert, K. R. (1994). *Effects of Particle Impingement Angle and Surface Wetting on Solid Particle Erosion of AISI 1018 Steel,*

ANSYS, F. (2006). FLUENT user's manual. *Software Release, 6*, 449-456.

Begg, R., & Palaniswami, M. (2006). *Computational intelligence for movement sciences: Neutral networks and other emerging technigues* IGI Global.

Bellman, R., & Levy, A. (1981). Erosion mechanism in ductile metals. *Wear, 70*(1), 1-27.

Bitter, J. G. A. (1963). A study of erosion phenomena part I. *Wear, 6*(1), 5-21. doi:10.1016/0043-1648(63)90003-6

Boeree, C. G. (2013). General psychology - the neuron. Retrieved, 2013, from http://webspace.ship.edu/cgboer/theneuron.html

Bolboaca, S., & Jäntschi, L. (2006). Pearson versus spearman, kendall's tau correlation analysis on structure-activity relationships of biologic active compounds. *Leonardo Journal of Sciences, 5*(9), 179-200.

Burnett, A., De Silva, S., & Reed, A. R. (1995). Comparisons between “sand blast” and “centripetal effect accelerator” type erosion testers. *Wear, 186*, 168-178.

Carpenter, G. A., & Grossberg, S. (1985). Category learning and adaptive pattern recognition: A neural network model. Paper presented at the *Proceedings, Third Army Conference on Applied Mathematics and Computing, ARO Report,* 86-81.

Cartis, C., Gould, N. I., & Toint, P. L. (2009). Trust-region and other regularisations of linear least-squares problems. *BIT Numerical Mathematics, 49*(1), 21-53.

Chase, D., Rybicki, E., & Shadley, J. (1992). A model for the effect of velocity on erosion of N80 steel tubing due to the normal impingement of solid particles. *Journal of Energy Resources Technology, 114*, 54.

Chen, X., McLaury, B. S., & Shirazi, S. A. (2004). Application and experimental validation of a computational fluid dynamics (CFD)-based erosion prediction model in elbows and plugged tees. *Computers & Fluids, 33*(10), 1251-1272.

Clark, H., & Burmeister, L. (1992). The influence of the squeeze film on particle impact velocities in erosion. *International Journal of Impact Engineering, 12*(3), 415-426.

Clift, R., & Gauvin, W. (1971). Motion of entrained particles in gas streams. *The Canadian Journal of Chemical Engineering, 49*(4), 439-448.

Conn, A. R., Gould, N. I., & Toint, P. L. (2000). *Trust region methods* Siam.

Cousens, A., & Hutchings, I. (1983). A critical study of the erosion of an aluminium alloy by solid spherical particles at normal impingement. *Wear, 88*(3), 335-348.

Cousens, A., & Hutchings, I. (1983). Influence of erodent particle shape on the erosion of mild steel. Paper presented at the *Erosion by Liquid and Solid Impact, Sixth International Conference,* 1983.

Danaher, S., Datta, S., Waddle, I., & Hackney, P. (2004). Erosion modelling using bayesian regulated artificial neural networks. *Wear, 256*(9), 879-888.

Dayhoff, J. E., & DeLeo, J. M. (2001). Artificial neural networks. *Cancer, 91*(S8), 1615-1635.

Demuth, H., & Beale, M. (1993). Neural network toolbox for use with MATLAB.

Denison, D., Mallick, B., & Smith, A. (1998). Automatic bayesian curve fitting. *Journal of the Royal Statistical Society: Series B (Statistical Methodology), 60*(2), 333-350.

Edwards, J. K. (2000). *Development, Validation, and Application of a Three-Dimensional, CFD-Based Erosion Prediction Procedure,*

Edwards, J., McLaury, B., & Shirazi, S. (1998). Supplementing a CFD code with erosion prediction capabilities. Paper presented at the *Proceedings of ASME FEDSM, , 98*

Efron, B. (1979). Bootstrap methods: Another look at the jackknife. *The Annals of Statistics,* , 1-26.

Efron, B., & Efron, B. (1982). *The jackknife, the bootstrap and other resampling plans* SIAM.

Evans, A., Gulden, M., & Rosenblatt, M. (1978). Impact damage in brittle materials in the elastic-plastic response regime. *Proceedings of the Royal Society of London.A.Mathematical and Physical Sciences, 361*(1706), 343-365.

Finnie, I. (1958). The mechanism of erosion of ductile metals. Paper presented at the *Proceedings of 3rd US National Congress of Applied Mechanics,* 527-532.

Finnie, I., & McFadden, D. (1978). On the velocity dependence of the erosion of ductile metals by solid particles at low angles of incidence. *Wear, 48*(1), 181-190.

Finnie, I., Stevick, G., & Ridgely, J. (1992). The influence of impingement angle on the erosion of ductile metals by angular abrasive particles. *Wear, 152*(1), 91-98.

Finnie, I., Wolak, J., & Kabil, Y. (1967). Erosion of metals by solid particles. *J.Mater, 2*(3), 682-700.

Finnie, I. (1960). Erosion of surfaces by solid particles. *Wear, 3*(2), 87-103. doi:10.1016/0043-1648(60)90055-7

Fluent, A. (2009). 12.0 theory guide, ANSYS. *Inc., Canonsburg, PA, 15317*

Forder, A., Thew, M., & Harrison, D. (1998). A numerical investigation of solid particle erosion experienced within oilfield control valves. *Wear, 216*(2), 184-193.

Foresee, F., & Hagan, M. T. (1997). Gauss-newton approximation to bayesian learning. Paper presented at the *Neural Networks, 1997., International Conference on, , 3* 1930-1935.

Gershenson, C. (2003). Artificial neural networks for beginners. *ArXiv Preprint cs/0308031,*

Gibbons, J. D. (1993). *Nonparametric measures of association* Sage.

Gibbons, J. D., & Chakraborti, S. (2003). *Nonparametric statistical inference* CRC press.

Grant, G., & Tabakoff, W. (1974). Erosion prediction in turbomachinery due to environmental solid particles. *AIAA Paper,* (74-16)

Hagan, M. T., Demuth, H. B., & Beale, M. H. (1996). *Neural network design* Pws Pub. Boston.

Hagan, M. T., & Menhaj, M. B. (1994). Training feedforward networks with the marquardt algorithm. *Neural Networks, IEEE Transactions on, 5*(6), 989-993.

Haider, A., & Levenspiel, O. (1989). Drag coefficient and terminal velocity of spherical and nonspherical particles. *Powder Technology, 58*(1), 63-70.

Harrington, P. d. B. (1993). Sigmoid transfer functions in backpropagation neural networks. *Analytical Chemistry, 65*(15), 2167-2168.

Haykin, S. (1994). *Neural networks: A comprehensive foundation* Prentice Hall PTR.

Hjertager, B., & Solberg, T. (1999). a review of computional fluid dynamics (cfd) modeling of gas explosions. *Prevention of Hazardous Fires and Explosions: The Transfer to Civil Applications of Military Experiences, 26*, 77.

Hockey, B., Wiederhorn, S., & Johnson, H. (1977). *Erosion of Brittle Materials by Solid Particle Impact.,*

Holland, P. W., & Welsch, R. E. (1977). Robust regression using iteratively reweighted least-squares. *Communications in Statistics-Theory and Methods, 6*(9), 813-827.

Humphrey, J. (1990). Fundamentals of fluid motion in erosion by solid particle impact. *International Journal of Heat and Fluid Flow, 11*(3), 170-195.

Hutchings, I. M. (2000). Ductile-brittle transitions and wear maps for the erosion and abrasion of brittle materials. *Journal of Physics D: Applied Physics, 25*(1A), A212.

Hutchings, I. (1979). Mechanisms of the erosion of metals by solid particles. *Erosion: Prevention and Useful Applications, ASTM STP, 664*, 59-76.

Hutchings, I. (1981). A model for the erosion of metals by spherical particles at normal incidence. *Wear, 70*(3), 269-281.

Hutchings, I., & Winter, R. (1974). Particle erosion of ductile metals: A mechanism of material removal. *Wear, 27*(1), 121-128.

Jahanmir, S. (1980). The mechanics of subsurface damage in solid particle erosion. *Wear, 61*(2), 309-324.

Kendall, M. G. (1948). Rank correlation methods.

Kendall, M. G. (1948). Rank correlation methods.

Klerfors, D. (1998). Artificial neural networks. *St.Louis University, St.Louis, Mo,*

Klopf, A. H. (1972). *Brain Function and Adaptive Systems: A Heterostatic Theory,*

Klopf, A. H. (1975). A comparison of natural and artificial intelligence. *ACM SIGART Bulletin,* (52), 11-13.

Kvam, P. H., & Vidakovic, B. (2007). *Nonparametric statistics with applications to science and engineering* Wiley. com.

Laitone, J. (1979). Aerodynamic effects in the erosion process. *Wear, 56*(1), 239-246.

Lawson, C. L., & Hanson, R. J. (1974). *Solving least squares problems* SIAM.

Lee Rodgers, J., & Nicewander, W. A. (1988). Thirteen ways to look at the correlation coefficient. *The American Statistician, 42*(1), 59-66.

Levenberg, K. (1944). A method for the solution of certain problems in least squares. *Quarterly of Applied Mathematics, 2*, 164-168.

Levy, A. V. (1981). The solid particle erosion behavior of steel as a function of microstructure. *Wear, 68*(3), 269-287.

Levy, A. V. (1995). *Solid particle erosion and erosion-corrosion of materials* ASM International (OH).

Levy, A. V., & Chik, P. (1983). The effects of erodent composition and shape on the erosion of steel. *Wear, 89*(2), 151-162.

Levy, A. V. (1986). The platelet mechanism of erosion of ductile metals. *Wear, 108*(1), 1-21. doi:10.1016/0043-1648(86)90085-2

Liebhard, M., & Levy, A. (1991). The effect of erodent particle characteristics on the erosion of metals. *Wear, 151*(2), 381-390.

MacKay, D. J. (1992). Bayesian interpolation. *Neural Computation, 4*(3), 415-447.

MacLeod, C.The back propagation algorithm. *An introduction to practical neural networks and genetic algorithms for engineers and scientists* ()

Marquardt, D. W. (1963). An algorithm for least-squares estimation of nonlinear parameters. *Journal of the Society for Industrial & Applied Mathematics, 11*(2), 431-441.

Marquardt, D. W. (1963). An algorithm for least-squares estimation of nonlinear parameters. *Journal of the Society for Industrial & Applied Mathematics, 11*(2), 431-441.

MATLAB curve fitting toolbox documentation. (2013). Retrieved, 2013, from http://www.mathworks.com/help/curvefit/index.html

MATLAB curve fitting toolbox user guide (2012).

MATLAB R2013b documentation. (2013). Retrieved, 2013, from http://www.mathworks.com/help/documentation-center.html

McCulloch, W. S., & Pitts, W. (1943). A logical calculus of the ideas immanent in nervous activity. *The Bulletin of Mathematical Biophysics, 5*(4), 115-133.

McLaury, B. S. (1993). *A Model to Predict Solid Particle Erosion in Oilfield Geometries,*

McLaury, B. S. (1996). *Predicting Solid Particle Erosion Resulting from Turbulent Fluctuations in Oilfield Geometries,*

McLaury, B. S., Rybicki, E. F., Shadley, J. R., & Shirazi, S. A. (1999). How operating and environmental conditions affect erosion. *Corrosion 99,*

McLaury, B. S., Shirazi, S. A., Shadley, J. R., & Rybicki, E. F. (1996). How erosion-corrosion patterns in a choke change as material losses in the choke progress. *Corrosion 96,*

McLaury, B., & Shirazi, S. (1998). Predicting sand erosion in chokes for high pressure wells. Paper presented at the *SPE Annual Technical Conference and Exhibition,*

McLaury, B., & Shirazi, S. (1999). Generalization of API RP 14E for erosive service in multiphase production. Paper presented at the *SPE Annual Technical Conference and Exhibition,*

McLaury, B., Wang, J., Shirazi, S., Shadley, J., & Rybicki, E. (1997). Solid particle erosion in long radius elbows and straight pipes. Paper presented at the *SPE Annual Technical Conference and Exhibition,*

Mehrotra, K., Mohan, C. K., & Ranka, S. (1997). *Elements of artificial neural networks* the MIT Press.

Mehrotra, K., Mohan, C. K., & Ranka, S. (1997). *Elements of artificial neural networks*. Cambridge, Mass: MIT Press. Retrieved from

http://search.ebscohost.com/login.aspx?direct=true&db=nlebk&AN=1416&site=ehost-live

Mohaghegh, S., & Ameri, S. (1995). Artificial neural network as a valuable tool for petroleum engineers. Paper presented at the *SPE Petroleum Computer Conference, Texas, SPE, , 29220*

Moré, J. J. (1978). The levenberg-marquardt algorithm: Implementation and theory. *Numerical analysis* (pp. 105-116) Springer.

Moré, J. J., & Sorensen, D. C. (1983). Computing a trust region step. *SIAM Journal on Scientific and Statistical Computing, 4*(3), 553-572.

Neilson, J., & Gilchrist, A. (1968). Erosion by a stream of solid particles. *Wear, 11*(2), 111-122.

Oka, Y. I., Okamura, K., & Yoshida, T. (2005). Practical estimation of erosion damage caused by solid particle impact: Part 1: Effects of impact parameters on a predictive equation. *Wear, 259*(1), 95-101.

Oka, Y., Ohnogi, H., Hosokawa, T., & Matsumura, M. (1997). The impact angle dependence of erosion damage caused by solid particle impact. *Wear, 203*, 573-579.

Oka, Y., & Yoshida, T. (2005). Practical estimation of erosion damage caused by solid particle impact: Part 2: Mechanical properties of materials directly associated with erosion damage. *Wear, 259*(1), 102-109.

Pearson, K. (1901). LIII. on lines and planes of closest fit to systems of points in space. *The London, Edinburgh, and Dublin Philosophical Magazine and Journal of Science, 2*(11), 559-572.

Perlovsky, L. (1987). Multiple sensor fusion and neural networks. DARPA neural network study.

Pourahmadi, F., & Humphrey, J. (1983). Modeling solid-fluid turbulent flows with application to predicting erosive wear. *PhysicoChemical Hydrodynamics, 4*, 191-219.

Rojas, R. (1996). *Neutral networks: A systematic introduction* Springer.

Rosenblatt, F. (1958). The perceptron: A probabilistic model for information storage and organization in the brain. *Psychological Review, 65*(6), 386.

Rumelhart, D. E., & McClelland, J. L. (1986). Parallel distributed processing: Explorations in the microstructure of cognition. volume 1. foundations.

Russell, R., Shirazi, D., & Macrae, J. (2004). A new computational fluid dynamics model to predict flow profiles and erosion rates in downhole completion equipment. Paper presented at the *SPE Annual Technical Conference and Exhibition,*

Salama, M., & Venkatesh, E. (1983). Evaluation of API RP 14E erosional velocity limitations for offshore gas wells. Paper presented at the *Offshore Technology Conference,*

Salik, J., & Buckley, D. H. (1981). Effects of erodant particle shape and various heat treatments on erosion resistance of plain carbon steel.

Sargent, G. (1982). Slurry erosion of materials. *Corrosion-Erosion-Wear of Materials in Emerging Fossil Energy Systems,* , 196-231.

Shahab, M., Bogdan, B., & Samuel, A. (1997). Permeability determination from well log data. *SPE Formation Evaluation, 12*(3), 170-174.

Sheldon, G. (1970). Similarities and differences in the erosion behavior of materials. *J Basic Eng Trans Asme, 92*(3), 619-626.

Sheldon, G., & Kanhere, A. (1972). An investigation of impingement erosion using single particles. *Wear, 21*(1), 195-209.

Sheskin, D. J. (2003). *Handbook of parametric and nonparametric statistical procedures* crc Press.

Shipway, P., & Hutchings, I. (1994). A method for optimizing the particle flux in erosion testing with a gas-blast apparatus. *Wear, 174*(1), 169-175.

Sivanandam, S., Sumathi, S., & Deepa, S. (2006). *Introduction to neural networks using matlab 6.0* Tata McGraw-Hill Education.

Smeltzer, C., Gulden, M., & Compton, W. (1970). Mechanisms of the erosion of metals by solid particles. *Journal of Basic Engineering, 19*, 639-654.

'Souza, C. (2009). **Neural network learning by the levenberg-marquardt algorithm with bayesian regularization (part 2)**. Retrieved, 2013, from http://crsouza.blogspot.com/2009/11/neural-network-learning-by-levenberg.html#regularization

Srinivasan, S., & Scattergood, R. O. (1988). Effect of erodent hardness on erosion of brittle materials. *Wear, 128*(2), 139-152. doi:10.1016/0043-1648(88)90180-9

Stigler, S. M. (1989). Francis galton's account of the invention of correlation. *Statistical Science, 4*(2), 73-79.

Suresh, A., Harsha, A., & Ghosh, M. (2009). Solid particle erosion studies on polyphenylene sulfide composites and prediction on erosion data using artificial neural networks. *Wear, 266*(1), 184-193.

Tabakoff, W., & Wakeman, T. (1979). Test facility for material erosion at high temperature. *ASTM Special Publication, 664*, 123-135.

Tilly, G. P. (1973). A two stage mechanism of ductile erosion. *Wear, 23*(1), 87-96. doi:10.1016/0043-1648(73)90044-6

Tukey, J. W. (1977). Exploratory data analysis. *Reading, Ma, 231*

Turenne, S., Chatigny, Y., Simard, D., Caron, S., & Masounave, J. (1990). The effect of abrasive particle size on the slurry erosion resistance of particulate-reinforced aluminium alloy. *Wear, 141*(1), 147-158.

Turenne, S., Fiset, M., & Masounave, J. (1989). The effect of sand concentration on the erosion of materials by a slurry jet. *Wear, 133*(1), 95-106.

Velten, K., Reinicke, R., & Friedrich, K. (2000). Wear volume prediction with artificial neural networks. *Tribology International, 33*(10), 731-736.

Vogl, T. P., Mangis, J., Rigler, A., Zink, W., & Alkon, D. (1988). Accelerating the convergence of the back-propagation method. *Biological Cybernetics, 59*(4-5), 257-263.

Werbos, P. (1974). Beyond regression: New tools for prediction and analysis in the behavioral sciences.

Werbos, P. J. (1988). Backpropagation: Past and future. Paper presented at the *Neural Networks, 1988., IEEE International Conference on,* 343-353.

WIDROW, B., & HOFF, M. E. (1960). Adaptive switching circuits.

Wolfe, D. A., & Hollander, M. (1973). Nonparametric statistical methods. *Nonparametric Statistical Methods,*

Yu, H., & Wilamowski, B. (2012). Neural network training with second order algorithms. *Human–Computer systems interaction: Backgrounds and applications 2* (pp. 463-476) Springer.

Zhang, Y. (2006). *Application and improvement of computational fluid dynamics(CFD) in solid particle erosion modeling*

Zhang, Y., McLaury, B. S., & Shirazi, S. A. (2009). Improvements of particle near-wall velocity and erosion predictions using a commercial CFD code. *Journal of Fluids Engineering, 131*(3)

Zhang, Z., Barkoula, N., Karger-Kocsis, J., & Friedrich, K. (2003). Artificial neural network predictions on erosive wear of polymers. *Wear, 255*(1), 708-713.

Zhang, Z., Barkoula, N., Karger-Kocsis, J., & Friedrich, K. (2003). Artificial neural network predictions on erosive wear of polymers. *Wear, 255*(1), 708-713.

Zhang, Z., & Friedrich, K. (2003). Artificial neural networks applied to polymer composites: A review. *Composites Science and Technology, 63*(14), 2029-2044.

Zhang, Y., Reuterfors, E. P., McLaury, B. S., Shirazi, S. A., & Rybicki, E. F. (2007). Comparison of computed and measured particle velocities and erosion in water and air flows. *Wear, 263*(1–6), 330-338. doi:10.1016/j.wear.2006.12.048

Biographical Information

Mr. Deval Pandya, completed his Bachelors in Mechanical engineering and Post Graduate Diploma in Industrial Relations and Personell management from India. He arrived in United States in 2008. After completion of his Master of Science degree in Aerospace Engineering from University of Texas, he started his doctoral studies at the same university in Mechanical Engineering. Deval Pandya is one of the four co-chairs of Next Generation Scientists for Biodiesel. His interests include modeling and simulations for energy sector including both oil and gas as well as renewable energy forms like biodiesel.